The Abdus Salam International Centre for Theoretical Physics

United Nations Educational, Scientific and Cultural Organization

IAEA International Atomic Energy Agency

20th International Workshop on Computational Physics and Materials Science: Total Energy and Force Methods | (SMR 3554)

23 Feb 2021 - 25 Feb 2021
Virtual, Virtual, Italy

P01 - ABJAOU Ali

The Magnetic Properties of High Entropy Alloys: Role of Cr on alloy based Al-Fe-Ni-Co

P02 - ACHEHBOUNE Mohamed

Structural, Electronic and optical properties of ZnO doped with Ytterbium (Yb): Overview of DFT calculation

P03 - ADANE Tsigie Getie

Electronic Properties of 2D Van der Waals Heterostructures of Janus Transition Metal Dichalcogenides with WS2 Monolayer for Photovoltaic Devices: A First Principle study

P04 - AGBAOYE Ridwan Olamide

Bandgap correction and spin-orbit coupling induced optical absorption spectra of CH3NH2CH3PbI3 for solar cell absorber

P05 - AKIODE Kolawole Olubunmi

FIRST PRINCIPLES MODELLING OF SINGLE WALLED CARBON NANOTUBE-METAL OXIDE NANOCOMPOSITE AS ANODE MATERIAL IN LITHIUM ION BATTERY

P06 - ALAM Khorsed

Determining dynamical, mechanical and thermdynamical stability of combinatorially designed ternary transition metal trichalcogenides for potential applications as hydrogen evolution reaction catalysts

P07 - ALAM Marwan

First Principles Study of Janus monolaye SnSSe

P08 - ALKHALDI Hanof

Computing the Tungsten–Nitrogen Phase Diagram at High Pressure and High Temperature and further ternary W–N compounds

P09 - ALLAN Linet

AB-INITIO STRUCTURAL AND ELECTRONIC PROPERTIES OF SELECTED TITANIUM OXIDES AND OXYNITRIDESS

P10 - ALVERTIS Antonios Markos

Non-perturbative modelling of exciton-phonon interactions in organic semiconductors

P11 - ASIRI Hassn A Yassmin

The harmonic vibrational effects on excitonic gap using QMC and the random thermal averages

P12 - ATAEI Seyedehsamaneh

Electronic and optical properties of electron-doped layered transition metal dichalcogenides

P13 - ATALAR Kemal

Accurate ab initio tight-binding model for twisted bilayer transition metal dichalcogenides

P14 - AYALA María Paula

Ab initio studies of spinel-based γ-Al2O3 surfaces

P15 - AYARI Sabrine

Phonon-assisted exciton/trion conversion efficiency in transition metal dichalcogenides

P16 - BABARIYA Sanjaybhai Bindiya

Tuning the electronic band gap and reflective optical response of 2D layered MoTe2: A DFT study

P17 - BADRI Ayda

State-to-state inelastic rate coefficients of phosphine in collision with He at low to moderate temperature

P18 - BANERJEE Rudra

Combinatorial search for efficient HER catalyst

P19 - BARBOSA RODRIGUES Joao Nuno

Identifying materials with charge-spin physics from first principles calculations

P20 - BASTOS Alves Vinicius

Beyond-DFT Studies for Thiophene and Furan Oligomers

P21 - BELAKROUM Karima

DFT Study of structural, electronic and magnetic properties of CuCrSnS4

P22 - BELLEFLAMME Edgard Amade Fabian *- not presenting*

Combining accuracy with linear-scaling efficiency: energies and nuclear gradients for a variational formulation of the Harris functional as correction to sub-system DFT

P23 - BHAGAT Brajesh Rajesh

Understanding site-dependence overall water splitting mechanism for energetically stable bilayer heptazine g-C3N4

P24 - BŁASZCZAK Jakub Michał

'Ab initio' studies of structural and electronic propoerties of orthorombic layered crystals

P25 - BONACCI Miki

Excitonic effects in C3N

P26 - BUSSY Augustin

Efficient and low-scaling linear-response time-dependentdensity functional theory implementation for core-level spectroscopy of large and periodic systems

P27 - BUSTAMANTE Carlos Mauricio

A simple approximation to the electron–phonon interaction in population dynamics

P28 - CARVALHO Costa Pamela

Investigation of local magnetic properties in metallic multilayered systems

P29 - CAZZANIGA Marco

Anharmonic calculations of vibrational spectra for molecular adsorbates: A divide-and-conquer semiclassical molecular dynamics approach

P30 - CHANEY Gracie

Benchmarking SCAN functional for two-dimensional crystal structures

P31 - CHANG Yueqing

z-dependent spin-momentum locking in monolayer 1T'-WTe2

P32 - CHIAROTTI Tommaso

A unified formalism for spectral and thermodynamic calculations in MBPT and its application to the HEG

P33 - CHIRCHIR Gabriel Kipkemei

INVESTIGATION OF ELECTRONIC, STRUCTURAL AND MECHANICAL PROPERTIES OF FeMnP 1-x A x (A=Si,Ga,Ge ; and) AS A POTENTIAL MAGNETOCALORIC REFRIGERANT ALLOY

P34 - COGOLLO OLIVO Beatriz Helena

Redefining the phase diagram of carbon dioxide within the quasi-harmonic approximation

P35 - COSTA ALBUQUERQUE Marcelo Fábio

XANESSimulations in Diamond-Like Two-Dimensional Material

P36 - DAS Bikram Kumar

Pure and B/ N doped Graphdiyne as a nano reactor for ORR, a competitor for Platinum: A first principles study

P37 - DAS Dr. Tisita

Enhanced Hydrogen Evolution Activity at the Edges of MPSe3 (M= Mn, Fe) Tri-chalcogenide Layers

P38 - DA SILVA Lora Estelina

Group Theory Analysis to Study Phase Transitions of Sr3Hf2O7

P39 - DAS Shreya

Understanding the curious magnetic state of Sr3OsO6

P40 - DE BREUCK Jacques M Pierre-Paul

Machine learning materials properties for small datasets

P41 - DEMIRTAS Merve

Design of two-dimensional ternary Ga2XO structures (X = S, Se, Te)

P42 - DIN Haleem Ud

Rashba spin splitting and photocatalytic properties of GeC–MSSe (M=Mo, W) van der Waals heterostructures

P43 - DONKOR Edward Danquah

Single-spin Dirac-like states in the rotational graphene phases on Co(0001)

P44 - DUTT Rajeev

Probing of Martensite phase and thermoelectric properties of CoxTaZ(x = 1,2 : Z = Si, Ge, Sn)

P45 - FOJT Tomasz Jakub

Dipolar coupling of nanoparticle-molecule assemblies: An efficient approach for studying strong coupling

P46 - GARCIA UC Fernando Luis

LDA vs GGA comparative study of the electronic and magnetic properties for dihydrated transition metal oxalate chains

P47 - GARZÓN ARMENDARIZ Nicole Doménica

Bandgap opening in graphene induced by patterned Flower-Like topological defects

P48 - GHORUI Supriti

Optoelectronic Properties and Defect Physics of Lead-free Photovoltaic Absorbers Cs2Au(I)Au(III)X6 (X = I, Br)

P49 - GHOSH Sukanya

Overcoming the asymmetry of the electron and hole doping for magnetic transitions in bilayer CrI3

P50 - GOLLAPALLI Prince

Chemically Graded Metal/Ceramic Interface - A High Throughput DFT Study

P51 - GOODWIN Anthony Holmes Zachary

The importance of long-ranged electron-electron interactions on the properties of twisted graphene moiré materials

P52 - GORELOV Vitaly

Ab-initio investigation of electronic excitations in bulk V2O5

P53 - GUANDALINI Alberto

Efficient GW calculations in two dimensional through the interpolation of the screened potential

P54 - GUO Jianqing

Hydration of NH + 4 in Water: Bifurcated Hydrogen Bonding Structures and Fast Rotational Dynamics

P55 - HASEEN Shariq

Computational structure search of Si3N4

P56 - HEHN Helena Anna-Sophia

Excited-state properties for semi-empirical tight binding

P57 - HERMAN František

Large twisting angles in Bilayer (Moiré) quantum dot structures

P58 - HIDALGO SACOTO Alejandro Raúl

Magnon valley Hall effect in CrI3-based van derWaals heterostructures

P59 - JACOBS Rychescki Matheus

Ab initio modelling of laser-induced ultrafast electronic dynamics at the perylene@MoSe2 interface

P60 - JAHANGIRZADEH VARJOVI Mirali

Tuning structural and electronic properties of two-dimensional aluminum monochalcogenides: Prediction of Janus Al2XX' (X/X' : O, S, Se, Te) monolayers

P61 - JANIK Norbert

Towards band gap engineering via biaxial and axial strain in group IV crystals

P62 - JAYACHANDRAN Pavithra

Structure and Excitation properties of Functionalized Tin porphyrins: A TDDFT study

P63 - JENNIFER G Abigail

Theoretical Insights on the Role of Bis-1,2,3-triazolebipyridine Ligands for Selective Separation of Am(III)/ Eu(III) in Nuclear Waste Management

P64 - JEYAPRAGASAM Meena Devi

Influence of shape on hydration of gold nanoparticles

P65 - JIANG Tonghuan

A full configuration interaction quantum Monte Carlo study of transition metal oxide molecules

P66 - JOSHI Himanshu

Modulation of Optical Absorption in Marcasite Fe1-xRuxS2 and Exploring the Stability of New Phase in RuS2

P67 - JUAN Dilson

Vacancy-driven Magnetic Changes on Doped Manganites: the Effect of a Localized Electronic Defect Level

P68 - KARUNAKARAN Indumathi

DFT STUDY ON GLOBAL REACTIVITY PARAMETERS OF PNA STACKS

P69 - KELLER Levi

Relativistic correction scheme for core-level binding energies from GW

P70 - KHAEMBA Kennedy Wamalwa

Weyl Chirality in Topological Semimetal Tantalum Phosphide

P71 - KITCHAEV A Daniil *- not presenting*

Probing unconventional electrochemistry with the RPA: oxidation of extended π-bonded molecular orbitals in a manganese oxide

P72 - KOHLI Kanika

Influence of Hydrogen Sulphide and its derivative on the hydrogen permeation through a model PdCu membrane by the first-principles study

P73 - KOLIOGIORGOS Athanasios

Electronic interaction and energy transfer between Si nanocrystals andorganic chromophores as a function of distance and orientation

P74 - KOTRI Abdelhadi

Static barrier of the clusters on the metallic Cu(111), Ag(111), and Au(111) surfaces

P75 - KO Tsz Wai

A fourth generation high-dimensional neural network potential

P76 - LINSCOTT Edward

Accurately predicting electron affinities with Koopmans spectral functionals

P77 - LIU Keyang

Ab initio molecular dynamics study of water TiO2 interface

P78 - MACHEDA Francesco

Theory and Computation of Hall Scattering Factor in Graphene

P79 - MAHAJAN Akshay

Decoupled Strain Response of Ferroic Properties in Multiferroic VOCl2 Monolayer

P80 - MAHAJAN Ruchika

Self-consistent DFT + U + V study of the structural, electronic, and magnetic properties of Pyrolusite (β – MnO2)

P81 - MALICA Cristiano

Temperature-dependent elastic constants from first principles

P82 - MARSILI Margherita

Combining GW-BSE and PCM approaches for the description of real time electronic dynamics of molecules close to a plasmonic nanoparticle: application to LiCN and p-nitro-aniline (PNA) molecules

P83 - MASROUR Rachid

Electronic, Magnetic properties and magnetocalori ceffect A2BC(A=Fe, Co,..; B=Mn,..; C=Ga, Al,...) Heusler compounds

P84 - MASSOTE Daniel Vasconcelos Pazzini

First principles study of atomic boron linear chains with substitutional nitrogen

P85 - MATERZANINI Giuliana

First-principles discovery of a high-temperature quasi-tetragonal phase in the Li+ conductor Li(3+x)GexP(1-x)O4

P86 - MAYDA BACAKSIZ Selma

The degradation of CdS-based paints

P87 - MENENDEZ PROUPIN Ariel Eduardo

Atomic scale model and electronic structure of Cu2O/CH3NH3PbI3 interfaces in perovskite solar cells

P88 - MERKEL Ernest Maximilian

CaFeO3 and LaMnO3: octahedral breathing versus Jahn-Teller distortion

P89 - MIESSEN Alexander

Variational Quantum Algorithms for Real Space Wave Packet Dynamics

P90 - MIRANDA De Paula Ivan

Ab-initio Gilbert damping on systems with lack of inversion symmetry: Fe50Co50(100) case

P91 - MISHRA Shashi Bhusan

Reactivity Order Among Low-index Facets of TiO2 for CO2 Adsorption and Conversion

P92 - MISSAOUI Jamil

Role of the valence band on the layer exfoliation in transition metal dichalcogenides: an ab initio study

P93 - MONDAL Unmesh

Fundamental studies on the role of nuclear quantum effects in terephthalic acid

P94 - MORAES Elizane

Assessment of Density Functionals on Carbon Dioxide intermolecular interactions

P95 - MUNOZ Reed Alexander *- not presenting*

A comparison of computed and experimental neutron diffraction intensity at large momentum for MnO and NiO

P96 - MUÑOZ SANTIBURCIO Daniel

Influence of electronic excitations on the formation of defects in GaAs

P97 - MUSSELI CEZAR Henrique

Revisiting greenhouse gases adsorption in carbon nanotubes: advances by ab initio optimized potentials

P98 - NAAZ Farha

High throughput computational screening of perovskites for photovoltaics

P99 - NAMSRAI Tsogbadrakh

First-principles calculation of magnetism and magnetocrystalline anisotropy in antiferromagnetic semiconducting chalcopyrite

P100 - NERY Juan Pablo

Ab-initio energetics of graphite and multilayer graphene: stability of Bernal versus rhombohedral stacking

P101 - NKOU Falonne Bertholde Sharone

Theoretical insights into magnetization in graphene containing single and interacting nanoporous defects

P102 - ODEYEMI Olusanmi Ebenezer

Structural, Electronic, Magnetic and Thermodynamic Properties for XCrGe (X: Hf and Zr) Half-Heusler compounds: First Principle Calculations

P103 - P Akhileshwari

of intermolecular interaction using Hirshfeld surface analysis and DFT calculations of chalcone derivatives

P104 - PANDEY Kumar Vineet

Effect of electron-phonon interaction on transprot properties Lead Iodide monolayer

P105 - PARK Heesoo

Cubic Phase Stability of Mixed-cation Perovskites: DFT calculations and machine-learning prediction

P106 - PATEL Manushi Jitendra

Ab-initio study of CsPbCl3 and Mn-doped CsPbCl3 monolayers as solar cell absorbers

P107 - PEREIRA CARDOSO Claudia Maria

Electronic and magnetic properties of well defined Gr/Co/Ir(111) and Gr/Fe/Ir(111) heterostructures

P108 - PETERSON Elizabeth

First-principles study of exchange-induced valley splitting in transition metal dichalcogenide monolayers

P109 - PITTS Christopher Thomas

Band-insulators with an odd numbers of electrons per unit cell and a restricted KS method for spin polarised systems

P110 - PRAKASH Roshme

Half-metallic ferromagnetism in XRuMnGa (X = Co & Ni) quaternary Heusler alloys -DFT study by using generalized gradient approximation (GGA) and modified Becke Johnson (mBJ) methods

P111 - PRASAD Babu Baijnath

Tunable spin Hall and spin Nernst effects in Dirac nodal line semimetals XCuYAs (X = Zr, Hf; Y = Si, Ge)

P112 - PUGA Anibal Fabian

In Silico prediction of antibacterial activity of sesquiterpene lactones using density-functional theory and quantitative structure-activity relationship methods

P113 - RAVAL Dharaben Vasantkumar

Ultrahigh carrier mobility and Strain Enhancement properties of 2D penta-PdX2 (X= As, P) monolayer: A DFT study

P114 - REHO Riccardo

Pressure-induced Phase Transitions in Fe4N

P115 - REYES LILLO Sebastian Eduardo

First principles calculation of the Hall coefficient in the high-temperature isotropic scattering-time limit

P116 - RIEMELMOSER Stefan

RPA-OEP for solids

P117 - ROSSMANNEK Max

Quantum HF/DFT-Embedding Algorithms for Electronic Structure Calculations

P118 - ROSTAMI Samare

Constructing the energy landscape for Ti{x}Zr{1-x}O2 via a neural-network potential through charge equilibration technique

P119 - R SARATHKUMAR .

Prediction of Structural, Electronic, Magnetic and Thermoelectric Properties for the InverseHeusler alloy Mn2NiSn: A first-principles study

P120 - SALAZAR MEJÍA Mateo Joshua

Ab-initio studies of ultra-thin CaF2 layers on the Si(100) surface

P121 - SAMBASIVAM Anitha

A DFT Study on the Relationship Between Structure and Antioxidant Properties of Thymoquinone

P122 - SANCHEZ NARANJO Anais Jennifer

Computational studies of the electronic structure and stability of TiO2 nanoclusters

P123 - SANTOS-PUTUNGAN Bernardo Alexandra

Strong chemisorption of CO2 on B10–B13 planar-type clusters

P124 - SAPPATI Subrahmanyam

Stability of variable protonation state of citrate on Fe3O4 nanoparticles

P125 - SHAPOVALOV Konstantin

Rotopolar coupling driving the antiferroelectric phase transition in PbZrO3

P126 - SHARMA Gautam

Structural, electronic and transport properties of BiI 3 /ZrS 2 van der Waals heterostructure: A first principle investigation

P127 - SHEIKH Ali Musharaf

Abinitio Studies on Permeation and Solubility of Hydrogen Isotopes in Iron (Fe), Tungsten (W) and Chromium (Cr)

P128 - SILVA GUILLÉN Jose Angel

Strain tuning of the anisotropy in the optoelectronic properties of the two-dimensional transition metal trichalcogenide TiS3

P129 - SONI Gaganbhai Kamalkumar

Compositional dependence of structure and chemical short-range order in Zr-Cu-Al Glass-forming alloys

P130 - SPRINGOLO Matteo

Flexoelectricity in two-dimensional materials

P131 - STEIN Frederick

Double-Hybrid DFT Functionals for the Condensed Phase: Gaussian and Plane Waves Implementation and Evaluation

P132 - STELLA Martina

Towards a systematic multi-scale method for excitations in molecular materials in the BigDFT code

P133 - TADOUT Mohamed

Effect of the cations distribution on the magnetic properties of SnFe2O4: First-principles study

P134 - TAGHIPOUR AZAR Yavar

Termination dependent Rashba-Dresselhaus band splitting in CsPbI3 slabs

P135 - TEUNISSEN Leonard Johannes

Automated design of a structural descriptor for radiation resistant perovskites

P136 - THOTTATHIL Reshmi

First Principle Study on Magneto-electric Multiferroics

P137 - TIMROV Iurii

Pulay forces and stresses in density-functional theory with extended Hubbard functionals: From nonorthogonalized to orthogonalized manifolds

P138 - TISI Davide

Heat transport in water from Deep Neural Network potentials

P139 - T Mohan Aswathi

CO2 capture, activation and dissociation on the Ti2C surface and Ti2C MXene: the role of surface structure

P140 - TREVIZAM DORINI Thiago

Two-dimensional ABO 3 /Me oxide quasicrystal approximants : insights from Density Functional Theory

P141 - TRIVEDI Kumar Ravi

Hydrogen Storage on TM metal doped Mgn and ZTC - A denstiy functional Investigation

P142 - TSIRKIN S. Stepan

Enhancing the speed and precision of Wannier interpolation with WannierBerri code

P143 - VACONDIO Simone

Higher order many-body perturbation theory applied to atomic systems

P144 - VAITHIYANATHAN Vetrivelan

Synthesis, Spectral, Hirshfeld surface analysis, DFT calculations and molecular docking studies on dioxol derivatives as potential antibacterial inhibitors

P145 - VARGAS TELLEZ Alberto Jorge

Improving density functional calculations of molecular polarizabilities using locally scaled self-interaction corrections

P146 - VÁSCONEZ Marcelo Edwin

First-principles studies of the electronic and mechanical properties of -Al/ -Al2O3(111) multilayer composite

P147 - VASILCHENKO Vasilii

Polarons In Two-dimensional Pnictogens

P148 - VAST Nathalie Madeleine Marguerite

Theoretical phase diagram of boron carbide from ambient to high pressure and high temperature

P149 - VATANKHAHAN Adeleh

Effect of Adsorption of Co and Mn atoms on magnetic and transport properties of hydrogenated borophene nanoribbons

P150 - VEGA David Jorge

Ab Initio study of the structural and electronic properties of Niobium Sulfide (NbS2) and Lithium Niobium Sulfide (LiNbS2) bulk and (001) surfaces

P151 - VELANKANNI Nandhakumar

DFT insights into electrocatalytic reduction of CO2 reduction on PdCu(110) surface

P152 - VIPIN KUMAR -

Electric field-induced band modulation of predicted ternary 2D MXC3 [M:X ¼ As:Ge, Sb:Sn and Bi:Pb] with strong stability and optical properties

P153 - VITALE Valerio

Chemical trends in the electronic structures of transition metal dichalcogenides

P154 - WAGNER Kyle Lucas

Direct Comparison of Many-Body Methods for Realistic Electronic Hamiltonians

P155 - WANG Yiyuan

The impact of chemical modification on charge injection at metal/polyolefin interfaces

P156 - WHEELER Ashwin William

PyQMC: an all-Python real-space quantum Monte Carlo code

P157 - WINES Daniel Thomas

A first-principles Quantum Monte Carlo study of two-dimensional (2D) GaS/Se and Janus GaSSe

P158 - WITT Charles (Chuck) William

Random structure searching with orbital-free density functional theory

P159 - WITTEMEIER Nils

Quantum transport with Spin Orbit Coupling

P160 - WOZNIAK Tomasz

Exciton g-factors of van der Waals heterostructures from first-principles calculations

P161 - YADAV Kedar

Novel low dense carbon allotropes from data mining approaches

P162 - YADAV Kumar Dinesh

Structural, elastic, electronic, and magnetic properties of MnNbZ (Z = As, Sb) and FeNbZ (Z = Sn, Pb) semi-Heusler alloys

P163 - YUNITASARI Sefty

The study of Dirac cones in graphene flakes using band-unfolding method

P164 - ZANOLLI Zeila

Defects in Transition Metal Dichalcogenides: towards quantum computing

P165 - ZIASHAHABI Azin

Enhanced optical adsorption at the surface of rutile TiO2 nanostructures by oxygen defects

P166 - SASANI Ali Resa

Magneto electric response in rare earth orthoferrites

P167 - TANNER Stephen Patrick Daniel

Electrostriction by DFT: a methodological study

P01

The Magnetic Properties of High Entropy Alloys: Role of Cr on alloy based Al-Fe-Ni-Co

Electronic structure of AlCo_x Cr_(1-X) FeNi (0≤ x ≤ 1) high-entropy alloys (HEAs) was calculated using the Korringa-Kohn-Rostoker method combined with the coherent potential approximation (KKR-CPA). Total energy minimization was performed for bcc and FCC structures in each alloy composition. The phase stability was investigated from the total energy analysis, which Finally allowed to determine the BCC-FCC phase transition for Chrome and Cobalt. It inspired us to synthesize AlCo_x Cr_(1-X) FeNi (0≤ x ≤ 1) using procedures . The XRD measurements evidently proved an occurrence of FCC or BCC structure and their coexistent, depending on Cr and Co concentration and temperature. This finding remains in good agreement with theoretical results from free energy analysis, when accounting for KKR-CPA total energy as well as entropy terms. Furthermore, the structure preference, from FCC to BCC HEAs, with increasing Cr content was discussed in view of total and atomic -dependent density of states computed in non-magnetic and paramagnetic -like states. Thus, the main objective of the present study is to study the effect of Co/Cr ratio on the magnetic properties of AlCo_x Cr_(1-X) FeNi (0≤ x ≤ 1) high entropy alloys. The systematic variation in composition was achieved via laser deposition of a compositionally graded alloy. Such a combinatorial approach permits the investigation of multiple compositional steps in a relatively fast, yet systematic manner, and leads to new insights related to the evolution of microstructure and its consequent influence on the magnetic properties.

P02

Structural, Electronic and optical properties of ZnO doped with Ytterbium (Yb): Overview of DFT calculation

M. achehboune[1,2], M. Khenfouch[2], I. Boukhoubza[1,2], I. Derkaoui[1,2], B. M. Mothudi[3], I. Zorkani[1], A. Jorio[1]

[1]Sidi Mohammed Ben Abdellah University, Faculty of Sciences Dhar el Mahraz, Laboratory of Solid State Physics, Group of Nanomaterials and Renewable Energies, PO Box 1796 Atlas Fez 30 000, Morocco.
[2]Africa Graphene Center, Department of Physics, College of Science, Engineering and Technology, Science Campus, University of South Africa, Cnr Christiaan de Wet & Pioneer Avenue Florida 1709, Johannesburg, South Africa.
[3]University of South Africa, Department of Physics, Private Bag X90, Florida, 1710, South Africa.

Corresponding author: achehboune.mohamed01@gmail.com

Abstract.
In this work, first-principles plane-wave ultrasoft pseudopotential method is employed to investigate band structures, density of states and optical properties in pure and Yb-doped ZnO theoretically. The energy band is still direct band gap after Yb doping, and band gap decreases with the increase of Yb concentration. The Fermi level moves upward into conduction band and the Density Of States (DOS) moves to lower energy with the increase of Yb concentration, which showing the properties of n-type semiconductor. The calculated optical properties imply that Yb doped causes a red-shift of absorption peaks, and enhances significantly the absorption of the visible light and the blue shift of reflectivity spectrum was observed. The research results in this work can provide a theoretical reference for subsequent researches of Yb-doped ZnO.

Keywords: Yb-doped ZnO, First-principles, Electronic structure, Optical properties.

Abstract

Building two-dimensional (2D) heterostructure emerges novel properties, with promising applications in photovoltaic (PV) cells. By performing density functional theory (DFT) based first principles calculations, electronic properties of WS2 and Janus transition-metal dichalcogenides (JTMDs) monolayers were calculated and depending on the lattice mismatch, layered 2D JTMDs/WS2 heterostructures were formed. The formation of the JTMDs/WS2 van der Waals (vdW) heterostructures have shown great potential for the design of novel electronic devices. In this study, Janus MoSSe/WS2, WSSe/WS2, and MoSTe/WS2 heterostructures were developed and their structural and electronic properties were evaluated using first principles calculations based on DFT calculations using Quantum ESPRESSO and VASP codes. It was found that the heterostructures bandgap is smaller than the Janus TMDs and WS2 monolayer. Structural relaxations were performed using generalized-gradient approximation (GGA) approaches for both the monolayers and heterostructures. Structural stability and electronic properties of JTMDs/WS2 vdW heterostructures with AC and AD stacking were investigated which are the most stable configuration compared with other configurations based on the binding energy and the interlayer distance. Results show that the Janus MoSTe/WS2, MoSSe/WS2, and AD-configuration of WSSe/WS2 vdW heterostructures are indirect bandgap semiconductor, but WSSe/WS2 with AC configuration is a direct bandgap. The JTMDs/WS2 vdW heterostructures exhibited a bandgap in the range of 1.54 to 0.54eV. In addition, MoSSe/WS2 and MoSTe/WS2 heterostructures displayed a type-II band alignment which is important to improve the photoelectric conversion efficiency. However, the band alignment of WSSe/WS2 heterostructure is difficult to identify and need additional calculations. First principles study shows that the investigated 2D heterostructures have a suitable bandgap for photovoltaic applications. Among the JTMDs/WS2 vdW heterostructures, MoSSe/WS2 and MoSTe/WS2 manifest type-II band alignment, making them promising candidates for photovoltaic (PV) applications.

P04

Bandgap correction and spin-orbit coupling induced optical absorption spectra of CH3NH2CH3PbI3 for solar cell absorber

In recent time, research aimed at improving solar cell materials' power conversion efficiency has become popular, amongst the materials of interest is the methylammonium lead iodide (CH3NH3PbI3) due to its high power conversion efficiency. This study used the density functional theory and the GW quasiparticle methods, to calculate the band structure and bandgap of optimized dimethylammonium lead iodide (CH3NH2CH3PbI3), considering the spin-orbit coupling effects on heavy metals. The real and imaginary dielectric tensors were calculated by solving the Bethe-Salpeter equations of the many-body perturbation theory with and without the effect of spin-orbit coupling. Spin-orbit coupling induces band splitting and bandgap reduction in both density functional theory and GW quasiparticle methods, while the GW quasiparticle method increases the density functional theory bandgap. This study reported the density functional theory band gap of 1.45 eV, while the effect of spin-orbit coupling reduces the bandgap to 0.51 eV. Similarly, the self-consistent GW quasiparticle method recorded a bandgap of 2.27 eV, and the effect of spin-orbit coupling on the self-consistent GW quasiparticle method reported a bandgap of 1.20 eV. The density of state results reveals that the iodine p orbital is most responsible for the valence band, while the Pb p orbital show more prominence in the conduction band. The absorption coefficient reaches the order of 106 in the ultraviolet and the visible region, which is higher than the absorption coefficient of CH3NH3PbI3, suggesting that CH3NH2CH3PbI3 has a better prospect as solar cell absorber.

P05

FIRST PRINCIPLES MODELLING OF SINGLE WALLED CARBON NANOTUBE-METAL OXIDE NANOCOMPOSITE AS ANODE MATERIAL IN LITHIUM ION BATTERY

Lithium ion batteries (LIBs) are energy storage devices based on Li-ion storage and conversion. The need for improved energy density has called for alternative anode materials that can replace the conventionally used low capacity graphite within LIBs. Metal oxides anode have shown high specific capacity while Single Walled Carbon Nanotube (SWCNT) anode exhibits long life cycle which combat the problem of volume expansion in metal oxides. Nanocomposite of Sn_3O_z (z= 3-7) with SWCNT is expected synergy that can improve anodic material for LIBs design. . Modelling and probing the nanocomposites of SWCNT isomers (arm-chair, chiral or zig-zag) with $Li_xSn_3O_3$ (SWCNT- $Li_xSn_3O_3$), structural stability and electronic properties in relation to electrochemical performance in LIBs were examined. Arm-chair SWCNT was best applicable for the formation of nanocomposites with $Li_xSn_3O_3$ nanoclusters due to its strong interactions mediated through Li-ions. The interaction increased with increase in number of x with strong cation-π interactions observed at x = 4, owing to high adsorption energy (4.24 eV). Destabilization of the nanocomposites occurred at x>4 but was reduced with the introduction of double walled carbon nanotube. Charge difference and Bader charge calculations showed successful charge transfer from the lithiated nanoclusters to SWCNT via Li-ions with highest charge transfer (2.0 electron charge) observed in SWCNT-$Li_4Sn_3O_3$ nanocomposite. Electronic density of states obtained confirmed the electronic properties of the nanocomposites. The minimum volume-expansion observed in SWCNT-$Li_xSn_3O_3$ nanocomposites with their maximum AIV values of ≈ 0.46 V indicated their good potential as anodic material for LIBs

P06 **Abstract:**

Recently few layered transition metal trichalcogenide compounds (TMTC), such as CoPS3, NiPS3, MnPSe3 and FePSe3, has been experimentally found to be efficient electrocatalysts for hydrogen evolution reaction (1,2). One intriguing question here would be whether there are other possible TMTC compounds which may not have yet been synthesized, but can be efficient HER catalysts. To address this question, in a recent work (3), we have combinatorially designed and computationally screened single layers of a large number of TMTC compounds, including those that are not reported in ICSD, for their efficiency as HER catalysts, by means of calculating the free energies of hydrogen adsorption (ΔG_{H*}) on the basal planes of these materials. Thirteen as yet unknown TMTC compounds are identified as efficient HER catalysts having ΔG_{H*} values close to zero. As a continuation of this project, we are currently studying the dynamical, mechanical and thermodynamic stability of these compounds to test the feasibility of their experimental synthesis. We have determined their dynamical stability by means of calculating their phonon band structures within the density functional perturbation theory framework. We have calculated the elastic constants of these materials and applied the Born stability criteria to determine their mechanical stability. Calculations for the thermodynamic stability are in progress, where we are constructing the convex hull on the ternary phase diagram for each of these compounds. So far, we have already established that few of these compounds are both dynamically, mechanically as well thermodynamically stable indicating the possibility that they can be experimentally synthesized and can be potential candidates as HER catalysts.

References:

1. Gusmao, et al., The Role of the Metal Element in Layered Metal Phosphorus Triselenides upon Their Electrochemical Sensing and Energy Applications. ACS Catalysis 2017, 7, 8159–8170.

2. Mayorga-Martinez et al., Layered Metal Thiophosphite Materials: Magnetic, Electrochemical, and Electronic Properties. ACS Applied Mater & Interfaces 2017, 9, 12563–12573

3. Sen et al, Combinatorial design and computational screening of 2D transition metal trichalcogenide monolayers: Toward efficient catalysts for hydrogen evolution reaction, The Journal of Physical Chemistry Letters, 2020,11, 3192–3197

P07

First Principles Study of Janus monolaye SnSSe

In the Modern technological era of semiconductor materials, 2D Transition Metal Dichalcogenides (TMDCs) are of much interest to researchers due to their outstanding structural, electronic, and optical properties. Efforts are still going on to find out many more such materials which would fill the gap of desirable conditions and all required properties for practical application in technology. In analogy to these TMDCs, inspired by experimental integration of Janus MoSSe Monolayer, We have predicted the Janus SnSSe monolayer. We performed first-principles calculations using density functional theory (DFT) implemented in Vienna Ab-Initio Simulation Package (VASP) package in order to investigate the structural, electronic, and optical properties and device absorption efficiency of Janus SnSSe monolayer. We have used HSE06 hybrid functional for electronic band structures, and optical properties were treated through Bethe-Salpeter equation. From the Phonon dispersion calculation it is observed that the 1T phase of Janus SnSSe is energetically and dynamically stable. The Janus SnSSe is a semiconductor with an indirect bandgap of 1.61 eV. From PDOS the Se-atoms have a dominant role in the VBMax as compared to S and Sn-atoms, while in CBMin and higher conduction band Sn-atoms has a major contrib ution. Dielectric constant has been determined to explain absorption coefficient, refractive index, reflectivity, extinction coefficient, and energy loss function of Janus SnSSe monolayer. In addition, Strong device absorption efficiency (approximately 90%) is observed for Janus SnSSe monolayer in visible, UV, and IR regions. Strong and efficient electronic and optical nature of the Janus SnSSe monolayer suggests it for Optoelectronic.

P08

Computing the Tungsten–Nitrogen Phase Diagram at High Pressure and High Temperature and further ternary W–N compounds

We compute the tungsten–nitrogen (W–N) pressure–temperature phase diagram through a combination of density functional theory and thermodynamic calculations. Augmenting standard enthalpy-pressure calculations by the chemical potential change of nitrogen at high pressure and high temperature conditions, we estimate Gibbs energies under nitrogen-rich conditions. The approach allows to predict temperature and pressure conditions necessary to synthesize W–N polymorphs and to locate optimum pressure/temperature conditions with maximum driving force for successful syntheses. Our investigations include W2N3, W3N5, W2N2(N2), WN6, and recently synthesized WN8-N2. Further studies address ternary Li–W–N compounds with W in high oxidation state, namely Li6WN4, Li6WN6, and Li6WN8.

P09

AB-INITIO STRUCTURAL AND ELECTRONIC PROPERTIES OF SELECTED TITANIUM OXIDES AND OXYNITRIDESS

ABSTRACT Titanium dioxide (TiO2) is an abundant, chemically stable, non-toxic, and highly versatile material, with applications ranging from photovoltaics to catalysis. For rutile and anatase phases, the band gap of TiO2 varies from 3.0 to 3.2 eV, which are too wide to absorb visible light, resulting in low photocatalytic efficiency. Continuous efforts have been made to form a band gap suitable for solar energy absorption to improve the photoactivity of TiO2 under visible light (400 nm to 700 nm). In particular, nitrogen doping into TiO2 has been able to narrow its band gap, creating an absorption tail in the visible-light region. However, TiO2 has limits to which it can be doped suggesting investigations of the oxygen-deficient corundum Ti2O3. Using the state-of-art density functional theory (DFT) as implemented in the Quantum ESPRESSO package, we present a study on the structural and electronic properties of corundum-type Ti2N2O (an example TinN2O2n−3 compound with n=2) which displayed the ability to absorb visible light with a better absorption threshold compared to other Ti-based oxides such as TiO2, TiO2: N and Ti2O3. The structural and electronic properties of the oxides were calculated using generalized gradient approximation (GGA) employing pseudopotentials and plain wave basis sets. Ti2O3 displayed metallic properties yet it is reported to have semi-conducting properties experimentally hence the DFT+U method was employed to correct the band gap of the oxides. On doping, the band gap reduced as dopant concentration was increased. Mid gap states, having shallower energies in 4%N doping than 2%N cases, were observed.

P10

Non-perturbative modelling of exciton-phonon interactions in organic semiconductors

The optoelectronic response of organic semiconductors is dominated by bound electron-hole pairs called excitons. The molecular character of these materials often leads to very strong exciton-phonon interactions, which makes perturbation theory insufficient for their description, making their first principles description challenging. Here we present a non-perturbative methodology for accurately capturing exciton-phonon interactions to all orders, based on a combination of finite differences methods for phonons with Green's function-based methods (GW-BSE) or time-dependent density functional theory (TD-DFT) for crystalline or isolated systems respectively. This allows us to show that the spatial delocalisation of an exciton is the main parameter controlling the magnitude and nature of its coupling to phonons, and to reveal the full microscopic mechanism of exciton energy temperature- and pressure-dependence in molecular crystals [1]. Furthermore, accounting for the coupling of excitons to nuclear quantum motion is found to be critical for achieving quantitative accuracy in the prediction of exciton energies, both for single molecules and crystalline molecular systems [1,2]. Overall, we provide a unified picture of exciton-vibration interactions in organic semiconductors, reconciling the complementary views of finite molecular clusters and periodic molecular solids. [1] A.M. Alvertis et al. Phys. Rev. B 102, 081122(R) https://journals.aps.org/prb/abstract/10.1103/PhysRevB.102.081122 [2] T.J.H. Hele, B. Monserrat, A.M. Alvertis, https://arxiv.org/abs/2011.10585

P11

The harmonic vibrational effects on excitonic gap using QMC and the random thermal averages

Many theoretical studies have enhanced our understanding of the various physical properties of materials and the behaviour of electrons in condensed matter. These properties are determined by solving the non-relativistic Schrödinger equation, although it is challenging to attain accurate approximate solutions of this equation. One of the most popular methods is DFT, which relies on the use of the best available approximation of the exchange-correlation (XC) energy. However, the DFT calculations fail to evaluate correctly band gap energies due to the difficulty of electron-phonon interactions calculations , even with the exact XC functional that produces the exact ground-state energy. Also, in situations where high accuracy is needed, the DFT method is considered unreliable, and it becomes necessary to use a more accurate method, such as the quantum Monte Carlo method (QMC). Many properties of material can be calculated within the static approximation, in which the effect of nuclear motion is neglected. However, the contribution of ZPE is very important in many systems, that consist of light or weakly bonded atoms, which reveal the necessity of taking into consideration the vibration correction for any comparison between the theoretical and experimental results. In this work, we have evaluate the renormalised vibrational expectation values of the electronic band gaps using random sampling of phonon normal coordinates. This approach implements the QMC sampling over a set of configurations parametrized by the temperature in interest with a small, size-independent number of sampling points. We found that the ZPE correction significantly contributed to the vibration energy.

P12

Electronic and optical properties of electron-doped layered Transition Metal dichalcogenides

S. Samaneh Ataei, Ali Sadeghi
Shahid Beheshti University, Department of Physics, Tehran, Iran

15/01/2021

Layered Transition Metal Dichalcogenides (TMDs) with promising physical properties, e.g. semiconductors with direct (indirect) energy gaps at visible range and large exciton binding energies due to the reduced screening, have recently attracted strong attention to investigate and tune the optical features in order to be applied for optoelectronic devices. Doping is one of the most relevant strategists to tune the single particle electronic band structure and absorption spectra of the materials. More ineterestingly, recent experiments have shown giant gating tunability of optical properties (ie. the refractive index) of TMDs. Electron doping leads to the Band gap renormalization (BGR) and enhanced screening in these materials. Starting from first principles calculations in the framework of Density Functional Theory (DFT) and Many Body Perturbation Theory (MBPT), we accurately study the role of BGR and screening on the electron hole pair binding of e-doped few-layer MoS_2. Our results show a non linear behavior for the reduction of the bandgap as a function of electron doping. Using GW approximation with Plasmon-Pole model (applied for the dynamical screening), the calculated band gap energies are in very good agreement with the measured data that has been recently published.

P13

Accurate ab initio tight-binding model for twisted bilayer transition metal dichalcogenides

The discovery of correlated insulating states and superconductivity in magic-angle twisted bilayer graphene has raised the question of whether similar correlated electron physics can be observed in other twisted systems such as twisted bilayer transition metal dichalcogenides (TMDs). In this work, we extend the ab initio tight-binding model of Fang et al. [1], developed for monolayer and untwisted bilayer TMDs, to study the electronic structure of twisted homo-bilayers and hetero-bilayers of the TMDs MoS2, MoSe2, WS2 and WSe2. To accurately describe twisted systems with atomic relaxations, we include pz-dz2 interlayer hopping parameters, the distance-dependence of interlayer hopping parameters, and the effect of the chemistry of the different layers on the tight-binding parameters. This poster will outline our implementation and the importance of including these features in the model by validating our results against large-scale density-functional theory calculations. [1] Shiang Fang, Rodrick Kuate Defo, Sharmila N. Shirodkar, Simon Lieu, Georgios A. Tritsaris, and Efthimios Kaxiras. Ab initio tight-binding hamiltonian for transition metal dichalcogenides. Phys. Rev. B, 92:205108, Nov 2015.

P14

Ab initio studies of spinel-based γ-Al2O3 surfaces

The γ-Al2O3 is a polymorph of alumina that is widely used for numerous technological applications such as catalysis, coatings, spacecraft industry, transistors, among others. A fundamental understanding of its properties from an atomistic approach holds the key for improving desired applications. Despite the relevance of γ-Al2O3, in the literature there are a limited number of studies at the nanoscale. The crystal structure of bulk and likely surfaces of γ-Al2O3 is still under scientific debate. In this work we take into account previous results for bulk models of γ-Al2O3 that have defective spinel structure. Using density-functional theory (DFT) within the strongly constrained and appropriately normed (SCAN) meta generalized gradient approximation (GGA), we compute the electronic and mechanical properties of the considered bulk models for γ-Al2O3. From those results, the (111), (110) and (100) surfaces of γ-Al2O3 were considered and the surface reconstructions, surface energies and corresponding electronic structure were computed. The simulations considered also non-stoichiometric phases. The results are compared and discussed in the light of available experimental data and previous computational models.

P15

Phonon-assisted exciton/trion conversion efficiency in transition metal dichalcogenides

Sabrine Ayari ,[1,] Sihem Jaziri,[1,2] Robson Ferreira,[3] and Gerald Bastard[3]

[1]*Faculté des Sciences de Bizerte, Laboratoire de Physique des Matériaux Structure et Propriétés, Université de Carthage, 7021 Jarzouna, Tunisia*

[2]*Faculté des Sciences de Tunis, Laboratoire de Physique de la Matière Condensée, Département de Physique, Université Tunis el Manar, Campus Universitaire 2092 Tunis, Tunisia*

[3]*Laboratoire de Physique de l'École normale supérieure, ENS, Université PSL, CNRS, Sorbonne Université, Université Paris-Diderot, Sorbonne Paris Cité, Paris, France*
*sabrineayaari8@gmail.com

Photoluminescence spectra show that monolayer transition-metal dichalcogenides (ML-TMDs) possess charged exciton binding energies, conspicuously similar to the energy of optical phonons. This enigmatic coincidence has offered opportunities to investigate many-body interactions between trion X^-, exciton X, and phonon and led to efficient excitonic anti-Stokes processes with the potential for laser refrigeration and energy harvesting. In this study, we show that in WSe_2 materials, the trion binding energy matches two phonon modes, the out-of-plane $A_1^{'}$ and the in-plane $E^{'}$ modes. In this respect, using the Fermi golden rule together with the effective mass approximation, we investigate the rate of the population transfers between X and X^-, mediated by a single phonon. We demonstrate that, while the absolute importance of the two phonon modes on the up-conversion process strongly depends on the experimental conditions such as the temperature and the dielectric environment (substrate), both modes lead to an up-conversion process on time scales in the range of few picoseconds to sub-nanoseconds, consistent with recent experimental findings. The conjugate process is also investigated in our study, as a function of temperature T and electron density N_e. We prove that the exciton to trion down-conversion process is very unlikely at low electron density $N_e < 10^{10} cm^{-2}$ and high temperature $T > 50$ K while it increases dramatically to reach few picoseconds time scale at low temperature and for electron density $N_e > 10^{10} cm^{-2}$. Finally, our results show that the conversion processes occur more rapidly in exemplary monolayer molybdenum-based dichalcogenides ($MoSe_2$ and $MoTe_2$) than tungsten dichalcogenides.

P16

Tuning the electronic band gap and reflective optical response of 2D layered $MoTe_2$: A DFT study

Bindiya Babariya[1], Dhara Raval[1], Sanjeev K. Gupta[2] and P. N. Gajjar[1,*]

[1]Department of Physics, University School of Sciences, Gujarat University, Ahmedabad 380 009, Gujarat, India

[2]Computational Materials and Nanoscience Group, Department of Physics and Electronics, St. Xavier's College, Ahmedabad 380 009, Gujarat, India

Email: bindiababariya293@yahoo.com, ravaldhara1994@gmail.com, sanjeev.gupta@sxca.edu.in, pngajjar@gujaratuniversity.ac.in*

ABSTRACT

Monitoring electronic band gap has become promising building block for desired applications. The structural properties, phonon dispersion curve, electronic band structure and reflective optical response of layered $MoTe_2$ have been investigated by means of first principle calculations. Positive frequency of phonon dispersion curve and cohesive energy indicate the structural stability of monolayer to quadlayer $MoTe_2$. For stable and relaxed geometry, the electronic band structure and reflective optical response have been computed. The indirect band gap decreases from 1.42 eV to 1.27 eV for monolayer to quadlayer $MoTe_2$, respectively which shows semiconducting character of layered $MoTe_2$. Considering the frequency gap between high and low frequency optical mode, layered $MoTe_2$ may be used in selective transmission of higher frequency range. The reflectivity increases as number of layers increase and maximum 68% of reflective response is achieved for quadlayer $MoTe_2$ in UV-C region. This high reflectivity depicts utility of quadlayer $MoTe_2$ as antireflection coating in UV-C region and good hot mirror material of ultrathin reflectors.

METHODOLOGY

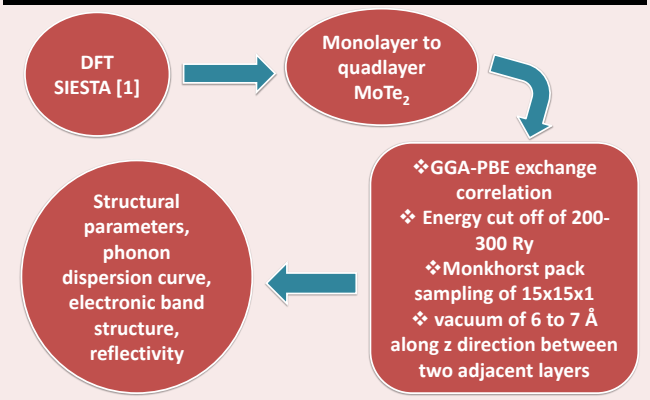

RESULTS

➢ $MoTe_2$ monolayer has 2D honeycomb like structure.
➢Monolayer to quadlayer $MoTe_2$ has semiconductor character with decreased band gap.

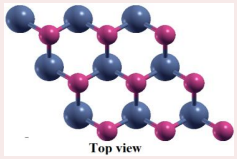

Material		a (Å)	Exp. a (Å)	d_{Mo-X} (Å)	d_{X-X} (Å)	θ_{X-Mo-X} (degree)	E_c (eV/atom)
$MoTe_2$	**Present**	**3.600**	3.522	**2.766**	**3.656**	**82.69**	**-2.05**
	Ref. [1]	3.56	[2]	2.73	3.60	-	-3.71

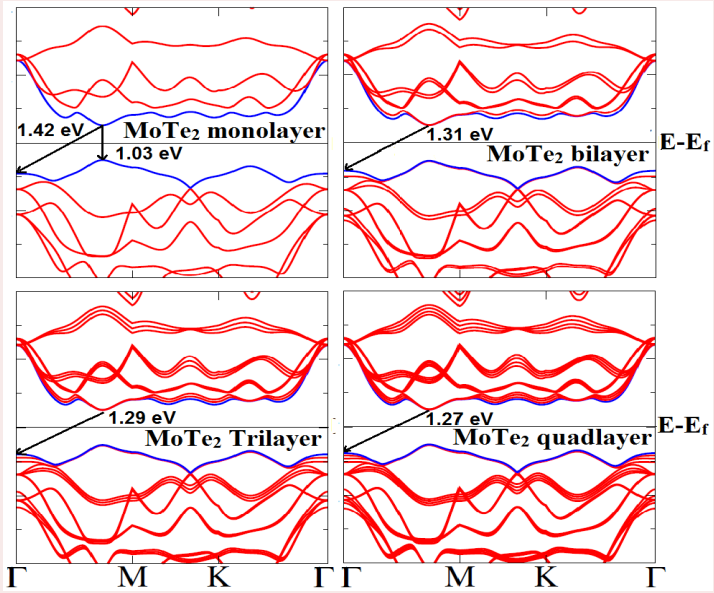

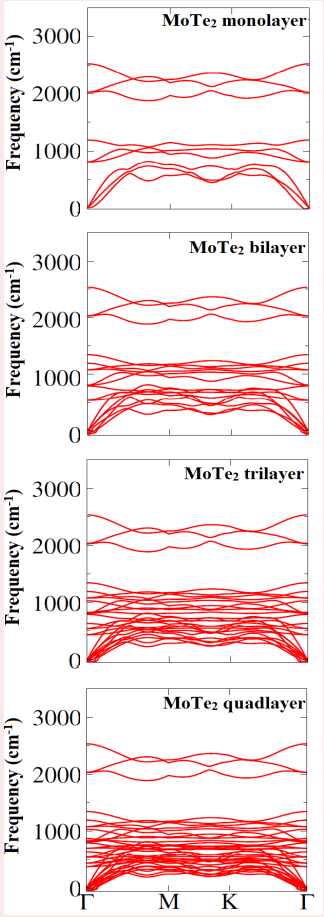

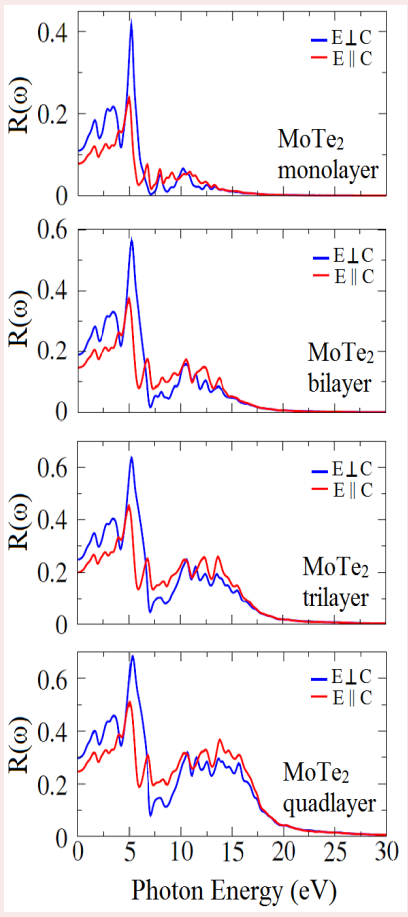

Fig. Electronic band structure and phonon dispersion surves along the high symmetrical direction in the Brillouin zone and Reflectivity R(ω) of layered $MoTe_2$

EXECUTIVE SUMMARY

➢The semiconducting behavior of layered $MoTe_2$ is observed with decrease in band gap with increase in the number of layers due to quantum confinement effect.
➢Layered $MoTe_2$ may be used in selective transmission of higher frequency range due to the frequency gap between lower and high and low frequency optical mode.
➢Reflectance up to 68% is seen for quadlayer $MoTe_2$ and so it is used as antireflection coating in UV-C region and hot mirror material of ultrathin reflectors also.

REFERENCES

1. J. M. Soler, E. Artacho, J. D. Gale, A. García, J. Junquera, P. Ordejón, and D. Sánchez-Portal, The SIESTA method for ab initio order-N materials simulation, *J. Phys. Condens. Matter* 14(11) (2002) 2745.
2. Lahourpour, F., Boochani, A., Parhizgar, S. S., & Elahi, S. M. (2019). Structural, electronic and optical properties of graphene-like nano-layers MoX_2 (X: S, Se, Te): DFT study. *Journal of Theoretical and Applied Physics*, 13(3), 191-201.
3. T. Böker, R. Severin, A. Müller, C. Janowitz, R. Manzke, D. Voß, P. Krüger, A. Mazur and J. Pollmann, Band structure of MoS_2, $MoSe_2$, and α−$MoTe_2$: Angle-resolved photoelectron spectroscopy and ab initio calculations, *Phys. Rev. B 64*(23) (2001) 235305.

ACKNOWLEDGEMENT

Support under DST-FIST Level-I , DRS-SAP-I and DRS-II SAP programmes are highly acknowledged.

P17

State-to-state inelastic rate coefficients of phosphine in collision with He at low to moderate temperature

Ayda Badri, Faouzi Najar, Cheikh T. Bop, Nejm-Eddine Jaidane and Majdi Hochlaf

Laboratoire de Spectroscopie Atomique Moléculaire et Applications- Université de Tunis El Manar- Faculté des Sciences de Tunis.

Laboratoire Modelisation et Simulation Multi Echelle, MSME UMR 8208 CNRS, 5 bd Descartes, 77454 Marne-la-Vallée, France.

LOMC–UMR 6294 CNRS, Université du havre, 25 rue Philippe Lebon, BP 1123, F-76063 Le Havre, France

Abstract: The 3D-PES was worked out by means of the standard coupled cluster with single, double and non-iterative triple excitation approach, in conjunction with the aug-cc-pVQZ basis set and complemented by mid bond functions. This 3D-PES presents a well of 34.92 cm −1 at {R, θ , phi}= {5.76a 0 , 90, 60}. Afterwards, we incorporated this 3D-PES into time-independent close-coupling quantum dynamical computations to derive the inelastic cross-sections of rotational excitation of (o)p-PH 3 after collision with He up to (1000) 500 cm −1. Subsequently, we evaluated the rate coefficients for temperatures up to (100 K) 50 K populating the (41)42 low-lying rotational levels of (ortho-) para-PH3 .These data were derived by averaging the cross-sections thermally over the Maxwell–Boltzmann velocity distribution. No general propensity rules are found. We also performed a comparison with the rates for NH3 –He. Our results should be of great help in determining accurate PH3 abundances and, more generally, constraining the interstellar PH3.

RESULTS

A. Cross-sections

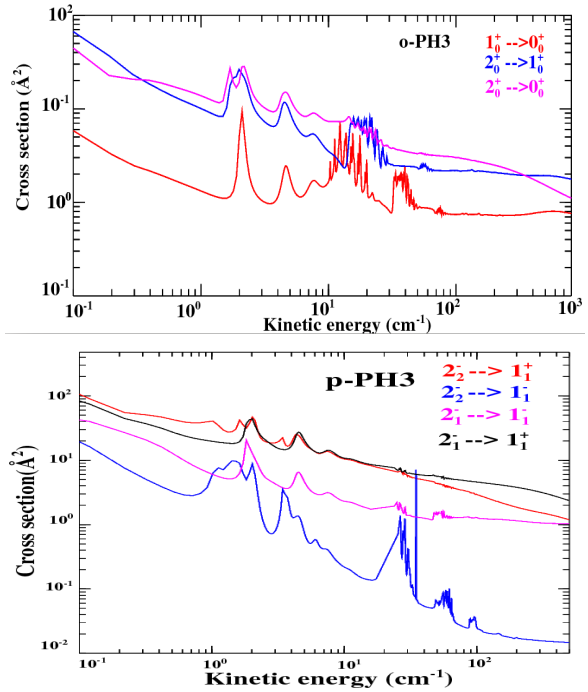

Figure1 : Inelastic cross-sections of o-PH3 , induced by collision with He

The cross-sections of ortho-PH 3 covering the range 9–1000 cm−1 allow us to generate the velocity coefficient for the transitions between the 41 low-lying rotational levels [up to j k = 10 0] for temperatures up to 100 K. Similary, the cross-sections of para-PH 3 covering the range 8.4–500 cm −1 allow us to generate the velocity coefficient for the transitions between the 41 low-lying rotational levels [up to j k = 7 1] for temperatures up to 50 K.

B.Rate coefficients

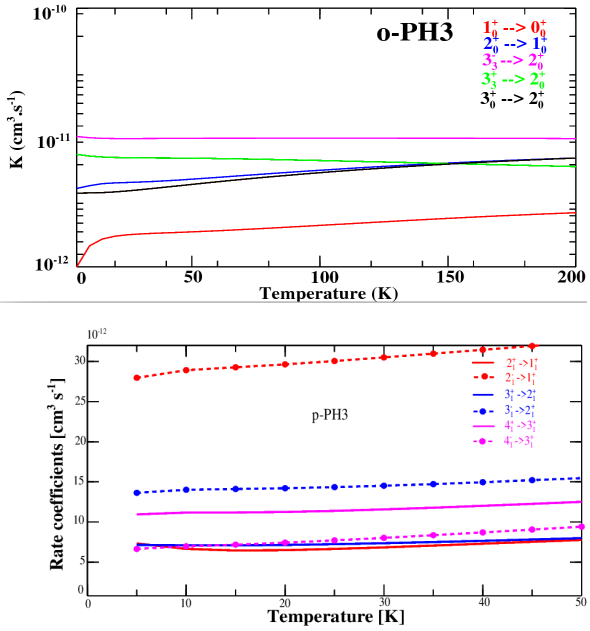

Figure 2: Inelastic cross-sections of p-PH 3 induced by collision with He versus kinetic energy

The The rate coefficients computed in this work were compared with those of Machin & Roueff (2005) for the NH3-He system, which is used to estimate the abundances of phosphine. Large differences are noticed.

Conclusion: The rate coefficients computed in this work were compared with those of Machin & Roueff (2005) for the NH 3 –He system, which is used to estimate the abundances of phosphine. Large differences are noticed, especially at low temperatures. Therefore, the results obtained in this work may be of great help to the astrophysical community, in order to model the physical conditions of media where phosphine was observed. Indeed, exact knowledge of the PH 3 abundance may be a clue to constrain the chemistry of interstellar phosphorus. In addition, the present data may help in the identification of PH3 in astrophysical media where other P-containing molecules were detected, e.g. in massive dense cores (Fontani et al. 2016) or the Galactic Centre (Rivilla et al. 2018).

References:

[1] Bouhafs N., Rist C., Daniel F., Dumouchel F., Lique F., Wiesenfeld L., Faure A., 2017, MNRAS, 470, 2204

[2] Agúndez M., Cernicharo J., Guélin M., 2007, ApJ, 662, L91.

[3] Machin L., Roueff E., 2005, Journal of Physics B: Atomic, Molecular and Optical Physics, 38, 1519

[4] Hutson J., Green S., 1994, Collaborative computational project Jiménez-Serra I., Viti S., Quénard D., Holdship J., 2018, ApJ, 862, 128

Contact:ayda.badri@fst.utm.tn

P18

Combinatorial search for efficient HER catalyst

Recent experiments showed that some layered ternary transition metal trichalcogenide compounds are efficient catalysts for the hydrogen evolution reaction (HER). Motivated by these, we have combinatorially designed and computationally screened, through an efficient, automated approach based on density functional theory, single layers of such compounds, including those not reported in widely used crystal structure database like the International Crystal Structure Database (ICSD), for their efficiency as HER catalysts. On the basis of our theoretical prediction of overpotentials determined from the reaction coordinate mapping corresponding to the HER mechanism, 13 of these compounds are found to be promising catalysts, out of which three are suggested to be as efficient as platinum, the best known HER catalyst to date.

P19

Identifying materials with charge-spin physics from first principles calculations

We present a quantity termed charge-spin susceptibility, which measures the charge response to spin degrees of freedom in strongly correlated materials. This quantity is simple to evaluate using both standard density functional theory and many-body electronic structure techniques, enabling comparison between different levels of theory. A benchmark on 28 layered magnetic materials shows that large values of charge-spin susceptibility correlate with unconventional ground states such as disordered magnets and unconventional superconductivity.

P20

Beyond-DFT Studies for Thiophene and Furan Oligomers

V. Alves-Bastos, T. J. da Silva and M. J. Caldas
Institute of Physics, University of São Paulo, Brazil

Combined Thiophene and Furan oligomers are an emerging class of pi-conjugated materials, relevant in particular for optoelectronic applications. Indeed structures formed by these materials can show enhanced properties [1], combining qualities of both systems. In this work, we compare properties of dimers of Thiophene (2T), Furan (2F) and Thiophene-Furan (Thienylfuran/TF), basic units to form more complex copolymers. We study structural and electronic properties adopting ab-initio calculations including many-body GW corrections on top of hybrid DFT+HF [2,3]. In terms of structural results we find that 2T adopts a non planar antiparallel configuration (as well known), however 2F and TF tend to be antiparallel but planar, as a consequence of the atomic effective repulsion sulfur-hydrogen and attraction oxygen-hydrogen in the molecules. We find that the HOMO charge distribution for 2T, 2F and TF are very similar, justifying the similar Ionization Potential values seen in the experimental results [4], and confirmed by our GW results. These similarities apply also to the LUMO states. We will discuss also the optical properties [5], which include other occupied and unoccupied states, focusing mostly on the TF molecule.

[1] A. E. Steen et al., J. Phys. Chem. C, 123, 15176 (2019); [2] M. Pinheiro Jr et al., Phys. Rev. B, 92, 195134 (2015); [3] V. Blum et al., Comput. Phys. Commun., 180, 2175 (2009); [4] I. Novak et al., J. Electron Spectrosc., 61, 177 (1992); [5] C. Liu et al., J. Chem. Phys. 152, 044105 (2020).

The authors thank LCCA-USP, and CNPq, FAPESP, CAPES via INCT-INEO.

P21

DFT Study of structural, electronic and magnetic properties of CuCrSnS4

In the crystallographic spinel structure, first solved by Bragg in 1915, the cations occupy 1/8 of the tetrahedral (A) and 1/2 of the octahedral (B) voids within the face-centred cubic (fcc)-lattice formed by the X anions. Interesting physics arises, when the B-site cations become mixed in valence. As the cations show different site preferences, by choosing the appropriate atoms it is possible to realize a selective magnetic dilution in one of the two sublattices. In the pseudo-binary systems CuCrS2-MS2 (M=Ti, Sn), spinel phases of the composition Cu2xCr2xM2-2xS4 have been discovered. The experimental evidence, to date, indicates that the Cu2xCr2xM2-2xS4 spinels are spin-glasses. These systems are very sensitive to the methods of preparation and deviations from stoichiometry. This effect was discussed with respect to a deficiency and excess of cations in tetrahedral or octahedral voids of the spinel structure. In this series, when the stoichiometric composition is passed through as 2x increases, drastic changes occur in (i) the electric resistivity: the activation energy drops, (ii) magnetic susceptibility: the Curie–Weiss temperature yp changes from negative to positive values, Contents lists available at which indicates that additional ferromagnetic couplings appear. Although there are numerous data available for powder materials, the studies of the effect of nonmagnetic Zr4+ substituted for Cr3+ atoms on the properties of the spinel structure are inconsistent. This raises the question about the proper location of the Zr ions and the metal excess of Cu in the spinel structre. We focus on the corresponding compounds CuCrZrSe4 and CuCrSnS4 to study

P23

Understanding site-dependence overall water splitting mechanism for energetically stable bilayer heptazine g-C_3N_4

B.R. Bhagat*, Kishan H. Mali and Alpa Dashora

Computational Material Science Laboratory, Department of Physics,

The M. S. University of Baroda, Vadodara 390002, India

** Email: bhagatbrajesh1996@gmail.com*

Among various allotropes of graphitic carbon nitride (g-C_3N_4), its heptazine planer sheets with modified layer orientation to relax N-2p and C-2p orbitals forces of bilayer to achieve least energy state is being considered for the study of oxygen/hydrogen evolution reaction (OER/HER) mechanism with intermediate adsorbed at different sites using Quantum ESPRESSO [1] code. Higher electron mobility than of holes decreases the rate of recombination and higher redox potential decides suitability of designed bilayer for photocatalytic activity. Lower oxidative overpotential than the monolayer (1.56 eV [2]) with efficient reduction overpotential which again decreased on addition of water molecule resulting from the separation of excitons at the energy disordered sites and interfacial charge transport makes it suitable for overall water splitting. Whereas, increase in overpotential when adsorption of intermediates are performed on both side of bilayer imply effect of van der Waals interaction on triplet exciton generation showing its applicability as coating material. Therefore, understanding of many body perturbative methods with excitons dynamics and time-dependent DFT methods will be convenient to analyse their respective roles.

[1] P. Giannozzi et al., J. Phys.: Condens. Matter, **21**, 395502 (2009).

[2] J. Wirth et al., Phys. Chem. Chem. Phys., **16**, 15917 (2014).

P24

'Ab initio' studies of structural and electronic propoerties of orthorombic layered crystals

The research covered ‘ab initio’ computational studies of Van der Walls orthorombic crystals, these are the transition metal monochalcogenides TMM (GeSe, GeS, GeTe, SnSe ans SnS). Preliminary steps included structures optimization joined with the study of the effect of various vdW corrections. Subsequently, calculations revealed band structures of bulk crystals and monolayers. In case of bulks the direct and the indirect band gaps were determined. Calculations for monolayers were only qualitative. Moreover, the matrix elements of momentum operator for bulks were calculated to determine the polarization of optical transitions. Furthermore, orbital contributions of transition metals and chalcogenides on the band structures were determined. Additionally, hydrostatic pressure was applied to bulk systems so as to evaluate the pressure coefficients of direct and indirect optical transitions. In conclusion, many of previously reported properties of TMM were confirmed. These include linear polarization dependence of optical transitions in band structure which stems from spacial geometry of a unit cell, band splitting on zigzag direction in case of monolayers which stems from symmetry breaking, and band structure dependence on hydrostatic pressure.

P25

Excitonic effects in C3N

Monolayer C3N is a two-dimensional indirect band gap semiconductor with emerging mechanical, thermal and electronic properties. In this work we present a full characterization of C$_3$N electronic and dielectric properties, focusing on the so-called momentum-resolved exciton band structure. The study is performed using the GW+BSE approach for finite momentum transfer, as implemented in the Yambo code. Excitation energies and oscillator strengths are computed in order to characterize bright and dark states. Activation of excitonic states is observed for finite transferred momentum. We find an indirect excitonic band gap of 0.7 eV, significantly lower than the direct optical band gap of 1.86 eV. Excitonic binding energies ranging from 0.5 eV to 0.9 eV for the lowest excitonic states, are indicative of strongly bound excitons. Excitonic wavefunctions are discussed with respect to the crystal symmetries.

P26

Efficient and low-scaling linear-response time-dependentdensity functional theory implementation for core-level spectroscopy of large and periodic systems

We present our implementation of linear-response time-dependent density functional theory (LR-TDDFT) for core level near-edge absorption spectroscopy. The method is based on established LR-TDDFT approaches to X-ray absorption spectroscopy (XAS) with additional accurate approximations for increased efficiency. We demonstrate that the method is suitable for extended systems in periodic boundary conditions and measure a favorable sub-cubic scaling of the calculation cost with system size.

P27

A simple approximation to the electron–phonon interaction in population dynamics

One alternative to include a quantum description of the nuclear degrees of freedom for the modeling of coupled electron–ion dynamics is provided by the kinetic model for electron–phonon interaction. This model provides an efficient approach for systems evolving with low amplitude fluctuations, in a quasi-stationary state. In this work, we propose an extension of the kinetic model to include the effect of coherences, which are absent in the original approach. The new scheme, referred to as Liouville–von Neumann + Kinetic Equation (or LvN + KE), was implemented in the context of a tight-binding Hamiltonian and employed to model the broadening, caused by the nuclear vibrations, of the electronic absorption bands of an atomic wire. The results show close agreement with the predictions given by Fermi's golden rule (FGR), which serve as a validation. The method was also applied to the electron–phonon interaction in transport simulations, adopting to this end the driven Liouville–von Neumann equation to model open quantum boundaries. In this case, the LvN + KE model qualitatively captures the Joule heating effect and Ohm's law.

P28

Investigation of local magnetic properties in metallic multilayered systems

Recently, the field of nanomagnetism has turned to the understanding of the formation, profiles, and physical properties of domain walls (DWs) due to its use in technological applications [1,2]. For instance, controlling DWs motions can be used on magnetic recording devices. In this context, the information can be interpreted via the DWs motion [1], which replaces the physical rotation of a hard disk. Here, we investigate the magnetic properties of the Co/Irn/Pt(111) (n = 0, 1, 2) and Ni/Irn/Pt(111) (n = 0, 1, 2) systems, aiming to inspect the formation and profiles of DWs. We focus on the analysis of the local magnetic moment, exchange interaction (Jij) and Dzyaloshinskii-Moriya interaction (DMI). The Real Space – Linear Muffin-Tin Orbital within the Atomic Sphere Approximation (RS-LMTO-ASA) method [3], in addition to the Local Spin Density Approximation (LSDA) [4] functional, is used in order to perform electronic structure calculations. The magnetic chirality is discussed in the light of a theory where the DMI and the exchange coupling parameter (Jij) can be calculated using first principles calculations, as implemented in the RS-LMTO-ASA [5]. References [1] S. S. P. Parkin et al., Science 320, 190 (2008). [2] S. Emori et al., Nat. Mater. 12, 611 (2013). [3] S. Frota-Pessôa, Phys. Rev. B 46, 14570 (1992). [4] U. von Barth et al., J. Phys. C 5, 1629 (1972). [5] R. Cardias et al., Sci. Rep. 10, 20339 (2020). Funding Acknowledgement: This work has been supported by CNPq, CAPES and FAPESP.

P29

Anharmonic calculations of vibrational spectra for molecular adsorbates: A divide-and-conquer semiclassical molecular dynamics approach

A theoretical investigation of vibrational properties of molecular adsorbates can help in understanding a large variety of phenomena, including surface catalysis. In the present work we aim in overcoming the harmonic approximation by accounting not only anarmonicities, but also quantum nuclear effects, such as overtones and combination bands. We achieve this objective by extending to the adsorption problem the divide-and-conquer semiclassical molecular dynamics approach [1], which already revealed successfully in describing vibrational levels in molecular systems. Relying on a standard Born-Oppenheimer classical trajectory of the full dimensional surface adsorbate system, we propagate at the semiclassical level only the adsorbate modes and few coupled surface ones. In this way, while containing the computational effort, we are able to obtain spectra which accounts for the effects coming from the molecular-surface interaction. We test our approach on CO, NO and H2O adsorbed on TiO2 Anatase(101), comparing our semiclassical results against the harmonic estimate and the classical power spectra computed on top on the same trajectory used for the semiclassical simulations [2]. [1] M. Ceotto, et al., Phys. Rev. Lett. 119, 010401 (2017) [2] M. Cazzaniga, et al., J. Chem. Phys. 152, 104104 (2020)

P30

Benchmarking SCAN functional for two-dimensional crystal structures

It has recently been reported that the strongly constrained and appropriately normed (SCAN) meta-GGA functional has performed exceptionally well for density functional theory (DFT) calculations involving molecular and crystalline systems. In addition, the computational cost of SCAN is argued to be much less than that of the highly demanding hybrid functional methods with comparable accuracy. SCAN has been applied to several three-dimensional systems, but has not been widely used for two-dimensional materials such as transition metal (M) monochalcogenides (MX), M dichalcogenides (MX2), and M trichalcogenides (MX3). In this study, we provide a comprehensive set of data obtained by SCAN, hybrid functionals (HSE), and PBE. Specifically, we compare lattice constants, band gaps, electronic/thermal transport and magnetic properties, and computational cost. We also study optical properties with GW approximation, using DFT orbitals obtained from SCAN and PBE. Our goal is to benchmark results from SCAN, PBE, HSE, PBE+GW, and SCAN+GW and to create a detailed picture of how SCAN performs compared to other well established DFT functionals. This work is the terminal paper for benchmarking different DFT functionals and will guide further theoretical studies involving 2D materials

P31

z-dependent spin-momentum locking in monolayer 1T'-WTe2

Monolayer 1T’-WTe2 is a quantum spin Hall insulator with a well-defined bulk gap and helical edge states. It has been predicted to undergo a topological phase transition upon breaking the inversion symmetry with gating [1]. Recent scanning tunneling microscopy (STM) experiments by Maximenko et. al. have found a surprising linear dependence of the gap on gating voltage. We present computational results of the electronic structure of monolayer 1T’-WTe2 with the effect of gating, using a tight-binding model derived from the Wannierised Kohn-Sham orbitals computed from density functional theory. We find that the top and bottom surfaces of the monolayer 1T’-WTe2 exhibit opposite spin-momentum locking properties. This effect causes the STM measured gap to show a linear response upon gating. [1] Zhang, Yang, et al. "Electrically tuneable nonlinear anomalous Hall effect in two-dimensional transition-metal dichalcogenides WTe2 and MoTe2." 2D Materials 5.4 (2018): 044001.

P32

A unified formalism for spectral and thermodynamic calculations in MBPT and its application to the HEG

Accurate predictions of Angle-resolved photo-emission spectroscopy (ARPES) experiments have been the center of great theoretical effort since the mid ‘50s. Many-body perturbation theory (MBPT) has been extensively used to predict material spectra for extended systems where ground-state theories are often not reliable (e.g. band-gap problem). The knowledge of the one-particle Green's function (GF) grants access to thermodynamic quantities such as the number of particle or the electronic total energy as well as spectral quantities e.g. the diagonal part of the spectral function (SF) as the outcome of an ARPES experiment. While this in true in principle, in practice spectral and thermodynamic calculations differ by methodology and numerical implementation. Here we present the sum-over-poles (SOP) formalism, able provide calculation of accurate thermodynamic quantities as well as material spectra among other advantages (see below). Propagators will be expanded in frequency as sum-over-poles (SOP) which will provide for the analytic calculation of thermodynamic quantities (using the momenta of the GF), convolutions (using Cauchy residue formula) and the Dyson inversion (using the so-called algorithmic inversion). We apply the methodology to the test case of the homogeneous electron gas (HEG) in the GW approximation at rs=4.

P33

INVESTIGATION OF ELECTRONIC, STRUCTURAL AND MECHANICAL PROPERTIES OF FeMnP 1-x A x (A=Si,Ga,Ge ; and) AS A POTENTIAL MAGNETOCALORIC REFRIGERANT ALLOY

Exhaustive ab initio calculations within the GGA are carried out to identify possible Fe 2 P-type giant magnetocaloric FeMnP 1-x Si x alloys. The calculated elastic constants confirm the mechanical stability for the Fe 2 P-type hexagonal FeMnP 1-x Si x at (and) alloys in both FM and AFM phases. The predicted elastic properties for FeMnP 0.67 Si 0.33 are close to those obtained for FeMnP 0.67 Ga 0.33 and FeMnP 0.66 Ge 0.33 using the same calculation scheme. The electronic density of states confirms that the FeMnP 0.67 Si 0.33 alloys have similar electronic structures to those of FeMnP 0.67 Ga 0.33 and FeMnP 0.66 Ge 0.33 . The results predict that FeMnP 0.67 Ga 0.33 is the best candidate refrigerant for room temperature magnetic refrigeration because of its high ductility during phase transition from ferromagnetic (FM) to AFM phase. On substituting Mn element in the 3g site with the Re element, ductility was acquired in all the three alloys that is FeMn 1-x Re x P 1-x A x (A= Si, Ga, Ge) alloys, making the alloys best refrigerants at room temperature.

P34

Redefining the phase diagram of carbon dioxide within the quasi-harmonic approximation

B. H. Cogollo-Olivo[1], S. Biswas[2], S. Scandolo[3] and J. A. Montoya[1]

[1]University of Cartagena, Colombia
[2]Goethe University Frankfurt, Germany
[3]The Abdus Salam ICTP, Italy

* bcogolloo@unicartagena.edu.co

The experimental study of the CO_2 phase diagram is hampered by strong kinetic effects leading to wide regions of metastability and to large uncertainties in the location of phase boundaries. Here we determine the CO_2 phase boundaries by means of ab-initio calculations of the Gibbs free energy of several molecular and non-molecular solid phases of CO_2. Temperature effects are included in the quasi-harmonic approximation. Contrary to previous results, we find that the boundary between non-molecular phases and phase V has a positive slope and starts at 21.5 GPa at T = 0 K. A triple point between phase IV, V, and the liquid phase is found at 35 GPa and 1600 K, indicating a broader region of stability for the non-molecular phases than previously thought. The experimentally determined boundary line between CO_2-II and CO_2-IV is reproduced by our calculations, indicating that kinetic effects are not relevant in that transition.

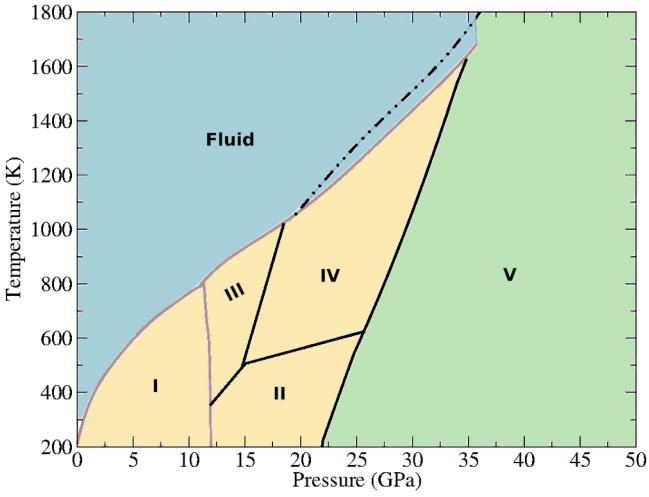

Fig. 1. Theoretical phase diagram for carbon dioxide at high pressure and temperature.

Acknowledgments: We acknowledge the ISCRA program of CINECA for provision of computational time under proposal HP10CVCDOB. B.H.C-O thanks COLCIENCIAS for a graduate scholarship and the support from the ICTP STEP programme. B.H.C-O and J.A.M. also thank the Vicerrectoría de Investigaciones of the Universidad de Cartagena, for the support through internal grants.

[1] B. H. Cogollo-Olivo et al., Phys. Rev. Lett. 124, 095701 (2020).
[2] M. Santoro et al., J. Chem. Phys. 181, 2780 (2004).
[3] M. Santoro and F. Gorelli, Phys. Rev. B 80, 184109 (2009)
[4] F. Datchi et al., Phys. Rev. B 94, 014201 (2016).

Keywords: carbon dioxide, high-pressure, DFT.

P35

XANESSimulations in Diamond-Like Two-Dimensional Material

In 2004 a new era on the searching for better-performance materials had given its jumpstart with the emergence of the thinnest material ever synthesized: the well-known graphene. Since then, many atomic-sized materials have been obtained from layered bulk materials and successfully characterized by many methods, including x-ray absorption spectroscopy (XAS). A few years ago, such a technique was employed to study bulk diamond-like materials, as well as graphite, in order to better characterize these sp2/sp3 bonded materials. Recently, researchers from Minas Gerais, Brazil, have theoretically and experimentally studied the formation and stabilization of diamondol, a 2D hydroxylated diamond-like layer, which arises from pressure-dependent charge injection on bi-, and multilayer graphene in a controlled ambient environment using scanning probe microscopy (SPM) along with electric force microscopy (EFM) measurements. Bearing that in mind, we have theoretically investigated sp2 and sp3 carbon-based materials through Density Functional Theory calculations and XANES (X-ray Near-Edge Spectroscopy) simulations. Diamondol, in turn, is composed of a mixture of sp2 and sp3 carbon bonding, and our simulations have shown that XANES may be an excellent way to characterize this kind of material.

P36

Pure and B/ N doped Graphdiyne as a nano reactor for ORR, a competitor for Platinum: A first principles study

The electrocatalytic activities of ABA stacked trilayer graphdiyne (Gdy) and its B/N doped configurations to carry out oxygen reduction reaction in their interlayer spacing are investigated through extensive first principles calculations. The rule of layer-wise B doping was found to be dependent on the orientation of the layers as B being electron deficient compared to C, prefers to substitute C atoms in closed-surroundings reducing the interlayer electrostatic repulsion. No such dependency was found for electron rich N doping. The diffusion of O2 molecules through the pores of the top layer was found to be highly feasible with low activation barrier of ~0.8 eV for all the configurations. Subsequent O2 adsorption was found to be feasible on both the pure/doped configurations in a dissociative manner on the two sp hybridized C atoms in the middle of the acetylene linkage except for B doped cases in which B-O-C epoxy configuration was found to be stable as an effect of back-donation interaction. Overall, O2 adsorption was found to be stronger in closed-surroundings as the thus formed dangling bonds find a way to saturate themselves via interlayer sigma bond unlike open-surroundings. Analysis of rest of the reaction pathway in terms of free energy reveals pristine and B doped Gdy to be excellent electrocatalyst for ORR with overpotential values less than 0.3 eV. The moderate binding of all the reaction intermediates on the catalyst surface as also described by an isolated descriptor and COHP analysis plays the key role for their high efficiency towards ORR.

P37

Enhanced Hydrogen Evolution Activity at the Edges of $MPSe_3$ (M=Mn, Fe) Tri-chalcogenide Layers

Tisita Das,[a,$] Khorsed Alam,[a] Sudip Chakraborty,[b] and Prasenjit Sen*[,a]

[a]*Harish-Chandra Research Institute, HBNI, Chhatnag Road, Jhunsi, Allahabad 211019, India*
[b] *Discipline of Physics, Indian Institute of Technology (IIT) Indore, Simrol, Indore 453552, India*
[$] Presenting Autor's Email: tisitadas@gmail.com

In this work we have investigated the hydrogen evolution reaction (HER) catalytic activity of two $MPSe_3$ (M: Mn, Fe) nano-ribbons with selected edge sites using first-principles density functional theory (DFT) based electronic structure calculations. Both these materials belong to the layered metal phosphite tri-chalcogenides family. In a very recent experiment[1], Gusmão et al. studied the HER activity of a series of these $MPSe_3$ bulk compounds among which $FePSe_3$, followed by $MnPSe_3$ showed the best efficiency, next to Pt (the best known HER catalyst till date), among their considered systems. On the other hand, in our earlier work,[2] we screened a large number of ternary transition metal tri-chalcogenide monolayers to study their hydrogen evolution activity on the corresponding basal planes, through determination of the hydrogen adsorption free energy (ΔG_{H^*}). At the end of our screening we found that both $FePSe_3$ and $MnPSe_3$ have quite large ΔG_{H^*} values indicating that these are not at all good catalysts for HER. This apparent discrepancy may have been caused by the fact that we adsorbed hydrogen only on the basal plane. There are materials (e.g. MoS_2 monolayer) where the basal planes are not active but the edge sites show efficient catalytic activity. This could be the case in our systems also. Therefore, to resolve this discrepancy, and to have a deeper understanding, we have studied catalytic activity of the edge sites of single layers of these materials.[3]

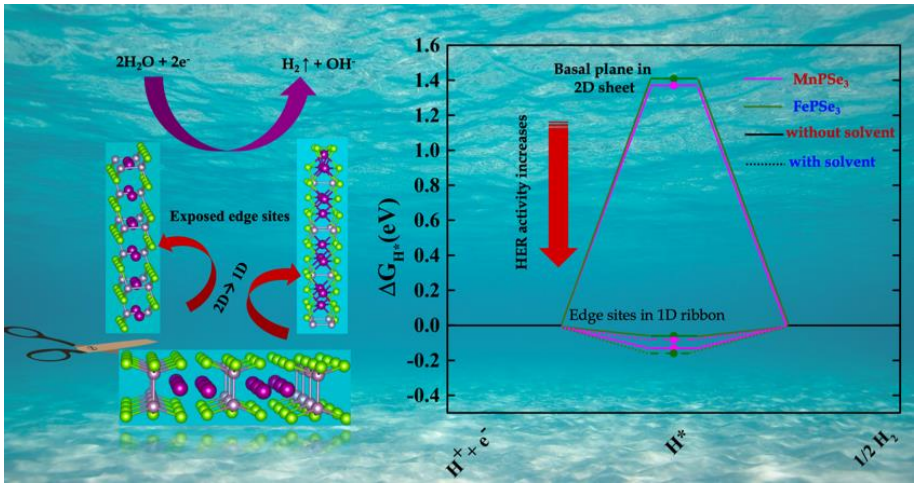

Different edges are exposed by constructing several nanoribbons from the corresponding monolayer. Thereafter, the stable most ribbon structures are considered for further investigation of their HER activity. The HER catalytic activity has been predicted through determination of the ΔG_{H^*} both with and without solvation effect. During this activity prediction, we have also explored the hydrogen coverage dependency. Based on Nørskov's approach of reaction coordinate mapping, we have envisaged the HER active edges for these two compounds while successfully addressing the correspondence between the experimental observation and theoretical prediction. From our DFT calculations it has been observed that the free energy of hydrogen adsorbed on the edge sites are much lower from our previously calculated values suggesting the edges as catalytically active regions in these materials.

References

1. R. Gusmão, Z. Sofer, D. Sedmidubský, Š. Huber and M. Pumera, *ACS Catalysis*, 2017, **7**, 8159–8170.
2. P. Sen, K. Alam, T. Das, R. Banerjee and S. Chakraborty, *The Journal of Physical Chemistry Letters*, 2020, **11**, 3192–3197.
3. Tisita Das, Khorsed Alam, Sudip Chakraborty and Prasenjit Sen, *Preprint*.

P38

Group Theory Analysis to Study Phase Transitions of Sr3Hf2O7

We present an ab-initio study performed by means of Density Functional Theory (DFT), group-subgroup symmetry analysis and lattice dynamics to probe the properties of the octahedral distortions, which occur during the structural phase transitions. Specifically, we focus our study on the Sr3Hf2O7 (SHO) system, which is characterized by a high-temperature I4/mmm (S.G. 139) centrosymmetric structure and a ground-state Cmc21 (S.G. 36) ferroelectric system. We have probed potential candidate phases that may form the I4/mmm → Cmc21 transition pathways, namely Fmm2 (S.G. 42), Ccce (S.G.68), Cmca (S.G. 64) and Cmcm (S.G. 63). We found that the band gap widths increase as the symmetry of the systems decreases, with the ground-state structure presenting the largest gap width (~5.95 eV). By probing the Partial Density of States (PDoS), we observe a direct relation regarding the tilts and rotations of the O perovskite cages as the transition occurs; these show large variations mostly of the O p-states which contribute mostly to the valence band maximum. Moreover, by observing the hyperfine parameters, namely the Electric Field Gradients (EFG) and asymmetric parameters, these vary as the transition occurs, and where the potential phase identification is demonstrated. We have also computed the macroscopic polarization and confirm that the Cmc21 phase is ferroelectric with a value of spontaneous polarization of 0.0478 C/m2. The ferroelectricity of the ground-state Cmc21 system arises due to a second order parameter related to the coupling of the rotation and tilts of the O perovskite cages together with the Sr displacements.

P39

Title: Understanding the curious magnetic state of Sr_3OsO_6

Name: Shreya Das[1], Anita Halder[1], Atasi Chakraborty[2], Prof. Indra Dasgupta[2] & Prof. Tanusri Saha-Dasgupta[1]

1. S. N. Bose Centre, Salt Lake, Kolkata.
2. Indian Association for the Cultivation of Science, Jadavpur, Kolkata.

Abstract:

Perovskites with general chemical formula ABO_3 (A = divalent alkaline/ trivalent rare-earth metal, B = transition metal) are well studied materials due to their wide variety in physical, chemical and magnetic properties. In recent years emphasis is put on the case of B site substituted perovskite oxides, namely double perovskites, $A_2BB'O_6$, due to their various interesting properties and possible applications [1].

Recently a ferromagnetic (FM) insulating compound Sr_3OsO_6 is reported with high T_C value of 1000K [2]. This is unusual since in general most of the ferromagneric compounds are known to be metal or half metal, and not insulator. Also, few ferromagnetic insulators known so far are low T_C materials, not high T_C. Here we have studied this curious behavior by employing first-principles calculations in conjunction with exact diagonalization of the full t_{2g} multiplet problem of two Os sites. Our analysis highlights the fact that stabilization of Sr_3OsO_6 in the cubic phase in epitaxially grown thin film is the key to both ferromagnetic correlation and the high-temperature scale associated with it. It also provides a natural explanation for why the sister compound Ca_3OsO_6, exhibits low-T_N antiferromagnetism in its monoclinic structure. We also uncover the origin of insulating behavior of ferromagnetic Sr_3OsO_6, which is found to be driven by the opening of a Mott gap in the half-filled spin-orbit coupled j = 3/2 manifold of d^2 Os. We thus conclude the registry to $SrTiO_3$ substrate is responsible for counter-intuitive stabilization of Sr_3OsO_6 in cubic phase, and key to its ferromagnetism.

References:

1. S. Vasala, M. Karppinen, Progress in Solid State Chemistry 43 (2015) 1-36.
2. Y. K. Wakabayashi et al., Nature Communications, 2019, 10.1038/s41467-019-08440-6.
3. Shreya Das, Anita Halder, Atasi Chakraborty, Indra Dasgupta, and Tanusri Saha-Dasgupta, Phys. Rev. B 101, 184422 (2020).

P40

Machine learning materials properties for small datasets

Pierre-Paul De Breuck, Geoffroy Hautier, Gian-Marco Rignanese

Institute of Condensed Matter and Nanosciences (IMCN), UCLouvain, 1348 Louvain-la-Neuve, Belgium

pierre-paul.debreuck@uclouvain.be

Background

- Machine Learning enables the prediction of any material property almost instantaneously, speeding up material discovery and design.
- Current models which have good accuracy can be categorized as:

Model	Any crystal type	Any property	Required data size
Ad-hoc	No	No	> 100
Deep graph	Yes	Yes	> 10 000

Ad-hoc: case per case study, targeted on a specific group of materials and a specific property, with hand-tailored descriptors and prior-knowledge.

Deep graph: based on deep convolutional neural networks, by representing the crystal as a graph.

- MODNet (this work) bridges the gap between these two categories by proposing a universal framework, with good accuracy on small datasets.

Usecases: band gaps within GW (80 materials), lattice thermal conductivity (101 materials), vibrational thermodynamics (1245 materials), most experimental properties, etc.

Methods

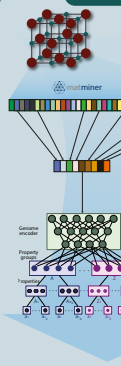

1. Feature generation A huge feature space is generated with matminer: they describe the crystal in terms of physical, chemical and geometrical properties. Compared to graph learning, these features contain preprocessed knowledge based on meaningful features.

2. Feature selection Not all features are useful. Too many features give rise to the curse of dimensionality. Features are chosen iteratively such that the next feature f has the highest $RR(f)$ score:

$$RR(f) = \frac{NMI(f,y)}{\left[\max_{f_s \in \mathcal{F}_s}\left(NMI(f,f_s)\right)\right]^p + c}$$

with y the target, $\mathcal{F}_s$ the current feature set and (p, c) two parameters determining the balance between redundancy and relevance.
The normalized mutual information (NMI) is bounded between 0 and 1 and provides a measure of any relation between two random variables X and Y. It goes beyond the Pearson correlation by taking any relation into account.

3. Joint Transfer Learning Possibility to learn on multiple properties. A neural network with a tree like architecture is used: depending on the similarity between properties, layers are shared among them. Successive blocks encode and decode the materials representation, each time getting more specific to the final property.

By learning properties together, knowledge from different properties are stored in common layers, improving the performance of the model. This is known as joint transfer learning.

Results

- Benchmarking (MAE) on formation energy (E_f [eV/atom]), band gap (E_g [eV]), non-zero band gap (E_g^{nr} [eV]) and refractive index (n [-]) for different training sizes (N_{train})

Property	N_{train}	MODNet	MEGNet	MEGNet*	SISSO
E_f	604	0.210	0.342	0.262	0.312
E_f	60 000	0.044	0.028	0.026	0.299
E_g	604	0.71	0.91	0.83	0.80
E_g	60 000	0.34	0.30	0.27	0.75
E_g^{nr}	604	0.87	0.98	0.86	0.94
E_g^{nr}	36 720	0.45	0.38	0.33	0.86
n	3 240	0.05	0.08	0.08	0.12

MODNet: our work
MEGNet: MatErials Graph Network, a deep graph learning model
MEGNet*: MEGNet with transfer learning from weights learned on the formation energy
SISSO: Sure Independence Screening and Sparsifying Operator

- Absolute error distribution on vibrationnal thermodynamics :

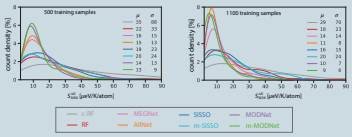

c-RF: Random forest with composition-only features
RF: Random forest with all generated features
AllNet: Neural network without feature selection
m-·-: Multi-target learning

Conclusion

- There is a clear distinction between physical-feature-based methods and graph-based models. Although the latter are often referred to as state-of-the art for many material predictions, the former are more powerful when learning on small datasets (below 4 000 samples).
- MODNet is based on feature selection (balancing relevance and redundancy) and joint transfer learning.
- State-of-the art model for predicting refractive indices and vibrational properties.
- The selection algorithm which determines the most important features can provide some understanding of the underlying physics.

Code availability

- The python package with pretrained models for the MODNet is available at https://github.com/ppdebreuck/modnet

Selected References

L. Ward, A. Agrawal, A. Choudhary, and C. Wolverton, npj Computational Materials 2, 16028

R. Ouyang, S. Curtarolo, E. Ahmetcik, M. Scheffler, and L. M. Ghiringhelli, Phys. Rev. Materials 2, 083802 (2018)

T. Xie and J. C. Grossman, Physical Review Letters 120

C. Chen, W. Ye, Y. Zuo, C. Zheng, and S. P. Ong, Chemistry of Materials 31, 3564 (2019)

G. Petretto, S. Dwaraknath, H. P. C. Miranda, D. Winston, M. Giantomassi, M. J. van Setten, X. Gonze, K. A. Persson, G. Hautier, and G.-M. Rignanese, Scientific Data 5, 180065 (2018)

F. Naccarato, F. Ricci, J. Suntivich, G. Hautier, L. Wirtz, and G.-M. Rignanese, Physical Review Materials 3, 044602 (2019)

fnrs FREEDOM TO RESEARCH
UCLouvain
C.E.C.I

P41

Design of two-dimensional ternary Ga2XO structures (X = S, Se, Te)

The possibility of breaking structural symmetry with realization of Janus monolayers offers new possibilities in the field of two-dimensional (2D) materials, and various ternary systems including the class of group-III monochalcogenides have been suggested. However, interaction of oxygen was shown to modify optoelectronic properties of gallium monochalcogenides, and design of ternary systems with oxygen as a third component has not been considered yet. We design and investigate 2D Ga2XO (X = S, Se, Te) systems by using first-principles calculations. Phonon spectra analysis and molecular dynamics simulations indicate that while Ga2SO and Ga2SeO are stable even at high temperatures Ga2TeO is dynamically unstable. Inclusion of oxygen makes Ga2SO and Ga2SeO less brittle when compared to their binary constituents. While GaX monolayers have indirect band gaps, Ga2SO and Ga2SeO become direct band-gap semiconductors and the band gap can be further tuned by tensile/compressive strain. Additionally, depending on the type of the system, strong optical absorption within the infrared, visible, and/or ultraviolet region is also predicted. Finally, structural and electronic properties of bilayers of Ga2XO are examined and compared with monolayers. Our results not only predict stable 2D ternary Ga2XO structures but also suggest them as promising materials for optoelectronic applications.

P42

Rashba spin splitting and photocatalytic properties of GeC-MSSe (M=Mo, W) van der Waals heterostructures

Haleem Ud Din[1,2], Bin Amin[2]

[1] College of Physics and Optical Engineering, Shenzhen University, Shenzhen 518060, Guangdong, P. R. China
[2] Abbottabad University of Science and Technology, Abbottabad 22010, Pakistan

ABSTRACT

Vertical stacking of ultrathin two-dimensional materials via weak van der Waals (vdW) interactions is identified as an important technique for tuning the physical properties and designing viable products for nanoelectronics, spintronics, and renewable energy source applications. The geometry, electronic, and photocatalytic properties of vdW heterostructures of GeC and Janus transition metal chalcogenides MSSe (M=Mo, W) monolayers are investigated by performing first-principles calculations. Two different possible models of GeC-MSSe heterostructures are presented with an alternative order of chalcogen atoms at opposite surfaces in MSSe. The most favorable stacking pattern of both models is dynamically and energetically feasible. A direct type-II band alignment is obtained in both models of understudy heterobilayer systems. The spin orbit coupling (SOC) effect causes considerable Rashba spin splitting in both MSSe monolayers. In particular, a greater Rashba spin polarization is demonstrated in model 1 (GeC-WSSe) than model 2 (GeC-MoSSe) caused by the alternative order of chalcogen atoms and larger SOC effect of heavier W than Mo atoms, which provides a platform for experimental and theoretical understanding of designing two-dimensional spintronic devices. More interestingly, the appropriate band alignments of model 1 with the standard water redox potentials enable its capability to dissociate water into H^+/H_2 and O_2/H_2O. In contrast to model 1, model 2 can only oxidize water into O_2/H_2O. The simulated design of GeC-MSSe is predicted for promising use in future electronic, spintronics, and photocatalytic water splitting.

CONTACT

Haleem Ud Din
1College of Physics and Optical Engineering, Shenzhen University, Shenzhen 518060, Guangdong, P. R. China
[2] Abbottabad University of Science and Technology, Abbottabad 22010, Pakistan
Email: b2scientist@gmail.com
Google scholar: https://scholar.google.com/citations?hl=en&user=hPJnkowAAAAJ#

INTRODUCTION

Interest in the field of two-dimensional (2D) materials, after the successful synthesis of graphene, has led the emergence of one-atom-thick materials exhibiting extraordinary electronic and optical properties. Beyond the gapless single layer graphene, 2D transition-metal dichalcogenidies (TMDCs) with general formulaMX_2(M=Mo, W;X=S, Se) have been extensively studied due to their fascinating properties. In particular, the high structure stability, suitable band-gap nature (ranging from 1.0 to 1.9 eV), and strong coupling between spin and valley degrees of freedom make these materials potential candidates for optoelectronics, field effect transistors (FETs), solar cells, and photocatalytic applications. [1].

Recently, selenization in MoS_2 and sulfurization in $MoSe_2$ through chemical vapor deposition (CVD) have successfully confirmed Janus MoSSe monolayers. Also, single layers of WSSe have been prepared by CVD method. The space group 2H-MX_2 is changed from D3h to C3v for Janus MXY (M=Mo, W;X, Y=S, Se) monolayers. Xiaet al. [2] recently reported the energetic feasibility and universality of electronic and photocatalytic properties of Janus MXY monolayers. SOC-induced Rashba spin splitting in these polar Janus MXY monolayers has also been demonstrated. It was shown that WSeTe monolayer has a significant Rashba spin splitting in the electronic band dispersion caused by intrinsic out-of-plane electric field induced due to the mirror asymmetry. The giant Rashba spin splitting in these single layers of Janus MXY renders their potentiality for out-of-plane piezoelectricity and future spintronic device applications [3]. Besides TMDCs and Janus TMDCs, the graphenelike hexagonal 2D compounds of group IV elements have also been gaining considerable attention due to their direct bandgap nature, which makes them a suitable candidate for designing optoelectronics, photovoltaic devices, and heterostructures [4]. GeC thin films have been prepared by laser ablation [5] and CVD techniques [6]. It has been reported that 2D GeC has a dynamically stable planar structure and exhibits excellent electronic and optical properties [7]. The single-layer GeC has higher Poisson's ratio and lower stiffness compared to graphene. Thus, the outstanding performance of single-layer GeC enables it for achieving enhanced electronic, optoelectronic, and photovoltaic device applications [9].

In this work, inspired by the highly energetic feasibility and satisfying lattice mismatch, we propose the vdW heterostructures of GeC and Janus MSSe to demonstrate the unprecedented properties by first-principles calculations. Two different models of vdW heterostructures based on the alternative order of chalcogen atoms with six possible stacking configurations are presented. It is found that both models with most favorable stacking configurations are dynamically stable. Further, a comprehensive insight is gained to explore the electronic properties, including Rashba spin splitting and photocatalytic response of the most stable configuration.

METHODOLOGY

We performed density-functional theory calculations with projector-augmented plane wave scheme in VIENNA AB INITIO SIMULATION PACKAGE [9]. The Grimme vdW correction with 500 eV cutoff was used in Perdew Burke Ernzerhof (PBE) functional to optimize the geometry until the forces and energy converged to 10^{-4} eV/Å and 10^{-5} eV, respectively. A 6×6×1 Γ-centered Monkhorst Pack k-mesh is used for structural relaxation, which is further refined to 12×12×1 for optimized structure. Artifacts of the periodic boundary conditions prevented by a vacuum layer of 25 Å were added along the z-axis. It is common that PBE functional underestimates the band-gap values of semiconductors, therefore, HSE06 (Heyd-Scuseria-Ernzerhof) functional is also used for electronic-structure calculations. However, due to high computational cost, HSE06 calculations are avoided to refine the k-mesh. SOC effect is significant in TMDCs and Janus monolayers, hence, SOC is also taken into account in our calculations. The SOC is incorporated by a second variational method, which uses scalar-relativistic basis, based on the reduction of original basis. Phonon spectrum calculations are performed by Phonopy code, which uses the harmonic interatomic force constants as input, obtained by density-functional perturbation theory. A 4×4×1 supercell with 6×6×1 k-mesh and 500 eV cutoff are used to ensure the convergence.

RESULTS and DISCUSSION

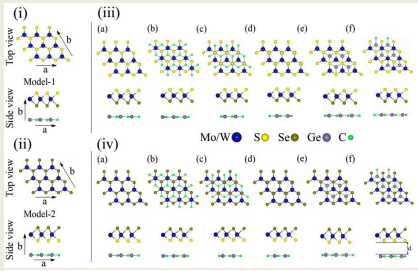

FIG. 1. Top and side view of (i) model 1 with Se atom located on bottom surface of Mo(W)SSe layer, (ii) model 2 with S atom placed at the bottom surface of Mo(W)SSe layer, and (iii), (iv) six possible stacking patterns of GeC-MSSe for both models (see text for details), and d represents the interlayer distance.

TABLE I. Binding energy (E_b, E_b, E_c, E_b, E_c, and E_f), interlayer distance ($d_{spacing}$), lattice constant (a), bond length (Ge-C and M-S/Se), and band gap (E_g (PBE/PBE–SOC), E_g (HSE06/HSE06–SOC) for both models of GeC-MSSe heterostructures.

Heterostructures	GeC-MoSSe		GeC-WSSe	
	Model 1	Model 2	Model 1	Model 2
E_b (eV)	−2.21	−1.91	−2.13	−1.81
$d_{spacing}$ (Å)	3.58	3.50	3.61	3.54
E_b (eV)	−3.23	−2.95	−3.11	−2.79
$d_{spacing}$ (Å)	3.24	3.11	3.27	3.14
E_c (eV)	−2.60	−2.48	−2.49	−2.30
$d_{spacing}$ (Å)	3.46	3.27	3.51	3.37
E_c (eV)	−2.86	−2.61	−2.74	−2.45
$d_{spacing}$ (Å)	3.35	3.20	3.42	3.31
E_f (eV)	−3.36	−2.88	−3.29	−2.75
$d_{spacing}$ (Å)	3.21	3.13	3.22	3.16
E_f (eV)	−2.09	−1.81	−2.03	−1.71
$d_{spacing}$ (Å)	3.63	3.55	3.26	3.26
a (Å)	3.26	3.26		
Ge-C (Å)	1.876	1.882	1.879	1.882
M-S/M-Se (Å)	2.42/2.53	2.42/2.54	2.42/2.54	2.42/2.54
E_g (PBE/PBE-SOC) (eV)	1.31/1.21	0.81/0.79	1.56/1.41	1.03/1.00
E_g (HSE/HSE-SOC) (eV)	1.87/1.86	1.31/1.30	2.16/2.06	1.62/1.58

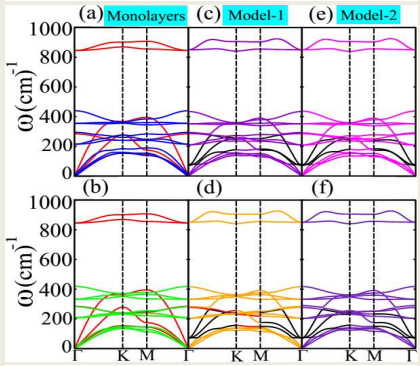

FIG. 2. Phonon spectrum of (a) GeC(MoSSe) in red (blue) (b) GeC(WSSe) in red (green) (c), (d) GeC-Mo(W)SSe in violet (orange) for model 1 (e), (f) GeC-Mo(W)SSe in magenta (indigo) for model 2, respectively.

REFERENCES

1. Adv. Mater. 29, 1605972 (2017)
2. J. Phys. Chem. C 123, 4549 (2019)
3. Nano Energy 40, 122 (2017)
4. Nanoscale 10, 34 (2018)
5. Phys. Rev. B 98, 165424 (2018)
6. Thin Solid Films 516, 3189 (2008)
7. Phys. Rev. B 80, 155453 (2009)
8. Phys. Lett. A 383, 1487 (2019)
9. Phys. Rev. B 47, 558 (1993)

RESULTS and DISCUSSION

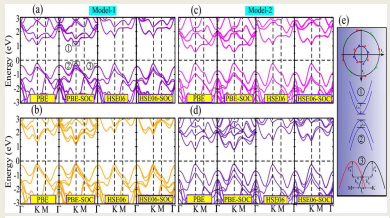

FIG. 3. Band structure of (a), (b) GeC-Mo(W)SSe in violet (orange) for model 1 (c), (d) GeC-Mo(W)SSe in magenta (indigo) for model 2. (e) Schematic of spin texture of two bands around Γ_v, and the encircled numbers (1 , 2, and 3) represent the magnified view of valence band-, conduction band-splitting at K-point and Rashba spin splitting around Γ_v, respectively.

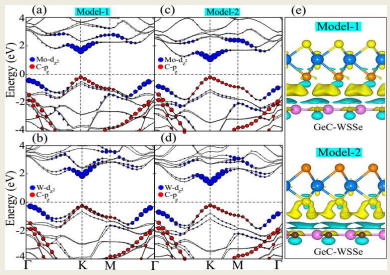

FIG. 4. Weighted band structure of (a), (b) GeC-Mo(W)SSe for model 1 (c), (d) GeC-Mo(W)SSe for model 2. (e) Schematic of charge density difference (with isovalue 0.00023e/Bohr^3), where the yellow and cyan colors represent the charge depletion and charge accumulation.

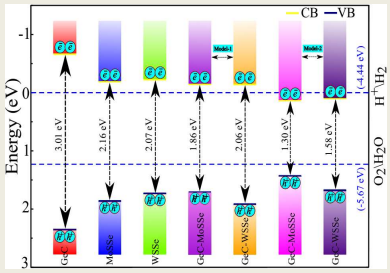

FIG. 5. The valence band (VB) and conduction band (CB) edge alignment of GeC, MoSSe, WSSe and their corresponding heterostructures; the blue dashed-lines represent the standard oxidation (−5.67 eV) and reduction (−4.44 eV) potentials for water splitting into O_2/H_2O and H^+/H_2, respectively.

CONCLUSIONS

- The most favorable vdW stacking of GeC with MSSe is energetically and dynamically feasible.
- GeC-MSSe vdW heterostructures have direct type-II band semiconducting nature.
- Larger Rashba spin splitting is found in model 1 than model 2 due to alternative order of chalcogen atoms and larger SOC.
- CB and VB edges of model 1 straddle the standard redox potentials for water splitting and are useful for dissociating water into H^+/H_2 and O_2/H_2O.

P43

Single-spin Dirac-like states in the rotational graphene phases on Co(0001)

The relevance of graphene as part of spintronics devices is drastically enhanced by interfacing it with ferromagnetic layers for the injection of spin-polarized electrons. The graphene/Co(0001) interface emerged as a great candidate for this scope after the recent experimental study reported single-spin Dirac-like "mini-cone" states of the epitaxially-aligned graphene on Co(0001). However, growth of a homogeneous phase of epitaxially-aligned graphene at large scale on cobalt thin films presents great challenges and most often leads to the creation of rotational graphene phases. Relevant to this point, here we show, with support from experimental work done at Elettra-Sincrotrone, Trieste, that the mini-cone states are also found in rotational graphene phases on Co(0001). Using ab-initio density-functional-theory calculations, we simulate graphene oriented at the experimentally-observed 19, 16 and 22-degree angles from the Co lattice, and compare with the epitaxial phase. We find the existence of the highly spin-polarized mini-cone states close to the Fermi energy at the K point in the band structures of all the three rotational phases unfolded to the primitive graphene cell, and we identify the origin of the mini-cone states. Our findings confirm, complete, and elucidate the photoemission results. Moreover, we discuss the energetics of the rotational graphene phases and compare the calculated Fermi velocities with the experimental ones. This work opens new possibilities for the inclusion of graphene/Co(0001) interfaces for spintronics applications.

P44

Probing the martensite transition and thermoelectric properties of Co_xTaZ (Z = Si, Ge, Sn and x = 1, 2): a study based on density functional theory

Rajeev Dutt[1,2,*], Dhanshree Pandey and Aparna Chakrabarti[1,2]

[1]*Homi Bhabha National Institute, Training School Complex, Anushakti Nagar, Mumbai-400094, India.*

[2]*Theory and Simulations Laboratory, Human Resources Development Section, Raja Ramanna Centre for Advanced Technology, Indore - 452013, India.*

**Email : duttrajeev35@gmail.com,duttrajeev@rrcat.gov.in*

Introduction

- Thermoelectric materials give us an option for the uncoventional source of energy, as well as they are important from the fundamental point of view.
- A large number of Co-based full Heusler alloys shows half-metallic character[1] and hence suitable for thermoelecctric materials
- **In the present study our aim is two-fold:**
  1. to explore if Co_2TaZ and CoTaZ (Z = Si, Ge,Sn) exhibit martensite transition
  2. to compare the thermoelectric properties of all these materials, in cubic (austenite) and possible tetragonal (martensite) phase

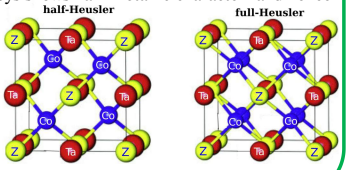

Fig 1: Structure of half and full Heulser alloys, where Z = Si, Ge and Sn

Computation Methodology

Structure optimization

- Spin polarized density functional theory (DFT) based calculation has been performed by VASP (Vienna Ab-initio Simulation Package) for structure optimization.
- For exchange-correlation, GGA-PBE functional has been used.
- Energy cut-off of 500 eV for the planewaves and k mesh of 19x19x19 have been used .
- Energy Convergence Criterion : 10^{-6} eV

• Electronic structure calculations

- Spin polarized electronic structure calculations have been performed by using WIEN2k software
- Linear augumented plane-wave (LAPW) method is used
- Energy convergence : $1x10^{-5}$ Ry.

Transport Properties

- Transport properties based on semi-classical Boltzmann transport theory were calculated by BoltzTraP software.

Probing of Martensite Phase

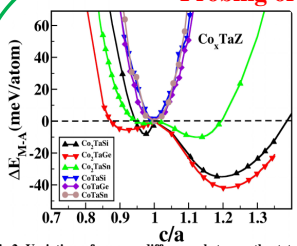

Fig 2: Variation of energy difference between the tetragonal (M) and cubic (A) phase (ΔE_{M-A}) in Co_xTaZ (Z = Si, Ge and Sn), x = 1, 2 with respect to c/a

- **All the full Heusler alloys (FHAs) found to have stable martensite phase configuration; half Heusler alloys (HHAs) prefer cubic phase.**
- **Tentative martensite transition temperature of Z = Si and Ge are to be above room temperature (400K), whereas for Z = Sn it is below the room Temperature**

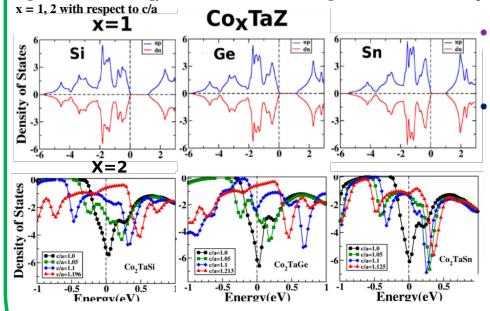

Fig 3: Upper panel shows the DOS of HHAs and Lower panel shows the DOS of down-spin for FHAs

- **HHAs show band gap value 1.246, 1.210 and 1.045 eV for Si, Ge and Sn respectively.**
- **Lower panel shows the down-spin DOS of FHAs, where a sharp peak has been observed for c/a =1 close to E_f and splitting of this peak take place with the variation of c/a in FHAs - indicating Jahn-Teller distortion and stability of the martensite (M) or tetragonal phase, as seen in case of Ni_2MnGa.**

Band structure and Fermi-surface Analysis

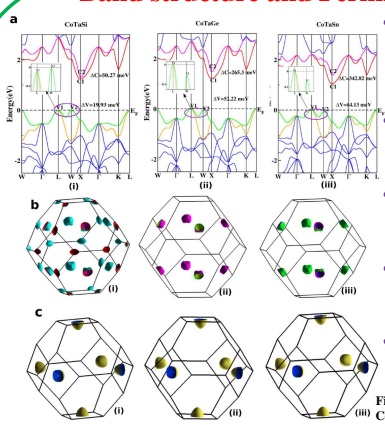

- **Valence band maxima have been observed at high symmetry point W (V2) for Si and at L (V1) for Ge, Sn.**
- **There is a hole valley observed at L (V1) for Si and at W (V2) for Ge and Sn respectively.**
- **$\nabla V = |V1-V2|$ found for Si, Ge and Sn as 19.93, 52.22, 64.13 meV respectively.**
- **$\nabla C = |C2-C1|$ values 50.27, 265.3, 342.82 meV for Si, Ge and Sn respectively.**
- **High valley degeneracy(N_V) has been observed for Si.**

Fig 6: a(i-iii) represents the band-structure of CoTaZ(Si,Ge,Sn) b(i-iii) and c(i-iii) represents iso-energy surface 25 meV below the VBM and 60 meV above the CBM.

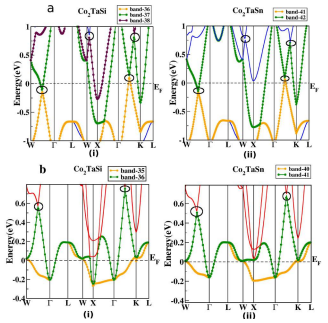

Fig 7: a(i-ii) and b(i-ii) represents band-structure of A phase of Co_2TaZ (Si, Sn) for up and down-spin respectively.

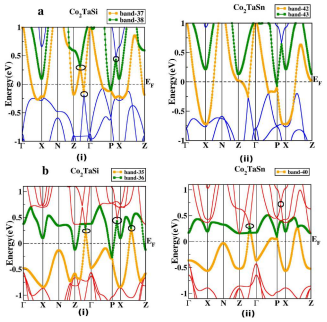

Fig 8: a(i-ii) and b(i-ii) represents band-structure of M phase of Co_2TaZ (Si, Sn) for up and down-spin respectively)

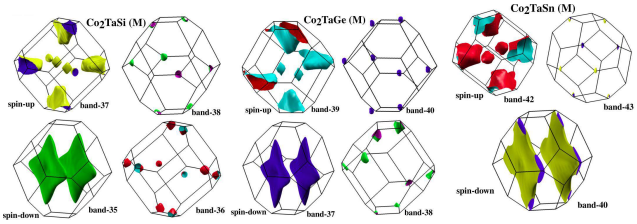

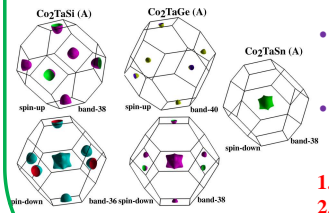

Fig 9: Fermi Surface of Co_2TaZ in A and M phase

- **Signature of linear band crossing and flat bands very close to the Fermi level have been observed for the A phase of all the FHAs.**
- **One order difference between the S value of A and M phase of FHAs is found due to the two reasons:**
  1. A high value of N_V in A phase than M phase.
  2. Large slope of DOS of A phase in the vicinity of E_F in comparison to the M phase.

Transport Properties

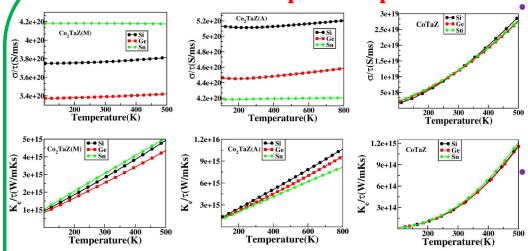

Fig 4: Electrical (σ/τ) & Thermal (κ/τ) (electronic) Conductivity

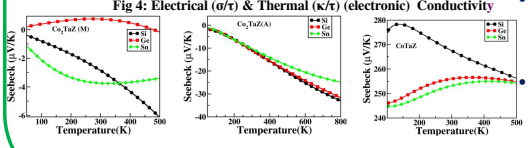

Fig 5: Seebeck coefficient (S) of Co_xTaZ (Z=Si,Ge,Sn) (x=1,2)

- **M phase of Co_2TaSn has the highest electrical and thermal conductivity among FHAs whereas these become the lowest for the austenite (A) phase in comparison to Si and Ge.**
- **Electrical and thermal conductivity of CoTaZ (Z=Si,Ge,Sn) show semiconducting behavior**
- **A phase for Co_2TaZ shows one order high value of S as compared to M phase.**
- **Among the HHAs CoTaSi found to exhibit higher value of S in comparison to other two.**

Conclusion

- **Tetragonal phase has been found to be stable for the FHAs.**
- **HHAs do not show any signature of tetragonal phase.**
- **DOS and elastic properties[1] confirm the stability of M phase of FHAs.**
- **FHAs found to be magnetic and metallic in both the phases, so they are likely to belong to the class of magnetic shape memory alloys.**
- **FHAs in M phase exhibit less value of S in comparison to the A phase which is further one magnitude lower than the HHAs.**
- **Band-structure and Fermi-surface analysis have been used to explain the comparative behavior of thermoelectric properties of the studied alloys.**

Acknowledgement

Authors thank Director, RRCAT, S.V. Nakhe for support and encouragement and A. Banerjee, S.R. Barman for discussion. Thanks for computer centre of RRCAT, Indore for computing facilities. RD thanks RRCAT and HBNI for financial support.

References

1. R. Dutt, D. Pandey and A. Chakrabarti, Journal of Physics: Condensed Matter 33, 045402 (2021) and references therein.

P45

Dipolar coupling of nanoparticle-molecule assemblies: An efficient approach for studying strong coupling

Strong light-matter interactions facilitate not only emerging applications in quantum and non-linear optics but also modifications of materials properties. In particular the latter possibility has spurred the development of advanced theoretical techniques that can accurately capture both quantum optical and quantum chemical degrees of freedom. These methods are, however, computationally very demanding, which limits their application range. Here, we demonstrate that the optical spectra of nanoparticle-molecule assemblies, including strong coupling effects, can be predicted with good accuracy using a subsystem approach, in which the response functions of the different units are coupled only at the dipolar level. We demonstrate this approach by comparison with previous time-dependent density functional theory calculations for fully coupled systems of Al nanoparticles and benzene molecules. While the present study only considers few-particle systems, the approach can be readily extended to much larger systems and to include explicit optical-cavity modes.

P46

LDA vs GGA comparative study of the electronic and magnetic properties for dihydrated transition metal oxalate chains

L. F. Garcia*, J. Hernández-Tecorralco, and R. de Coss

Departamento de Física Aplicada, Centro de Investigación y de Estudios Avanzados del Instituto Politécnico Nacional Unidad Mérida, Yucatán, México

Abstract

Nowadays, density functional theory (DFT) is a powerful tool to calculate the ground-state properties of materials in fields as physics, chemistry, and materials science. However, the accuracy of the calculation is driven by the choice of the exchange-correlation (xc) functional, so it is essential to choose the right one for the problem in question. In the first part of this work, we evaluated the performance of local density approximation (LDA) and generalized gradient approximation (GGA) to calculate the electronic and magnetic properties of 1D chains of dihydrated transition metal oxalates (MOx with M=Fe, Co, and Ni). The MOx systems are interesting from the fundamental research point of view due to their fascinating magnetic properties. The study of these 1D systems comes from a simplification of the problem since the bulk is formed by chains that are held together by hydrogen bonds. Besides, these MOx systems could add an extra challenge to DFT due to electronic correlation effects. Thus, in the second part of this work, we have used the DFT+U correction to describe the electronic and magnetic properties of these systems to compare with the available experimental evidence. Our calculations are based on the plane wave and pseudopotential method as is implemented in the Quantum Espresso code. The structural and magnetic properties obtained by GGA gives results in qualitative agreement with experimental observations. Besides, the DFT+U correction improves the bandgap opening observed in these materials. The results show a correlation between the filling of d orbitals and the gradient corrections effects on the ground state prediction.

*e-mail: luisf.garcia@cinvestav.mx

BANDGAP OPENING IN GRAPHENE INDUCED BY PATTERNED FLOWER-LIKE TOPOLOGICAL DEFECTS

P47

Doménica N. Garzón, Henry P. Pinto
Yachay Tech University, domenica.garzon@yachaytech.edu.ec

To identify applications of graphene, a deep study of its properties is necessary, including defects. One class of those defects is topological, i.e. grain boundary loops (GBL) [1]. It has been observed through scanning tunneling microscopy (STM) flower-like patterns. Recent measurements suggest that some of these one-dimensional topological defects can have unique electronic properties, such as a one-dimensional conductivity [2]. In this work, we propose and investigate a hypothetical system formed by a hexagonal array of such flower-like defects with different separations forming a superlattice. Using *ab initio* density-functional theory within the meta-GGA approximation provides a high level of accuracy and flexibility in the simulation of the properties of these superlattices.
Atomic and electronic structure, formation energies, and simulated scanning tunneling microscopy images of these superlattices are computed and analyzed.

FLOWER-LIKE DEFECTS

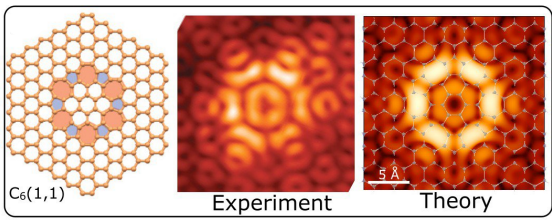

Figure 1. The C_6 (1, 1) with 24 atom core, left shows the experimental STM image in topographic mode with tunneling current of 100 *pA* and bias voltage of 0.3 *V* at T = 4.3 *K*; right panel is the DFT computed STM image (0.3 *V*), the corresponding lattice is superimposed in the image (Adapted from [1]).

METHODOLOGY

Simulations

[3]

Functional SCAN + rVV10 [4], which includes the Van der Waals dispersions. Cutoff energy of 950 eV. The separation of the k-point mesh was 0.032

STM images

[5]

Tersoff-Hamann approximation

Computed pristine graphene and 5x5, 6x6 ,7x7 ,8x8, 9x9, superlattices

RESULTS

System	a_{op}(Å)	N_{atom}	E_c (eV)	E_g(eV)
Pristine	2.45	2	7.61	0
5x5	12.371	50	7.45	0
6x6	14.803	72	7.50	0.54
7x7	17.242	98	7.53	0
8x8	19.679	128	7.55	0
9x9	22.123	162	7.57	0.33

Table 1. The results of the calculations for pristine graphene and 5x5,6x6,7x7,8x8,9x9 arrangements. a_{op} is the optimal defective lattice, N_{atom} is the number of atoms. E_C is the cohesive energy per atom, E_g represents the bandgap.

5x5

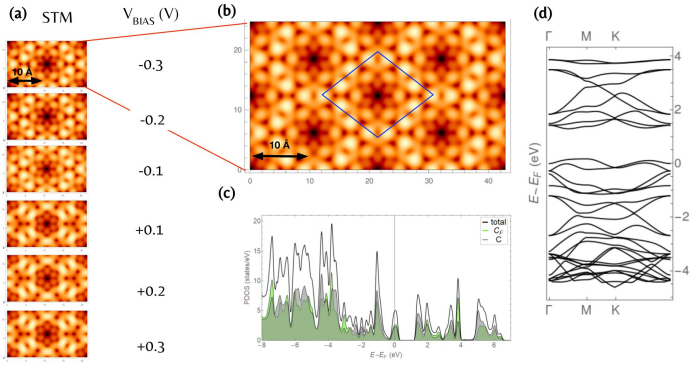

Figure 2. Computed STM for hexagonal array of defects with pattern 5x5. (a) shows the computed STM images for a series of VBIAS voltages. (b) Computed partial density of states (PDOS) where the gray (green) region belongs to the pristine-like C (flower region C_F) atoms. (c) shows a larger view of the hexagonal patterned 5x5 supercell for V_{BIAS} = -0.3 *V*; notice the scalebars in Å. The blue line denotes the unit cell of the displayed structures.

6x6

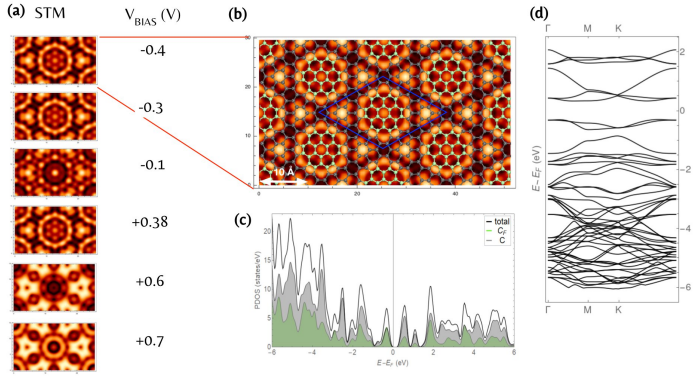

Figure 3. Computed STM for hexagonal array of defects with pattern 6x6. (a) shows the computed STM for a series of voltages. (b) shows a larger view of the hexagonal patterned 6x6 for VBIAS -0.3V .The blue line denotes the unit cell of the displayed structures.(c) Computed partial density of states (PDOS) for the deformed-undeformed region in green-gray. (d) Computed Band structure, it is shown *E-Ef*, where *Ef* is the Fermi level at 2.52(eV).

CONCLUSION

Results demonstrate the existence of a bandgap opening in defective graphene superlattice, induced by the FLD defect when arranged at certain distances with hexagonal configuration. In the 6x6 and 9x9 superlattices, we observe a band gap opening of 0.4 (eV) and 0.2 (eV) respectively. The magnitude of the cohesive energy per atom (E_C) decreases from pristine graphene to 9x9 arrangement. In future research, it will be analyzed the cause of this phenomenon and the nano-electronic applications.

ACKNOWLEDGMENT

The authors would like to acknowledge HPC-Europa3 (HPC17WE2EY) for providing state-of-the-art high-performance computing facilities for this research; also to the School of Physical Sciences and Nanotechnology at Yachay Tech University for the support in this work.

REFERENCES

[1] E. Cockayne, G. M. Rutter, N. P. Guisinger, J. N. Crain, P. N. First, and J. A. Stroscio, "Grain boundary loops in graphene," Phys. Rev. B, vol. 83, p. 195425, May 2011.
[2] H. Pinto and J. Leszczynski, Fundamental Properties of Graphene, Handbook of Carbon Nano Materials. World Scientific, mar 2014.
[3] G. Kresse and J. Furthmller, "Efficiency of ab-initio total energy calculations for metals and semiconductors using a plane-wave basis set," Computational Materials Science, vol. 6, no. 1, pp. 15 – 50, 1996.
[4] H. Peng and J. P. Perdew, "Synergy of van der waals and self-interaction corrections in transition metal monoxides," Phys. Rev. B, vol. 96, Sep 2017.
[5] K. Palot´as and W. A. Hofer, "Multiple scattering in a vacuum barrier obtained from real-space wavefunctions," Journal of Physics: Condensed Matter, vol. 17, no. 17, p. 2705, 2005.

P48

Optoelectronic Properties and Defect Physics of Lead-free Photovoltaic Absorbers Cs2Au(I)Au(III)X6 (X = I, Br)

Stability and toxicity issues with the hybrid lead iodide perovskite MAPbI3 necessitate a hunt for potential alternatives. Here, we shed light on promising photovoltaic properties of gold mixed-valence halide perovskites Cs2Au2X6(X=I, Br, Cl). They satisfy fundamental requirements such as nontoxicity, better stability, a band gap in the visible range, and a low excitonic binding energy. Our study shows a favorable electronic structure, resulting in a high optical-transition strength, and thus a sharp rise in the absorption spectrum near the band gap. This, in turn, yields a very high short-circuit current density and hence higher simulated efficiency compared with MAPbI3. However, careful investigation of defect physics reveals the possibility of deep-level defects (such as V_X, V_Cs, X_Au, X_Cs, Au_i, and Au_X, X=I,Br), depending on the growth conditions. These can act as carrier traps and become detrimental to photovoltaic performance. The present study should help in taking necessary precautions in synthesizing these compounds in a controlled chemical environment, which should minimize performance-limiting defects and pave the way for future studies on this class of materials.

P49

Overcoming the asymmetry of the electron and hole doping for magnetic transitions in bilayer CrI3

Electrical control of magnetism has great potential for low-power spintronics applications and the newly discovered two-dimensional van-der-Waals magnetic materials are promising systems for this type of applications. In fact, it has been recently shown experimentally (Jiang et al. 2018 Nat. Nanotechnol. 13, 549–553) that upon electrostatic doping by electrons bilayer CrI3 undergoes an antiferromagnetic-ferromagnetic (AFM-FM) phase transition, even in the absence of magnetic field. Doping by holes, on the other hand, does not induce the same transition in the experiment, which points to an intrinsic asymmetry in the hole and electron doping that limits the control of the transition by doping. We here show, based on first-principles calculations, that the asymmetry originates in the relativistic nature of the valence-band-edge states of the pristine bilayer, which inhibits the magnetic transition upon hole doping. Based on this finding, we propose an approach to engineer this system so that it displays the AFM-FM transition for both hole and electron doping by using moderate uniaxial strain along the soft direction of the bilayer.

P50

Chemically Graded Metal/Ceramic Interface - A High Throughput DFT Study

Prince Gollapalli, Satyesh Kumar Yadav
Department of Metallurgical and Materials Engineering, Indian Institute of Technology (IIT) Madras, Chennai 600036, India.

The interface in nano-sized metal-ceramic heterostructure plays an important role in dictating their properties. Interfaces between metals and ceramics are assumed to be atomically sharp, but recent studies suggests that Ti(metal)-TiN(ceramic) system is atomically compositionally graded across the interface[1]. This chemically graded interface can potentially find applications in wear resistance coatings, barrier layer for IC interconnects, hetero-catalysts, etc. Such chemically graded interfaces have some unusual characteristics like, gradual variation of elastic modulus across the interface. Bonding at the interface could improve due to smooth variation in lattice parameter, elastic modulus and other properties. To explore other combinations of metal/ceramic systems that could plausibly result in chemically graded interface by experimental effort is formidable. Here, we performed first-principles calculations based on density functional theory to predict the formation of chemically graded interface. In Ti-TiN, chemical gradation is attributed to creation of N vacancy in TiN; and diffusion of N into interstitial site of Ti. This provides a quantitative way to calculate driving force to form a chemically graded interface. We calculate vacancy formation energy, interstitial formation energy; sum of two quantities give estimate of driving force to form chemically graded interface. We have considered different combinations of metals (M) and ceramics (M_aX_b) to evaluate if they can form a chemically graded interface, where M = Ti, Zr, Hf, V, Nb, Ta, Al, Mg, Cr, and Fe; and X = C, N, and O.

References

1. E.B. Watkins et al., Thin Solid Films, 616, 399 (2016).

P51

The importance of long-ranged electron-electron interactions on the properties of twisted graphene moiré materials

Besides the most intensively studied twisted bilayer graphene (tBLG) system, there are several other graphene-based twisted moiré materials that have been found to exhibit correlated insulator states and superconductivity, including graphene twisted between two aligned graphene sheets, referred to as singly twisted trilayer graphene (tTLG), and twisted double bilayer graphene (tDBLG). We use an atomistic tight-binding model to investigate the interacting quasiparticle properties of these graphene-based moiré materials as a function of doping and twist angle, and we explicitly include long-ranged electron-electron interactions within the Hartree approximation. For tBLG and tTLG we find that long-ranged electron-electron interactions have a significant influence on the quasiparticle properties when the system is doped with holes or electrons, even away from the so-called magic angle, whereas the behaviour of tDBLG is qualitatively different and long-ranged interactions have negligible effect. We also investigate the magnetic ordering of tBLG as a function of doping and twist angle around the magic angle. We find that the phase diagram is qualitatively different when long-ranged interactions are included. In particular, we predict that the correlated insulating phases at doping levels of 1 and 3 holes per moiré unit cell should be less prominent than at other dopings, in good agreement with experimental observations.

P52

Ab-initio investigation of electronic excitations in bulk V2O5

We present an ab-initio investigation of electronic excitations in bulk V2O5. Time-dependent Density-Functional Theory (TDDFT) calculations were performed to obtain the dielectric function within the linear response. When crystal local field effects are included, we find a quantitative agreement between theoretical and experimental electron energy loss spectra (EELS) for all the momentum transfers considered in the experiment [1]. The observed anisotropy of the EELS is analyzed. We also discuss photoemission and optical spectra including corrections from Many-Body Perturbation Theory. [1] S. Arzkern et al. Phys. Rev. B 61, 12792 (2000)

P53

Efficient GW calculations in two dimensional through the interpolation of the screened potential

The GW self-energy approximation is able to accurately predict quasiparticle (QP) properties of several classes of materials. However, the calculation of the QP band structure of 2D semiconductors is challenging due to the sharp q-dependence of the dielectric function in the long-wavelength limit (q->0). In this case, a very dense q-sampling of the Brillouin zone is usually needed to obtain properly converged quantities. In this work, we assess the possibility to drastically improve the convergence of the QP corrections of 2D semiconductors with respect to the q-sampling, by combining Monte Carlo integration techniques and interpolation schemes of the screened potential. We test our method by computing the bandgap for three prototypical materials: a wide bandgap insulator (2D-hBN), a transition metal dichalcogenide (MoS2), and an anisotropic semiconductor (phosphorene). A speed-up of at least two orders of magnitude is found for all the systems considered.

P54

Hydration of NH + 4 in Water: Bifurcated Hydrogen Bonding Structures and Fast Rotational Dynamics

Understanding the hydration and diffusion of ions in water at the molecular level is a topic of widespread importance. The ammonium ion (NH+4) is an exemplar system that has received attention for decades because of its complex hydration structure and relevance in industry. Here we report a study of the hydration and the rotational diffusion of NH+4 in water using ab initio molecular dynamics simulations and quantum Monte Carlo calculations. We find that the hydration structure of NH+4 features bifurcated hydrogen bonds, which leads to a rotational mechanism involving the simultaneous switching of a pair of bifurcated hydrogen bonds. The proposed hydration structure and rotational mechanism are supported by existing experimental measurements, and they also help to rationalize the measured fast rotation of NH+4 in water. This study highlights how subtle changes in the electronic structure of hydrogen bonds impacts the hydration structure, which consequently affects the dynamics of ions and molecules in hydrogen bonded systems. Guo et al., Phys. Rev. Lett. 125, 106001

P55

Computational structure search of Si3N4

Silicon nitride is a material which exhibits high-temperature stability, chemical durability, and useful mechanical properties. While α-Si3N4 and β-Si3N4 are the only known polymorphs of Si3N4 stable at ambient conditions, a cubic form of Si3N4, -Si3N4, was recently synthesized under high pressure and temperature. In order to investigate whether additional phases of silicon nitride may exist we perform a comprehensive structure search of Si3N4. We first rapidly generate thousands of network models of Si3N4 through classical molecular dynamics using the Stephen-Garofalini (SG) potential. Models are subsequently screened and then optimized within Density Functional Theory (DFT). We report new hypothetical phases of Si3N4 and calculate mechanical properties.

P56

Excited-state properties for semi-empirical tight binding

Anna Hehn, Fabian Belleflamme, Jürg Hutter

Department of Chemistry, University of Zurich, Winterthurerstrasse 190, 8057 Zurich, Switzerland.

Understanding properties of electronic excited states is fundamental for describing various kinds of spectroscopy and for modeling photochemical phenomena. The therefore required analytical excited-state gradients have been reported for time-dependent density functional theory for Gaussian and plane wave basis sets and have become a standard tool in quantum chemistry program packages [1, 2]. Based on these developments, but aiming now for a highly efficient semi-empirical approach suitable for excited-state dynamics and large-scale applications on confined materials, we present excited-state gradients for the simplified Tamm-Dancoff approximation (sTDA) [3] as implemented in the mixed Gaussian and plane waves framework of the CP2K program package [4]. For electronic spectra, sTDA was already proven to be a powerful alternative to conventional hybrid density functionals, enabling to treat larger system sizes of thousands of atoms while still yielding reasonable accuracy with deviations in the range of 0.5 eV. We outline the implementation strategy for corresponding excited-state properties and show first benchmark results in comparison to standard time-dependent density functional theory approaches.

[1] F. Furche, R. Ahlrichs, *J. Chem. Phys.* **117**, 7433 (2002).

[2] J. Hutter, *J. Chem. Phys.* **118**, 3928 (2003).

[3] S. Grimme, *J. Chem. Phys.* **138**, 244104 (2013).

[4] The CP2K developers group. CP2K is freely available from http://www.cp2k.org/.

P57

Large twisting angles in Bilayer graphene

Moiré quantum dot structures

Jozef Bucko & František Herman

Department of Experimental Physics, Comenius University, Bratislava

herman2@uniba.sk

Abstract

*Recent exploration of the commensurate structure in the turbostratic double layer graphene shows that the large angle twisting can be treated by the decrease of the effective velocity within the energy spectra of the single layer graphene [1]. Within our work, we use this result as a starting point, aiming towards understanding the physics of by a large angle twisted double layer graphene (i.e. Moiré) quantum dot systems **(BGM-QD)**. We show that within this simple approach using the language of the first quantization, yet another so far unrealized (not up to our knowledge), illustrative property of the commutation relation appears in the graphene physics. Intriguingly, large twisting angles show to be a suitable tunning knob of the position symmetry in the graphene systems. Complete overview of the large angle twisting on the considered dot systems is provided.*

(Large angle) twisted bilayer graphene quantum dots

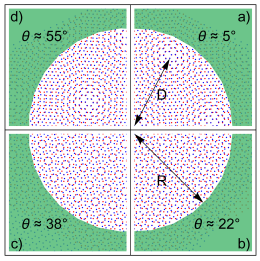

Figure 1: Moiré pattern situation close to the boundary of the cartoon $7\,nm$ wide BGM-QD system considering different values of the large twisting angle θ. R represents radius of the dot and D corresponds to the Moiré period.

Model

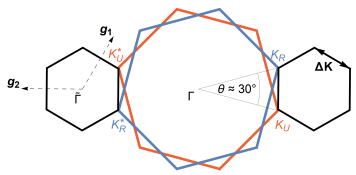

Figure 2: Brillouin zone of the unrotated (red), rotated (blue) single layer graphene, as well as twisted bilayer graphene (black).

- Effective velocity:

$$v_F(\theta) = v_F^{SL}\left(1 - \frac{\alpha}{\Delta K^2}\right), \quad \Delta K = \frac{4}{3a_0}\sin\frac{\theta}{2}.$$

v_F^{SL}: the single layer Fermi velocity.
α: the binding constant element between states in indiv. graphene layers.
ΔK: the distance of valleys in the individual graphene layers.
a_0: $(0.142nm)$, the shortest distance between Carbon atoms in the graphene layer.
θ: the twisting angle.

- Hamiltonian:

$$H^\tau(\theta) = v_F(\theta)\left(\mathbf{p} + e\mathbf{A}\right).\boldsymbol{\sigma} + \tau\Delta\sigma_z + U\left(\boldsymbol{r}\right),$$

$\mathbf{p}$: the momentum operator.
$\mathbf{A}$: the vector potential for magnetic field parallel to the z-axis $\mathbf{A} = B/2(-y, x, 0)$.
σ: the Pauli matrices.
τ: the valley number.
Δ: the constant mass term creating gap 2Δ induced by the underlying substrate.
$U(\mathbf{r})$: the confining potential assuming $U(\mathbf{r}) = 0$, $(U(\mathbf{r}) = U_0)$ for $r \leq R$, $(r > R)$ respectively.

Uncertainty principle

Theory

- Commutator of the Hamiltonian (assuming the vector potential $\mathbf{A} = \mathbf{0}$) together with the position operator $\mathbf{r}$:

$$[H^\tau(\theta), \mathbf{r}] = v_F(\theta)\,[\mathbf{p}, \mathbf{r}]\cdot\boldsymbol{\sigma},$$
$$= -i\hbar v_F(\theta)\boldsymbol{\sigma}.$$

- Twisting angle θ entering the reduced effective velocity works as a tuning knob of the deviance from the exact symmetry of the position operator and the Hamiltonian.

- Assuming radially symmetrical system $\langle r\rangle = 0$:

$$\Delta E\Delta\mathbf{r} \geq \mathbf{0}.$$

- Uncertainty principle allows us in principle to have well localized states together with the exact values of energy. All that due to the symmetry of our system and the equation of motion.

Experiment

- In the real life experimental conditions, we would expect Δr to be on the same scale as the radius of the dot R:

$$\Delta E R \approx \hbar v_F(\theta).$$

Reduced energy scale

- Reduced Fermi velocity (which leads to the reduction of the energy scale occurring in the graphene physics) affects the behavior of the allowed energies as well as states in the dot problem with the twisting angle θ:

$$\frac{\hbar v_F^{SL}}{R} \to \frac{\hbar v_F(\theta)}{R}.$$

Numerical Analysis

Formulation of the Eigenproblem

- Dirac equation of motion describing BGM-QD system:

$$H^\tau(\theta)\Psi^\tau(\theta) = E^\tau(\theta)\Psi^\tau(\theta),$$

- The two-site envelope wave function (due to cylindrical symmetry) can be factorized as:

$$\Psi^\tau(r,\varphi) = \frac{e^{im\varphi}}{\sqrt{r}}\begin{pmatrix}1 & 0\\ 0 & e^{-i\varphi}\end{pmatrix}\Psi_1^\tau(r),$$

where r and φ are the polar spatial coordinates and $\Psi_1^\tau(r)$ is the remaining part of the envelope wave-function.

- The final eigenenergies as well as final form of the eigenvectors can be found from the solution of the boundary condition (at $r = R$) using states inside $(<)$ and outside $(>)$ of the dot:

$$\Psi_<^\tau(R,\varphi) = \Psi_>^\tau(R,\varphi).$$

- The difference between solutions inside and outside of the dot is coming from the bounding potential $U(\boldsymbol{r})$.

Results and discussion

Energy states scaling

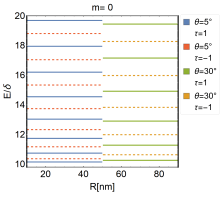

Figure 3: Energy levels of the BGM-QD considering $m = 0$, potentials $U_0 = \Delta = 10\delta$, where $\delta = \hbar v_F(\theta)/R$, two different valleys $\tau = \pm 1$ (+1 solid, -1 dashed), as well as two different values of twisting angle $\theta = 5°$ (red and blue) and $\theta = 30°$ (green and orange).

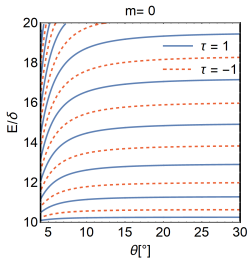

Figure 4: Evolution of the states in the conduction band as a function of the twisting angle θ considering both valleys $\tau = \pm 1$. Each of the curves plotted in the figure can be fitted by an empirical formula (motivated by the second order perturbation theory):

$$\varepsilon' = \varepsilon_0\left(1 - \gamma\csc^2\left(\frac{\theta}{2}\right)\right),$$

considering fitting parameters ε_0 and γ

Envelope wave-function

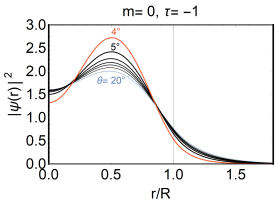

Figure 5: Wave function of the twisted bilayer quantum dot as a function of the twisting angle θ. Parameters related to the considered model: $m = 0$, $\tau = 1$, $U_0 = \Delta = 2\delta$, $R = 25\,nm$, $\rho = 1$, and the twisting angle is changing from $\theta = 4°$ (top curve) to $\theta = 20°$ (bottom curve).

Summary

- Small graphene flakes suitable for the quantum dots are not a problem to produce. Therefore the demand regarding the theory [2, 3] as well as experiment [4, 5, 6].

- Twisting the BGM-QD system in the regime of large angles shows to be suitable tool in order to get better localized states. Such a state also has lower energy due to reduced velocity.

- Use of the better localized states is natural in the tunneling applications [7, 8] (and references therein).

- Tunable distance of the energy levels on the infrared scale ranging from $\delta \approx 7\,meV$ (considering $R = 100\,nm$) already up to $\delta \approx 700\,meV$ (considering $R = 1\,nm$) craves for the application in the infrared spectroscopy area.

All of the mentioned ideas show promising research future in the field of the twisted bilayer graphene quantum dot physics. Our modest contribution to the fast developing field lays in the direction of the very simple description of the tuning by the large angle twisting of two graphene flakes placed above each other. It shows, that this effect leads to the decrease of the electron velocities. Described effect causes several features in the energy and state description including e.g. higher localization of the envelope wave-function.

References

[1] S. Shallcross et al. "Electronic structure of turbostratic graphene". In: *Physical Review B* 81.1 (Apr. 2010), p. 165105.

[2] Eliska Greplova et al. "Fully Automated Identification of Two-Dimensional Material Samples". In: *Phys. Rev. Applied* 13 (June 2020), pp. 064017–. URL: https://Journals.aps.org/prapplied/abstract/10.1103/PhysRevApplied.13.064017.

[3] Jozef Bucko et al. "Automated exploration of bound states in twisted bilayer graphene quantum dots". In: *To be published* (2021).

[4] C. Volk et al. "Electronic Excited States in Bilayer Graphene Double Quantum Dots". In: *Nano Letters* 11 (Aug. 2011), pp. 3581–3586. URL: https://pubs.acs.org/doi/10.1021/nl201295s.

[5] Marius Eich et al. "Spin and Valley States in Gate-Defined Bilayer Graphene Quantum Dots". In: *Physical Review X* 8 (Feb. 2018), p. 031023.

[6] A. Kurzmann et al. "Excited States in Bilayer Graphene Quantum Dots". In: *Physical Review Letters* 123.026803 (Sept. 2019), pp. 1–5. URL: https://Journals.aps.org/prl/abstract/10.1103/PhysRevLett.123.026803.

[7] Tobias Wenz et al. "Quantum dot state initialization by control of tunneling rates". In: *Physical Review B* 99 (May 2019), 201409(R)–. URL: https://arxiv.org/pdf/1903.02395.pdf.

[8] Niels Ubbelohde et al. "Partitioning of on-demand electron pairs". In: *Nature Nanotechnology* 10 (Dec. 2015), pp. 46–49. URL: https://www.nature.com/articles/nnano.2014.275.

Acknowledgements

We are grateful for financial support from the Swiss National Science Foundation through Division II (Grant No. 184739). We are also grateful to Eliska Greplova, Peter Rickhaus, Fokko de Vries and Frank Schäfer for many useful and interesting comments and discussions.

P58

Magnon valley Hall effect in CrI3-based van derWaals heterostructures

Magnonic excitations in the two-dimensional (2D) van der Waals (vdW) ferromagnet chromium triiodide (CrI3) are studied. We find that bulk magnons exhibit a nontrivial topological band structure without the need for Dzyaloshinskii-Moriya interaction. This is shown in vdW heterostructures, consisting of single-layer CrI3 on different 2D materials such as MoTe2, HfS2, and WSe2. We find numerically that the proposed substrates substantially modify the out-of-plane magnetic anisotropy on each sublattice of the CrI3 subsystem. The induced staggered anisotropy, combined with a proper band inversion, leads to the opening of a topological gap of the magnon spectrum. Since the gap is opened nonsymmetrically at the K+ and K– points of the Brillouin zone, an imbalance in the magnon population between these two valleys can be created under a driving force. This phenomenon has a close analogy to the so-called valley Hall effect and is thus termed the magnon valley Hall effect. In linear response to a temperature gradient, we quantify this effect by the evaluation of the temperature dependence of the magnon thermal Hall effect. These findings open a different avenue by adding the valley degrees of freedom besides the spin in the study of magnons.

P59

Ab initio modelling of laser-induced ultrafast electronic dynamics at the perylene@$MoSe_2$ interface

Matheus Jacobs, Jannis Krumland, and Caterina Cocchi

January 2021

Hybrid interfaces formed by atomically thin semiconductors, such as transition-metal dichalcogenides and physisorbed organic molecules, host intriguing charge-transfer dynamics effects that are relevant for opto-electronics [1]. In the framework of real-time time-dependent density functional theory [2,3], we investigate the ultrafast electronic dynamics at the type-II interface formed by perylene molecule physisorbed on a $MoSe_2$ monolayer. We monitor the evolution of the charge carriers in the electronic bands under a resonant femtosecond pulse. Our results provide a valuable starting point to explore further relevant dynamical effects, such as vibronic coupling.

[1] M. Jacobs *et. al.*, Adv. in Phys.: X 5, 1749883 (2020)
[2] N. Tancogne-Dejean *et. al.*, J. Chem. Phys. 152, 124119 (2020)
[3] J. Krumland *et. al.*, J. Chem. Phys. 153, 054106 (2020)

P60

Tuning structural and electronic properties of two-dimensional aluminum monochalcogenides: Prediction of Janus Al2XX' (X/X' : O, S, Se, Te) monolayers

The realization of ternary, single-layer transition metal dichalcogenides has suggested a promising strategy to develop two-dimensional (2D) materials with alternative features. In this study, we design and investigate Janus aluminum monochalcogenide monolayers, Al2XX' (X/X' = O, S, Se, and Te) by using first-principles methods. Starting from binary constituents, the ternary structures are optimized without any constraint and ground-state configurations are obtained. The stability of these systems is tested by performing phonon spectra analysis and ab initio molecular dynamics simulations and all Al2XX' monolayers other than Al2TeO are confirmed to be dynamically stable. Mechanical properties are examined by calculating Young's modulus and Poisson's ratio and subsequently compared with binary counterparts. Monolayers of Al2XX' have a brittle character but oxygenation makes them less stiff. The electronic structure is also analyzed and variation of the band gap with the type of chalcogen atoms is revealed. It is found that different from their binary counterparts, Al2XO monolayers are direct band-gap semiconductors. Additionally, modification of the electronic structure in the presence of biaxial compressive or tensile strain is investigated by taking into account possible indirect-direct band-gap transitions. Our results not only predict stable 2D ternary Al2XX' structures but also point out them as promising materials for optoelectronic applications.

P61

Towards band gap engineering via biaxial and axial strain in group IV crystals

Applying strain is one of major ways for tuning the electronic structure. In this work, DFT based ab initio studies of the effect of strain on electronic structure of group IV crystals were performed. Isotropic as well as axial and biaxial strains with respect to [1 0 0], [1 1 0] and [1 1 1] directions were considered. First, the structural and elastic characteristics were evaluated. The band structures evolution were represented by changes in energy gaps between valence band maximum at the gamma point of the Brillouin Zone and conduction band minima at gamma, as well as minima lying along lambda and delta lines. The important and known features observed are: sharp non-smooth behavior close to zero strain, the removal of the star degeneracy along delta and lambda lines, the transitions from indirect to direct band gap as well as closing/opening the gaps. The typical deformation potentials were calculated for Si and Ge directly from ab initio data, using the slab method for establishing unified energy reference point. The evaluated effective masses in valleys along delta and lambda lines exhibit a sudden increase in electron or hole effective masses under small strains, which is also reflected in significant changes in carrier mobility. An excellent agreement of computational results with available experimental data is observed, except for the deformation potentials related to the VB top absolute position, whose values seem to remain still an open question.

P62

Structure and Excitation properties of Functionalized Tin porphyrins: A TDDFT study

Metalloporphyrins are the most commonly used chromophores as they show strong absorption bands in the visible region and also for their natural light harvesting properties The present study highlights the impact of axial ligands (OH^-, Cl^-, and H_2O) and protonation at pyridine sites on the structure and electronic spectra of Sn(IV)tetrakis(4-pyridyl) porphyrins (SnTP) using time-dependent density functional theory (TDDFT). The considered 8 SnTP molecules such as i) $[SnTP]^{2+}$, ii) $[SnTPH]^{6+}$, iii) $[(OH^-)Sn(OH^-)TP]$, iv) $[(OH^-)Sn(OH^-)TPH]^{4+}$, v) $[(Cl^-)Sn(Cl^-)TP]$, vi) $[(Cl^-)Sn(Cl^-)TPH]^{4+}$, vii) $[(H_2O)Sn(H_2O)TP]^{2+}$ and viii) $[(H_2O)Sn(H_2O)TPH]^{6+}$ were optimized at B3LYP/6-31+G* level of theory with LANL2DZ basis set for Sn metal. The optimized geometries were later used in calculating single point energies using the same level of theory in Gas, THF and DMF phases with the conductor-like polarizable continuum (C-PCM) model. The excitation energies are obtained for 30 singlet states and it is observed that the absorption bands are located in the near UV-visible region between 250nm and 550nm signifying π- π^* transitions. The observed structural effects correlate well with the experimental data and clearly depict the impact of axial ligands on the SnTP ring. The absorption spectra along with the frontier orbitals in all three phases show noticeable dependence of axial ligation on the photophysical properties of SnTPs. This in turn provokes to study the effect of different axial ligands on the excitation properties of Sn porphyrins and the application of $[(OH^-)Sn(OH^-)TP]$ and $[(Cl^-)Sn(Cl^-)TP]$ as photosensitizers.

P63

Theoretical Insights on the Role of Bis-1,2,3-triazolebipyridine Ligands for Selective Separation of Am(III)/ Eu(III) in Nuclear Waste Management.

Abigail Jennifer G & Dr Rajadurai Vijay Solomon*

Department of Chemistry, Madras Christian College (Autonomous), East Tambaram, Chennai 600 059.

Email: vjsolo@gmail.com

Nuclear power has drawn attention to generate ample reliable energy to meet the global energy demands as an alternative to that previously sourced from fossil fuels. However, the long-term storage of significant amounts of the radioactive Spent Nuclear Fuel (SNF) generated as waste from these nuclear power plants pose as an obstacle for its application. While most of the short-lived fission products and uranium are less hazardous, the long-lived actinides (Am, Cm, Np) are highly radiotoxic[1]. This necessitates the need to eliminate or reduce the radiotoxicity by separation or transmutation of the long-lived minor actinides into short-lived or stable elements. 2,6-bis-1,2,4-triazin-3-yl-pyridines (BTPs) and 6,6′-bis-1,2,4-triazin-yl-2,2′-bipyridines (BTBPs) have been extensively studied for An/Ln separation[2]. These ligands and their derivatives have been reported to exhibit limitations such as instability in highly acidic conditions, limited solubility in non-polar dilutants, and moderately slow phase-transfer kinetics. In order to overcome these limitations, a class of tetradentate nitrogen donor ligands: 6,6′-bis(1-R-1H-1,2,3-triazol-4-yl)-2,2′-bipyridines (R = alkyl or aryl) or BTzBPs have been experimentally synthesised[3]. However, the origin of selectivity for effective complexation with metal nitrates has not been fully explained. This work aims to provide theoretical insights into the binding efficiencies, Frontier Molecular Analysis, Energy Decomposition Analysis, Charge Analysis, Bond Order Analysis and QTAIM calculations for the stage for full-scale application with respect to hydrophilic and hydrophobic substituents.

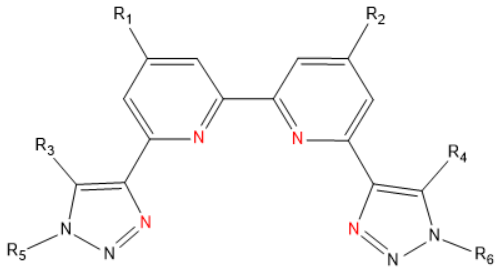

R1, R2 – Hydrophilic and hydrophobic groups R3, R4, R5, R6 - Methyl

Keywords: BTzBP ligands, Radioactive minor actinides, Actinide separation, Am^{3+}/Eu^{3+} stripping, Nuclear Waste Management.

References

1) Ebenezer, C.; Solomon, R. V. Insights into the Extraction of Actinides from Lanthanides Using 3,3'-Dimethoxy-phenyl-bis-1,2,4-triazinyl-2,6-pyridine Ligand – A DFT Study. Chemistry Select (2020)., 5(44), 13895–13901.
2) Panak, P. J.; Geist, A. Complexation and Extraction of Trivalent Actinides and Lanthanides by Triazinylpyridine N-Donor Ligands. Chem. Rev. 2013, 113 (2), 1199−1236.
3) Muller, J. M.; Nash, K. L. Synthesis and Characterization of 6,6′- bis(1-(2-ethylhexyl)-1H-1,2,3-triazol-4-yl)-2,2′-bipyridine (EH−BTzBP) for Actinide/Lanthanide extraction and Separation. Solvent Extr. Ion Exch. 2016, 34 (4), 322−333

P64

Influence of shape on hydration of gold nanoparticles

G. Jayabalaji and J. Meena Devi*

Centre for Nanotechnology & Advanced Biomaterials (CeNTAB) and School of Electrical & Electronics Engineering (SEEE), SASTRA Deemed University, Thanjavur-613401, Tamilnadu, India.

Keywords: Gold nanoparticles, Shape, Hydration and Molecular Dynamics simulation

Abstract:

Gold nanostructures of diverse shapes such as gold nano rods, cubes, stars and plates have variety of optical, chemical, biological applications and medical applications due to their fine tunable, physical, chemical and novel properties. The simulation studies on the gold nanoparticles of various shapes in water is important to acquire better understanding to facilitate the design of nanomaterials with desired functions for biological and technological applications. In the present work, molecular dynamics simulations have been employed to study the hydration of the gold nanoparticles of various shapes such as sphere, cube, rod and wire, focusing on their interactions with water at the interface. The wettability of the gold nanoparticles and the micro structure and dynamics of their interfacial water molecules were found to vary with the shape of the gold nanoparticles. This observed difference can be due to complex factors and may be attributed to the difference in their surface area, and degree of anisotropy. The present simulation result suggests, that the surface interactions of the gold nanoparticles with the aqueous medium can be modified by altering their shape. The outcome of this work may aid biological and technological applications.

P65

A full configuration interaction quantum Monte Carlo study of transition metal oxide molecules

Accurate ab initio calculations of 3d transition metal monoxide molecules have attracted extensive attention. In this poster, we show our recent study of transition metal oxide molecules using full configuration interaction quantum Monte Carlo (FCIQMC). We applied state of the art developments in FCIQMC and have tackled challenging problems in transition metal oxide molecules. The FCIQMC results are used to assess the performance of other wave function theory and density functional theory methods.

P66

Modulation of Optical Absorption in Marcasite Fe1-xRuxS2 and Exploring the Stability of New Phase in RuS2

A first-principle computational method have been used to investigate the effects of Ru dopants on the electronic and optical absorption properties of marcasite FeS2. In addition, we have also revealed a new marcasite phase in RuS2, unlike most studied pyrite structures. The new phase has fulfilled all the necessary criteria of structural stability and its practical existence. The transition pressure of 8 GPa drives the structural change from pyrite to orthorhombic phase in RuS2. From the thermodynamical calculation, we have reported the stability of new-phase under various ranges of applied pressure and temperature. Further, from the results of phonon dispersion calculated at Zero Point Energy, pyrite structure exhibits ground state stability and the marcasite phase has all modes of frequencies positive. The newly proposed phase is a semiconductor with a band gap comparable to its pyrite counterpart but vary in optical absorption by around 106 cm-1. The various Ru doped structures have also shown the similar optical absorption spectra in the same order of magnitude. We have used crystal field theory to explain high optical absorption which is due to the involvement of different electronic states in formation of electronic and optical band gaps. Löwdin charge analysis is used over the customarily Mulliken charges to predict 89% of covalence in the compound. Our results indicate the importance of new phase to enhance the efficiency of photovoltaic materials for practical applications.

P67

Vacancy-driven magnetic changes on doped manganites: the effect of a localized electronic defect level

Dilson Juan[1,2,3], **Miguel Pruneda**[2], **and Valeria Ferrari**[1,3]

[1]Instituto Sabato, UNSAM - CNEA, Av. Gral Paz 1499, San Martín, 1650 Buenos Aires, Argentina.
[2]Catalan Institute of Nanoscience and Nanotechnology - ICN2, CSIC and BIST, Campus UAB, 08193 Bellaterra, Spain.
[3]Instituto de Nanociencia y Nanotecnología, CNEA - CONICET. Departamento de Física de la Materia Condensada, GIyA, CAC - CNEA, Av. Gral Paz 1499, San Martín, 1650 Buenos Aires, Argentina.

ABSTRACT

Oxygen vacancies are common to most metal oxides and usually play a crucial role in determining the properties of the host material. In this work, we perform *ab initio* calculations to study the influence of vacancies in doped manganites $La_{(1-x)}Sr_xMnO_3$ (LSMO), varying both the chemical composition and the vacancy concentration within the ferromagnetic-metallic range ($0.2 < x < 0.5$). We find that the presence of a localized electronic defect level modifies the magnetic and electronic properties. The occupation of this level, which can be tuned by the number of available electrons in the system, does not only affect the half-metallic properties of LSMO along with a compression/expansion of the lattice parameters, but also reduces the strength of the double-exchange interaction, thus favoring spin-flipped configurations (local antiferromagnetism) and the deterioration of the metalicity. Our results provide theoretical evidence shedding light on the long-standing puzzle regarding the experimentally observed degradation of the magnetic and transport properties found in reduced manganites.

DFT STUDY ON GLOBAL REACTIVITY PARAMETERS OF PNA STACKS

P68

[1]K. Indumathi, [2]A. Abiram and [1]G. Praveena*
[1]Department of Physics, PSGR Krishnammal College for Women, Tamil Nadu
[2] Department of Physics, Karunya Institute of Technology and Sciences, Tamil Nadu
Corresponding author e-mail: *gopalpraveena@gmail.com*

ABSTRACT

Peptide nucleic acid (PNA) is a synthetic oligonucleotide, which is widely studying due to its unique properties such as high affinity, great specificity and stability [1, 2]. In this work, we have selected three sequential forms of peptidic chain tailored dimeric structures such as GG-CC (shown in Fig 1), AA-TT and AA-UU to reveal their reactivity properties. All the considered systems were subjected to optimize using B3LYP/6-31G* level of theory. The global reactivity descriptors (GRD) such as vertical ionization potential(*VIP*), vertical electron affinity(*VEA*), electronegativity(χ), chemical potential(μ), chemical hardness(η), chemical softness(S), electrophilicity(ω), HOMO-LUMO gap(E_{gap}) and polarizability (α) has been calculated for all the considered systems to understand the effect of replacing peptidic backbone instead of sugar phosphate group. On comparing the results with natural backbone, it is observed that peptidic chain containing strands have enhanced reactivity properties [3].

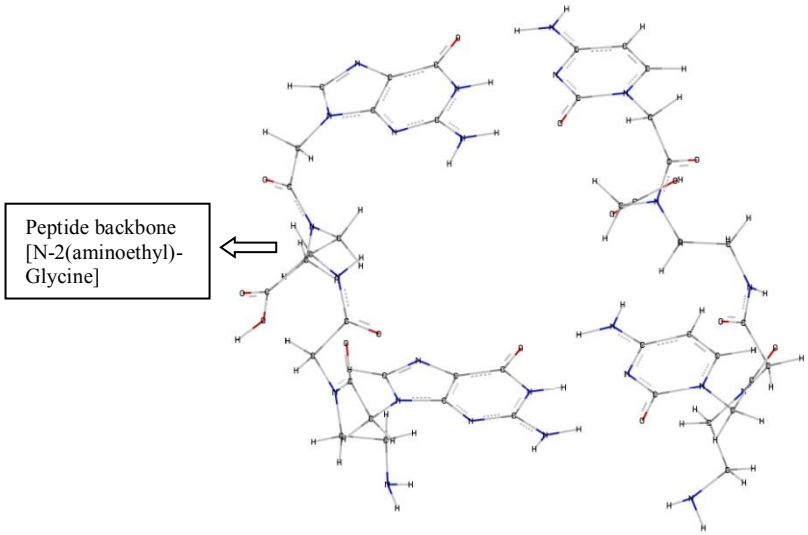

Fig 1: Optimized structure of GG-CC PNA dimeric strand at B3LYP/6-31G* level of theory.

References
1. P. E. Nielsen, M. Egholm, R. H. Berg, O. Buchart, *science*, 254 (1991) 9677-78.
2. Mologni, L., leCoutre, P., Nielsen, P.E. and Gambacorti-Passerini, C., *Nucleic. Acids. Res.* 1998, 26, 1934-1938.
3. K. Indumathi, A. Abiram & G. Praveena , *Molecular Physics*, 118:1 (2020) DOI: 10.1080/00268976.2019.1584682.

P69

Relativistic correction scheme for core-level binding energies from GW

We present a relativistic correction scheme to improve the accuracy of 1s core-level binding energies calculated from Green's function theory in the GW approximation, which does not add computational overhead. An element-specific corrective term is derived as the difference between the 1s eigenvalues obtained from the self-consistent solutions to the non- or scalar-relativistic Kohn–Sham equations and the four-component Dirac–Kohn–Sham equations for a free neutral atom. We examine the dependence of this corrective term on the molecular environment and the amount of exact exchange in hybrid exchange–correlation functionals. This corrective term is then added as a perturbation to the quasiparticle energies from partially self-consistent and single-shot GW calculations. We show that this element-specific relativistic correction, when applied to a previously reported benchmark set of 65 core-state excitations [D. Golze et al., J. Phys. Chem. Lett. 11, 1840–1847 (2020)], reduces the mean absolute error (MAE) with respect to the experiment from 0.55 eV to 0.30 eV and eliminates the species dependence of the MAE, which otherwise increases with the atomic number. The relativistic corrections also reduce the species dependence for the optimal amount of exact exchange in the hybrid functional used as a starting point for the single-shot G0W0 calculations. Our correction scheme can be transferred to other methods, which we demonstrate for the delta self-consistent field (ΔSCF) approach based on density functional theory.

P70

Weyl Chirality in Topological Semimetal Tantalum Phosphide

Weyl semimetal materials have attracted a lot of interest in quantum physics and industry. These materials provide the first realization of Weyl fermions and exhibits protected Fermi arc surface states and have found application in spintronics and valleytronics when spin-Orbit coupling (SOC) is turned on. Tantalum phosphide (TaP) was predicted and later experimentally realized as a Weyl semimetal. TaP is a topological Weyl semimetal though little has been studied despite being predicted for use in spintronics. It may be because the material has not been well understood in terms of its physical regime and its symmetrical properties (Weyl chirality) when SOC is turned on. In this study, we shall calculate Weyl chirality in TaP in real space integration using the maximally localized Wannier Functions (MLWFs) in order to depict if the Weyl nodes in TaP are sinks or troughs. This research will employ the state-of-the-art density functional theory as implemented in Siesta code. Norm conserving pseudopotentials will be used using fully relativistic approaches. This knowledge will guide the material designers in making TaP related materials with tailored properties basing on our findings.

P72

Influence of Hydrogen Sulphide and its derivative on the surface properties and hydrogen permeation through a model PdCu membrane by the first-principles study.

Kanika Kohli,[†] Debabrata Chattaraj,[‖] Chiranjib Majumder,[‖,⊥] and Prasenjit Ghosh[*,‡,§]

[†]Department of Chemistry, Indian Indian of Science Education and Research, Dr. Homi Bhabha Road, Pune, India

[‡]Depatment of Physics, Indian Indian of Science Education and Research, Dr. Homi Bhabha Road, Pune, India

[§]Centre for Energy Sciences, Indian Institute of Science Education and Research, Dr. Homi Bhabha Road, Pune, India

[‖]Product Development Division and [⊥]Chemistry Division, Bhabha Atomic Research Centre, Mumbai 400085, India

Abstract

Dense metallic membranes based on Pd alloys are being employed for the purification of hydrogen produced from “Steam-Methanol Reforming”(SMR) or “Water-Gas shift” reaction, because of their high hydrogen permeability and catalytic activity concerning hydrogen dissociation. However, they are susceptible to poisoning, induced by impurities in the gasifier effluent streams like H_2S, in the form of corrosion or catalyst deactivation[1,2]. In this work, we report a systematic theoretical study of the dissociation process of H_2S, its influence on the H_2 adsorption and dissociation process. Moreover, the effect of its derivative (sulphur) on the hydrogen adsorption, dissociation and hydrogen penetration via the solution diffusion mechanism through a model PdCu(110) membrane as a function of the sulphur coverage have also been studied. We found that the dissociation of H_2S on PdCu(110) is facile, with an energy barrier of 0.27 eV. Additionally, we observe slight lowering of H_2 dissociation barrier in the presence of H_2S as compared to that observed on the clean PdCu(110) membrane. Our calculations also suggest that there is a significant decrease in the hydrogen adsorption energy in the vicinity of the sulphur adatoms. Irrespective of the hydrogen coverage, blocking of hydrogen adsorption happens only for higher sulphur coverages. Based on the energy barrier calculations, we find that while sulphur promotes the H_2 dissociation process on PdCu(110) surface, it inhibits H penetration into the subsurface (one of the important steps in H penetration at the feeder side of the membrane). The poisoning effect of sulphur occurs at higher sulphur coverages. Since, the temperature is one of the controlling factors for the stability of hydrogen-permeable membranes, further, we are also studying the temperature dependant kinetics of the dissociation and penetration steps involved in the permeation mechanism using a microkinetic model, and the rate-limited flux prediction study.

References:

[1]. Casey P O’Brien, Bret H Howard, James B Miller, Bryan D Morreale, and Andrew J Gellman. Inhibition of hydrogen transport through pd and pd47cu53 membranes by h2s at 350°c. Journal of Membrane Science, 349(1-2):380{384, 2010.

[2]. Wilke, M.; Scheffler, M., Poisoning of Pd(100) for the dssociations of H2: a theoretical study of co adsorption of hydrogen and sulphur. Surface Science Letters 1995, 329, L605-L610.

P73

Electronic interaction and energy transfer between Si nanocrystals andorganic chromophores as a function of distance and orientation

The interaction between a silicon nanocrystal (Si NC) and aprotoporphyrin IX molecule (PPIX) is studied by first-principles simulations(DFT and TDDFT) at the ground state and at the excited state fordifferent distances and orientations of the PPIX molecule relative to the SiNC. The spectral overlap integral of the Si NC/PPIX pair is calculated,where Si acts as acceptor and PPIX as donor. The electronic couplingbetween the two parts is calculated using the transition density cube(TDC) method. Based on the TDC couplings and the spectral overlapintegral, the energy transfer rates are calculated. There is an electroniceffect on both PPIX and Si NC due to mutual proximity. A parallelorientation of PPIX relative to Si exhibits the strongest coupling andenergy transfer rates, albeit rapidly decreasing as a function of distance.The upright orientation yields stronger coupling for larger distances.Implications for designing energy harvesting systems are discussed. Thestudy also demonstrates a computational paradigm for use of the TDCmethod on semiconductor systems and for the simulation of relativelylarge nanocrystals that are in the area between strongly confinednanostructure and bulk material.

P74

Static barrier of the clusters on the metallic Cu(111), Ag(111), and Au(111) surfaces

A. Kotri [1,2], E. El koraychy[1], M. Mazroui[1]

[1] Laboratoire de Physique de la Matière Condensée, Faculté des Sciences Ben M'sik, Université Hassan II, B. P. 7955, Casablanca, Maroc.
[2] ERMAM, Faculté Poly-disciplinaire de Ouarzazate, Université Ibn Zohr Agadir, Maroc

Abstract

The diffusion properties of small clusters Ag_n, Cu_n, and Au_n on the Cu(111) and Au(111) surfaces have been studied using molecular statics, to understand the atomistic processes underlying the motion. Here, the atomic interaction is modeled by the semi-empirical potential. We found that on the tow surfaces Cu(111) and Au(111), the small clusters diffuse via the zigzag mechanism and the concerted jump. The static energies are found by the drag method, and The activation energy associated with the various diffusion mechanisms has been deduced. In addition, We have found that the value of this physical quantity always has a tendency to decrease in the case of the tetramer for all the systems treated. The same results have been found by various scientific researches, which confirm the validity of our EAM model.

P75

A fourth generation high-dimensional neural network potential

Machine learning potentials (MLP) have become an important tool for performing reliable atomistic simulations, since they provide nearly ab-initio accuracy while the computational costs are comparable to empirical force fields. To date, the majority of MLPs relies on the representation of energies and charges as a function of the local chemical environments. They are thus unable to capture global changes in the electronic structure due to long-range charge transfer and cannot describe systems in multiple charge states. Recently, non-local MLPs have been introduced to overcome these limitations. Here we propose a fourth-generation high-dimensional neural network potential (4G-HDNNP) that is able to take global charge redistributions and the corresponding non-local effects into account. We illustrate the improved accuracy of 4G-HDNNPs for several benchmarking systems including molecular and periodic systems.

P76

Accurately predicting electron affinities with Koopmans spectral functionals

Density functional theory (DFT) is a popular method for electronic-structure calculations. But while Kohn-Sham eigenvalues can loosely mirror experimental quasiparticle energies, there is formally no connection between the two (except for the HOMO in exact DFT). Furthermore, the presence of self-interaction errors in semi-local DFT can make those eigenvalues an even poorer proxy for quasiparticle energies. This poster will discuss Koopmans spectral functionals, an efficient approach for recovering spectral properties in a beyond-DFT formulation at very little additional computational cost. They have already been shown to lead to accurate molecular ionization potentials, and I will present the latest results, including accurate predictions of molecular electron affinities in the GW100 set.

P77

Ab initio molecular dynamics study of water TiO2 interface

Interfacial water on transition metal oxides such as TiO2 has been widely studied because of their structural complexity and scientific relevance in e.g. photocatalysis and ice growth. In this poster, I will discuss some of our recent works on this interface using ab initio molecular dynamics. I will show some interesting interfacial water structure that is newly identified in our simulations, and how these new structures can impact out understanding of the solid liquid interface.

P78

Theory and Computation of Hall Scattering Factor in Graphene

The Hall scattering factor, r, is a key quantity for establishing carrier concentration and drift mobility from Hall measurements; in experiments, it is usually assumed to be 1. We use a combination of analytical and ab initio modeling to determine r in graphene. Although at high carrier densities $r \approx 1$ in a wide temperature range, at low doping the temperature dependence of r is very strong with values as high as 4 below 300 K. These high values are due to the linear bands around the Dirac cone and the carrier scattering rates due to acoustic phonons. At higher temperatures, r can instead become as low as 0.5 due to the contribution of both holes and electrons and the role of optical phonons. Finally, we provide a simple analytical model to compute accurately r in graphene in a wide range of temperatures and carrier densities.

P79

Decoupled Strain Response of Ferroic Properties in Multiferroic $VOCl_2$ Monolayer

Akshay Mahajan* and Somnath Bhowmick

Department of Materials Science and Engineering, Indian Institute of Technology, Kanpur, Kanpur 208016, India

*Email: amahajan@iitk.ac.in

Abstract

Two-dimensional (2D) magnetoelectric multiferroic materials are a special class of 2D materials that holds promising applications in the miniaturization of logic and memory devices, along with the possibility to realize new low-dimensional device architectures. In this work, we have reported a strain-engineering-based study for a 2D multiferroic material, $VOCl_2$ monolayer, that shows independent control of magnetic and ferroelectric properties via applying strain along the different in-plane crystallographic directions. An in-plane strain of around 4% along the non-polar axis was found to cause a transition from an antiferromagnetic (AFM) ground state with an out-of-plane magnetization to a ferromagnetic (FM) ground state with in-plane magnetization. Additionally, the tensile strain along the polar axis enhances the ferroelectric polarization. An increase in the ferroelectric switching energy barriers and the magnitude of the magnetic exchange coupling parameter suggest enhancing ferroelectric and ferromagnetic stability with tensile strain. The work reveals the $VOCl_2$ monolayer as a strain-tuneable multiferroic material holding great promises for future generation nanoelectronic devices.

P80

Self-consistent DFT + U + V study of the structural, electronic, and magnetic properties of Pyrolusite ($\beta - MnO_2$)

Ruchika Mahajan[1], Iurii Timrov[2], Nicola Marzari[2] and Arti Kashyap[1]
[1]Indian Institute of Technology Mandi, Kamand, Mandi (HP)-175005, India
[2] Theory and Simulation of Materials (THEOS), and National Centre for Computational Design and Discovery of Novel Materials (MARVEL), École Polytechnique Fédérale de Lausanne (EPFL), CH-1015 Lausanne, Switzerland

Email: arti@iitmandi.ac.in

Abstract:

Pyrolusite ($\beta-MnO_2$) is one of many polymorphs of MnO_2 which contains 1x1 tunnels within the crystal structure causing immense selectivity towards ions or electron transfer kinetics. Hence it has been widely used in charge storage systems as an electrode materials or bifunctional catalyst [1]. In previous DFT+U works that used the empirical U = 4 and 6 eV it was found that the ferromagnetic configuration of β-MnO_2 is the most stable one [2]. However, experimentally it is known to have a helical noncollinear magnetic configuration with a band gap in the range of 0.26 to 0.3eV [3]. Here, we present the study based on the use of the self-consistent on-site (U) and inter-site (V) Hubbard parameters computed from first principles using density-functional perturbation theory [4]. We show that the inter-site Hubbard V is very relevant for the accurate description of the structural and electronic properties of $\beta-MnO_2$. We find that the G-type antiferromagnetic configuration is energetically more stable than the ferromagnetic one, and also we correctly predict the insulating properties of this material. Modelling of the helical noncollinear magnetic configuration in this material is challenging when including U and V, and this is the goal of our future studies which would highlight whether the inter-site Hubbard V is able to reproduce the experimental magnetic configuration.

References

[1] Yao, Wentao and Odegard et al., Nano Energy, 48(301--311), 2018.

[2] Franchini, Cesare and Podloucky et al., *Physical Review B,* 75(9): 195128, 2007.

[3] Yu, XL and Wu, SX et al., *Solid state communications,* 146(3-4): 166—168, 2008.

[4] Iurii Timrov, Nicola Marzari, and Matteo Cococcioni. *Physical Review B,* 98(8):085127, 2018.

P81

Temperature-dependent elastic constants from first principles

We present ab-initio calculations of the quasi-harmonic temperature dependent elastic constants (EC). The isothermal EC are computed from the second derivatives of the Helmholtz free energy, derived from phonon frequencies, with respect to the strain. The EC calculated for a grid of crystal parameters are interpolated at the geometry that minimizes the Helmholtz free energy at each temperature. This method is compared with the standard approach where the Helmholtz free energy as a function of the crystal parameters and strains is interpolated by a polynomial and its second derivatives are evaluated at the temperature dependent crystal parameters. Finally thermodynamic relationships are applied to compute adiabatic elastic constants in order to compare them with the experimental measurements. The work-flow is implemented in the thermo_pw code, a driver of the Quantum ESPRESSO routines for the calculation of material properties. We apply the method to several metals (Al, Ag, Au, Cu, Pd, and Pt) and semiconductors (Si and BAs).

P82

Combining GW-BSE and PCM approaches for the description of real time electronic dynamics of molecules close to a plasmonic nanoparticle: application to LiCN and p-nitro-aniline (PNA) molecules

In the presence of a plasmonic nanoparticle (NP) the optical response of molecules is strongly modified leading to significant effects such as surface enhanced Raman scattering, surface enhanced infrared absorption and metal enhanced fluorescence. The theoretical modelization of these phenomena is challenging due to the inherent multiscale nature of the system. Recently], the simulation of the simultaneous electronic dynamics of molecule and NP has been achieved by combining a time-dependent configuration interaction approach for the molecule, and a description of the NP as a continuous medium of given shape and dielectric function. The model takes into account the coupling of the system to a probing electromagnetic field as well, and its modification due to the plasmonic resonance of the nanoparticle. In this work we combine this approach with the description of the molecule's electronic structure and neutral excited states at the GW-BSE level and show the application of these combined methodologies to the study of Rabi oscillations of the ground and excited states population of a LiCN molecule, an ideal test system for the study of optical dipole switching. The molecule is set at increasing distances with respect to a spherical plasmonic nanoparticle probing the local field enhancement and the strength of the mutual interaction. The population and dipole dynamics of the prototypical push–pull PNA molecule in proximity of a tip-shaped nanoparticle is studied as well looking at the different responses that are obtained when the tip scans the different positions on the molecule.

P83

Electronic, Magnetic properties and magnetocalori ceffect A2BC(A=Fe, Co,..; B=Mn,..; C=Ga, Al,...) Heusler compounds

First principles calculations of structural and magnetic properties of A2BC(A=Fe, Co,..; B=Mn,..; C=Ga, Al,...) Heusler compounds with face-centered cubic, have been studied using a full potential linearized augmented plane wave within the density functional theory. Partial and total magnetic moments of magnetic ions have been determined as well the bulk modulus using the generalized gradient approximation proposed by Wu and Cohen. A2BC(A=Fe, Co,..; B=Mn,..; C=Ga, Al,...) Heusler compounds exhibit spin compensation and first-order behavior. The studied system undergoes a first-order phase transition between an ordered ferrimagnetic (or ferromagnetic) to paramagnetic. Transition and compensation temperatures have been determined using Monte Carlo simulation. Magnetic hysteresis cycle has been found for different temperatures.

P84

First principles study of atomic boron linear chains with substitutional nitrogen

In this ongoing study, we propose the first principles calculations of 1D atomic boron chains modified by nitrogen atoms. Since the discovery of borophene layers in 2015, we expect that boron derived nanomaterials may provide another possibility to monoelemental materials. With that in mind, we proposed a systematic study of boron chains due to the presence of a different element, such as N. We already expect that nitrogen may open electronic energy gaps. We are concerned with atmospheric contamination in vaccum chambers, which could help or destroy the modulation of properties of the chain.

P85

First-principles discovery of a high-temperature quasi-tetragonal phase in the Li^+ conductor $Li_{3+x}Ge_xP_{1-x}O_4$

Giuliana Materzanini[1,2], Elisa Gilardi[2,3], Daniele Pergolesi[2,3] and Nicola Marzari[1,2]

[1]Theory and Simulations of Materials (THEOS), École Polytechnique Fédérale de Lausanne, CH-1015 Lausanne, Switzerland

[2]National Centre for Computational Design and Discovery of Novel Materials (MARVEL), CH-1015 Lausanne, Switzerland

[3]Research with Neutrons and Muons (NUM), Paul Scherrer Institute, CH-5232 Villigen, Switzerland

In the light of recent first-principles molecular dynamics simulations (Materzanini et al., Phys. Rev. Mater. 2020, accepted) predicting high Li-ion conductivity in hypothetical tetragonal $Li_{10}GeP_2O_{12}$ (LGPO), we aim at enlightening possible entropy-driven phase transitions from the existing orthorhombic LISICON structure (α-o-LGPO) to the fast conductive hypothetical tetragonal α-t-LGPO. We perform extensive variable-cell (NPT) Car-Parrinello molecular dynamics at temperatures between 600 K and 1200 K, starting both from α-o-LGPO and α-t-LGPO structures, that we simulate in 100-atom supercells. We show that, at T $\sim$1100 K, both α-o-LGPO and α-t-LGPO transform into a quasi-tetragonal new phase (β-t-LGPO), that is stable at 600 K and is predicted, through DFT cell relaxation, to be the lowest-energy phase of LGPO. Interestingly, we monitor a phase transition to the same structure also from α-o-LGPO and α-t-LGPO at another stoichiometry, namely $x = 0.67$ in $Li_{3+x}Ge_xP_{1-x}O_4$. Experimental work is being conducted to investigate the formation of β-t-LGPO, and the possible competing processes that could dominate over α-o-LGPO phase transformation at high temperatures. Although, from the calculations, β-t-LGPO shows an improvement in conductivity against the original LISICON structure only at high temperatures, its stabilization can be regarded as an important challenge for synthesis and characterization of novel oxide superionic materials.

P86

The degradation of CdS-based paints

S.Mayda[1], F. Vanmeert[2,3], A. Romani[4,5], L. Monico[2,4,5], K. Janssens[2], B. Partoens[6], D.Lamoen[1]

[1]*EMAT & Nanolab Center of Excellence, Department of Physics, University of Antwerp, Groenenborgerlaan 171, 2020 Antwerp, Belgium*

[2]*AXES & Nanolab Center of Excellence , Faculty of Science, University of Antwerp, Groenenborgerlaan 171, 2020 Antwerp, Belgium*

[3]*Laboratories of the Royal Institute for Cultural Heritage (KIK−IRPA), Parc du Cinquantenaire 1, 1000 Brussels, Belgium*

[4]*CNR-SCITEC, via Elce di Sotto 8, 06123 Perugia, Italy*

[5]*SMAArt Centre and Department of Chemistry, Biology and Biotechnology, University of Perugia, via Elce di Sotto 8, 06123 Perugia, Italy*

[6]*CMT & Nanolab Center of Excellence, Department of Physics, University of Antwerp, Groenenborgerlaan 171, 2020 Antwerpen, Belgium*

Cadmium sulfide (CdS)-based yellows have been used in many historical artworks. These historical heritages are threatened by the degradation of the CdS-based paints. Although the origin of this process has been studied for many years, the details are still not fully understood. Here, we present a theoretical study for CdS and compounds such as $CdCl_2$ and Cd(OH)Cl that have been demonstrated to play a key role in the oxidation process of CdS together with high humidity levels[1]. We perform our calculations within the framework of DFT using the PBE and HSE functionals, and the GW approximation with the VASP code. In order to understand the oxidation mechanism of CdS to $CdSO_4$ and the influence of humidity and chlorine-compounds on this oxidation, we have calculated the band offsets between CdS, $CdCl_2$ and Cd(OH)Cl. Relative band positions are determined from slab calculations and by aligning the branch point energies[2]. Our results suggest that a single layer of Cd(OH)Cl is a polar semiconductor, featuring a built-in electric field. Stacking of several layers of Cd(OH)Cl creates a pocket of holes at the Cl-terminated surface, and a pocket of electrons at the OH-terminated surface, which attempt to compensate for the built-in electric field. This results in a difference in ionization energy at both surfaces of approximately 5.8 eV (PBE). The resulting band alignment between Cd(OH)Cl and CdS will therefore strongly depend on which Cd(OH)Cl surface is in contact with CdS. We believe this effect plays an important role in the observed degradation processes in some CdS-based paints.

[1] Monico, L. et al., Sci. Adv. 2020, **6**, eaay3514.
[2] Schleife, A. et al., Appl. Phys. Lett. 2009, **94**, 012104.

P87

Atomic scale model and electronic structure of Cu2O/CH3NH3PbI3 interfaces in perovskite solar cells

Cu2O has been proposed as hole transport layer in perovskite solar cells. Using density functional theory, we study the interfaces of CH3NH3PbI3 with Cu2O to assess their influence on device performance. Several atomic scale models of these interfaces are presented, considering different compositions of the interface atomic planes. The interface electronic properties are discussed on the basis of the optimal theoretical situation, in connection with the experimental realizations and device simulations. It is shown that the formation of vacancies in the Cu2O terminating planes is essential to eliminate dangling bonds and trap states. The four interface models that fulfill this condition present a band alignment favorable for photovoltaic conversion. Energy of adhesion, and charge transfer across the interfaces are also studied. The termination of CH3NH3PbI3 in PbI2 atomic planes seems optimal to maximize the photoconversion efficiency. See more at https://arxiv.org/abs/2006.15161.

P88

CaFeO3 and LaMnO3: octahedral breathing versus Jahn-Teller distortion

In the perovskites CaFeO3 (CFO) and LaMnO3 (LMO), the transition-metal cations have the same nominal d^4 electronic configuration. Both materials exhibit an insulating phase at intermediate to low temperatures where the degeneracy of the eg states is lifted by a structural distortion. However, while LMO exhibits a classical Jahn-Teller distortion, CFO exhibits a breathing distortion of the oxygen octahedra, resulting in alternating large and small octahedra, and thus two inequivalent Fe sites. To clarify the origin of the different behavior of LMO and CFO, we perform ab-initio calculations using density-functional theory and dynamical mean-field theory (DFT+DMFT), in combination with DMFT calculations for a simplified, semi-realistic tight binding model. Concretely, we seek to explain the different behavior of the materials by analyzing various quantities, such as the eg bandwidth, distortion stiffness, electron-distortion coupling constants, and electron-electron interactions parameters.

P89

Variational Quantum Algorithms for Real Space Wave Packet Dynamics

Variational quantum algorithms (VQAs) have become the new paradigm in applied quantum computing, enabling calculations on current-day quantum hardware that would be far out of reach otherwise. The triumph of hybrid quantum-classical schemes over purely-quantum methods has led to numerous further-developments and applications to stationary problems in recent years, yet the most widely used method for quantum dynamics simulation remains the Trotterization of the unitary time-evolution operator. However, it relies on deep quantum circuits and is therefore hampered by the substantial limitations of available quantum technology, which prohibits its use for practical tasks in the near future. Developing a variational time-evolution (VTE) algorithm was an important and necessary step. Nonetheless, VTE faces the difficulty of finding a representation of the wave function, which can maintain satisfactory accuracy throughout an evolution without diverging from the true state trajectory. While heuristic ansätze enjoy popularity, findings suggest that they require exponentially many parameters to offer enough flexibility, jeopardizing potential quantum advantages. One hypothesized way out of this dilemma is using a physically motivated ansatz, which samples from a reduced variational space by taking into consideration model-specific symmetries. In this work, we aim to explore this possibility by studying the dynamics of molecular vibrations as well as a spin-boson model. They are tested in the simulation of various system's dynamics. Our results indicate that it is indeed possible to find a compact yet accurate variational ansatz by leveraging symmetries of the system under study, requiring far less than exponentially many parameters.

P90

Ab-initio Gilbert damping on systems with lack of inversion symmetry: $Fe_{50}Co_{50}(100)$ case

I. P. Miranda[1], A. B. Klautau[2], A. Bergman[3], D. Thonig[3,4], H. M. Petrilli[1], and O. Eriksson[3,4]

[1] *Universidade de São Paulo, Instituto de Física, Rua do Matão, 1371, 05508-090, São Paulo, SP, Brazil*

[2] *Faculdade de Física, Universidade Federal do Pará, Belém, PA, Brazil*

[3] *Department of Physics and Astronomy, Uppsala University, Box 516, SE-75120 Uppsala, Sweden and*

[4] *School of Science and Technology, Örebro University, Fakultetsgatan 1, SE-701 82 Örebro, Sweden*

Gilbert damping has a critical importance in determining the lifetime, diffusion, transport and stability of domain walls, magnetic vortices, skyrmions, and other complex magnetic configurations. Given its high scientific interest, the possibility to obtain this quantity in a first-principles fashion [1] opens new perspectives of optimizing materials for devices. A way to do that is to use Kambersky's breathing Fermi surface (BFS) [2] and torque-correlation (TC) [3] models, which have been explored in terms of pure/alloy bulk and surfaces via reciprocal-space methods. However, considering the nonlocality of the damping parameter that is predicted for bulk itinerant magnets [4] there is a gap in literature for systems with lack of translation symmetry. Therefore, we will discuss a recent implementation of an ab-initio calculation of the damping in the real-space RS-LMTO-ASA method [5], based on the BFS/TC models. This allowed us to capture the orginis of the large damping anisotropy observed in $Fe_{50}Co_{50}(100)$ surface [6, 7].

---

[1] K. Gilmore *et al.*, Phys. Rev. Lett. **99**, 027204 (2007).

[2] V. Kamberskỳ, Czech. J. Phys. B **26**, 1366 (1976).

[3] V. Kamberský, Czech. J. Phys. **34**, 1111 (1984).

[4] D. Thonig *et al.*, Phys. Rev. Mater. **2**, 013801 (2018).

[5] S. Frota-Pessôa, Phys. Rev. B **46**, 14570 (1992).

[6] Y. Li *et al.*, Phys. Rev. Lett. **122**, 117203 (2019).

[7] I. P. Miranda *et al.*, arXiv:2101.02794 (2021).

P91

Reactivity Order Among Low-index Facets of TiO_2 for CO_2 Adsorption and Conversion

Understanding the atomic-scale interaction mechanism of CO_2 and H_2O on TiO_2 surface is crucial to establish a correlation between the catalytic efficiency with its exposed facet. Here, with the aid of a three-state model, nudged elastic band simulations, and DFT calculations, we examine the chemical restructuring of these molecules during the process of adsorption, coadsorption, and conversion on (001) including (1×4)-reconstructed, (010), and (101) facets of anatase TiO_2 and thereby, evaluate the step selective reactivity order. The study reveals that the change in exchange-correlation energy before and after adsorption can be considered as one of the quantitative factors to explain the nature of adsorption. Thus, the results reveal the unexplored non-trivialities in the reaction mechanisms. For the most stable (101) facet, we show that the unfavorable carbonate complex formation becomes favorable by switching the reaction from endothermic to exothermic in the presence of water. Further, we find that small binding energy does not necessarily imply physisorption. It can also give rise to chemisorption, where the loss in energy due to repulsive Hartree and Madelung interactions is comparable to the energy gained through the chemical bonding. Such a scenario is demonstrated for the CO_2 adsorption on (010) and (101) facets. Though (001) remains the most reactive surface, if it undergoes reconstruction, which happens at ultrahigh vacuum and high temperature, the number of active sites is reduced by three-fourths.

P92

Role of the valence band on the layer exfoliation in transition metal dichalcogenides: an ab initio study

The control of friction at the atomic scale is fundamental to optimize the exfoliation of layered materials. To this aim, we perform density functional simulations to study the the effect of intercalated molecules on the nanoscale friction of van der Waals transition metal dichalcogenides. We find that the molecule does not interact with the electronic density of the layers directly; nonetheless it determines the features of the valence band of the system. In particular, the valence-band width appears to be a promising parameter to correlate the electronic properties with the nanofrictional response; it then constitutes a guide for the automatic search of intercalation molecules suitable for layer exfoliation. The present outcomes also constitute a theoretical tool for future investigations on the effect that intercalated species have on the intrinsic friction in layered materials.

P93

Title: **Fundamental studies on the role of nuclear quantum effects in terephthalic acid.**

Authors: Unmesh Mondal[a] , Ali Hassanali[b], Prasenjit Ghosh[c]

a) Department of Chemistry, Indian Institute of Science Education and Research, Pune-411008, India
b) Condensed Matter Physics Section, The Abdus Salaam International Center for Theoretical Physics, Strada Costiera 11, 34151 Trieste Italy
c) Department of Physics and Center for Energy Sciences, Indian Institute of Science Education and Research, Pune-411008, India

Abstract:

Multiple proton transfer (MPT) is the movement of several protons along hydrogen bonds with interesting manifestations in a variety of chemical and biological processes. From proton hopping in water to proton transfer in DNA base pairs, the science of MPT is crucial and needs detailed investigation. As a lot of factors affect the nature of proton transfers in complex systems, we decided to study a less complex prototypical molecular crystal, terephthalic acid (TPA). TPA molecule is a dibenzoic acid with the carboxyl groups at the para position of the benzene. Each TPA molecule binds to two neighbouring TPA molecules through O-H---O bonds to form linear chains. Multiple chains experience weak C-H---O hydrogen bonds to form a sheet and eventually multiple sheets stack on top of each other through weak van der Waals interactions to form the crystal. Based on the stacking and crystal structure, TPA exists in three crystal forms[3,4] namely Form I, II and III, out of which Form III is stable at high temperature whereas Form I and II are both debated to be the most stable configuration at low temperatures. However, our *ab* initio calculations (using BLYP exchange-correlation functional) find Form I to be the most stable configuration at 0K. Existing experimental reports[1,2,6] suggest the hydrogen atoms along the O-H---O bond shuttles between the two TPA molecules . This double proton transfer (DPT) is believed to onset around 70 K and is commonly termed as the order-disorder transition.

In this study we intend to find the answers of the following questions:

(a) What is the nature of the double proton transfer? Is it stepwise or concerted?
(b) Are there any correlations between DPT occurring at two different H-bond sites(intralayer and interlayer)?
(c) How do molecule-molecule interaction and the crystal field affect the double proton transfer?
(d) How are the proton transfer and the correlations (if any) modulated by nuclear quantum effects(NQE)?
(e) Since the proton is significantly delocalized due to NQE, is there any coupling between the proton and the electronic degrees of freedom?

In order to address the aforementioned questions we performed *ab initio* molecular dynamics (AIMD) simulation with classical treatment of the nuclei at 70, 200 and 300 K. At low temperatures, NQE are overly pronounced for hydrogen atoms, therefore generalized langevin equation based path integral molecular dynamics simulations[7] (PIGLET) were performed to determine accurate statistical properties and thermostatted ring polymer molecular dynamics

simulations[8] (t-RPMD) for dynamical properties at the above mentioned temperatures. Classical nuclei AIMD simulations do not show any proton transfer (along O-H---O and C-H---O hydrogen bonds) at 70 and 200 K whereas at 300 K we do find diminutive proton transfer for the two hydrogen atoms along O-H---O hydrogen bonds at the chain junction. DPT is also found to have a concerted mechanism at the chain junction. However, DPT occurring at two adjacent H-bond sites along the linear chain is stepwise and does not occur simultaneously at 300 K. Incorporation of NQE enhances the proton transfer by tunneling and as a result small DPT is observed at 70 K. The proportion of proton transfers continuously increases with increase in temperature. Similar to the classical case at 300 K, the DPT is mostly concerted but we do find a non-negligible proportion of protons to be closer to one molecule than its neighbour. Such instances might induce fractional charge on the participating molecules for an overall neutral system. Unlike the classical case at 300 K, correlations of DPT at two adjacent H-bond sites can be both stepwise and concerted. At 70 K, the stepwise correlation is dominant whereas the increase in temperature makes the two processes comparable. In order to understand the dynamical properties, quantum t-RPMD simulations were used to approximately calculate the infrared(IR) spectra. The IR spectra shows considerable broadening in the O-H stretching region as the temperature is increased, thus, enabling a direct relationship with proton transfer. Additionally, we looked into deuterated TPA at 70 K and found no proton transfer and a consequent less broad O-D stretching in the IR spectra.

The shuttling hydrogen atom operates under a double well formed by the O atoms of the neighbouring TPA molecules. Due to symmetry, the double well potential experienced by hydrogen atoms in a TPA dimer is symmetric but becomes asymmetric in the crystal due to lattice effects. Previous reports[1,2,6] argue the asymmetric nature of the potential well to cause protons to tunnel and show NQE at low temperatures around 70 K. The exact nature of the lattice effects is difficult to understand through experiments. Therefore, we looked into NQE in the gas phase low-dimensional models of TPA namely dimer, chain and sheet. Both the classical and quantum simulations present zero proton tunneling at 70 K along with increased O---O bond distances w.r.t the crystal. The absence of proton transfer for low dimensional systems suggests the role of stacking of the TPA sheets to asymmetrize the double well in the crystal.

References:

[1] H. Fjaer, and E. J. Samuelson. Journal of Physics C: Solid State Phy., 30, 5945 (1986).
[2] P. Fischer, et al., J. of Sol. State Chem. 61, 109 (1986).
[3] M. Bailey, and C. J. Brown, Acta Crystallographica 22, 387 (1967).
[4] M. Sledz, J. Janczak, and R. Kubiak, J. of Mol. Str. 595, 77 (2001).
[5] R. J. Davey, et al, Nature 366 (1993).
[6] Meier, B. H., Meyer, R., Ernst, R. R., Zolliker, P., Furrer, A., & Hälg, W. Chemical physics letters 103(3), 169-174 (1983)
[7] Ceriotti, Michele, Giovanni Bussi, and Michele Parrinello. Physical review letters, 103(3) 030603 (2009).
[8] Rossi, M., Kapil, V., & Ceriotti, M. The Journal of chemical physics, *148*(10), 102301 (2018)

P94

Assessment of Density Functionals on Carbon Dioxide intermolecular interactions

Elizane E de Moraes[1] , Alexsandro Kirch [1] , Julio Romano Meneghini[2] and Caetano R. Miranda[1]

[1]Instituto de Física (IFUSP), DFMT, Universidade de São Paulo, São Paulo, SP, Brazil
[2]Departamento de Engenharia Mecânica-Escola Politécnica, Universidade de São Paulo, São Paulo, SP, Brazil

The need to reduce carbon dioxide (CO_2) emissions is one of the most significant environmental challenges facing society. Carbon capture and storage (CCS) is a major strategy to decrease CO_2 emissions from fossil fuel sources to the atmosphere. Understanding CO_2 interaction is crucial for the development of successful carbon capture and storage technologies. In this work we investigated the performances of the implemented functionals were investigated in the SIESTA: the van der Waals (vdW) dispersion correction with the (i) BH [1], (ii) C09[2], (iii) KBM [3], LMKLL [4], and (v) VV [5] version, and the generalized gradient approximation version GGA [6] to describe the interactions of the CO_2 homodimers through the density functional theory. The use of these functionals for the CO_2 has not been reported in the literature. Therefore the energy interaction between the CO_2 homodimers, the vibrational modes, and the solid phase was calculated using vdW-DF3-types. The calculation of the interaction energy between the dimers, we observed that the T-shaped (TS) and parallel displaced (PD) configurations are the most stable configurations. The qualitative and quantitative behavior of the functional vdW-DF-C09 for the PD configuration is in agreement with the works by Kalugina et al.[7]/Bukowski et al. [8], they used high-level CCSD(T)/aug-cc-pVXZ (X = D,T,Q,CBS)/SAPT theory. In addition, the functional vdw-DF-C09 was able to reproduce experimental data from the solid phase of CO_2 and the vibrational modes symmetrical, asymmetric and bending stretching. The comparison between different types of functional features of vdW can offer guidance for parameterization of force fields suitable for classical simulations to potentially bring insights into industrial solvent studies and optimize properties of materials designed for CO_2 capture and storage.

[1] Berland K and Hyldgaard P 2014 Phys. Rev. B **89** 035412
[2] Cooper V R 2010 Phys. Rev. B **81** 161104
[3] Klimeš J, Bowler D R and Michaelides A 2009 J. Phys.: Cond. Matter **22** 022201
[4]Lee K, Murray É D, Kong L, Lundqvist B I and Langreth D C 2010 Phys. Rev. B **82** 081101
[5] Vydrov O A and Van Voorhis T 2010 J. Chem. Phys. **133** 244103
[6] Perdew J P, Burke K and Ernzerhof M 1996 Phys. Rev. Lett. **77** 3865
[7]Kalugina Y N, Buryak I A, Ajili Y, Vigasin A A, Jaidane N E and Hochlaf M 2014 J. Chem. Phys. **140** 234310
[8]Torchet G, Bouchier H, Farges J, De Feraudy M and Raoult B 1984 J. Chem. Phys. **81** 2137–2143

Assessment of Density Functionals on Carbon Dioxide intermolecular interactions

Elizane E de Moraes[1] , Alexsandro Kirch [1] , Julio Romano Meneghini[2] and Caetano R. Miranda[1]

[1]Instituto de Física (IFUSP), DFMT, Universidade de São Paulo, São Paulo, SP, Brazil

[2]Departamento de Engenharia Mecânica-Escola Politécnica, Universidade de São Paulo, São Paulo, SP, Brazil

The need to reduce carbon dioxide (CO_2) emissions is one of the most significant environmental challenges facing society. Carbon capture and storage (CCS) is a major strategy to decrease CO_2 emissions from fossil fuel sources to the atmosphere. Understanding CO_2 interaction is crucial for the development of successful carbon capture and storage technologies. This work performs a benchmark of the exchange-correlation functionals to describe the van der Waals

interactions of the CO_2 through the density functional theory. The use of these functionals for the CO_2 has not been reported in the literature. Therefore the energy interaction between the CO_2 homodimers, the vibrational modes, and the solid phase was calculated using vdW-DF3-types. The functional vdW-DF-C09 accurately described the energy interaction between the different configurations of the dimers and the symmetrical, asymmetric, and bending stretch. The types of functional vdw-DF3 studied in this work described the solid phase of the dry ice correctly. The comparison between different types of functional features of vdW can offer guidance for parameterization of force fields suitable for classical simulations to potentially bring insights into industrial solvent studies and optimize properties of materials designed for CO_2 capture and storage.

P96

Influence of electronic excitations on the formation of defects in GaAs

Solar cells in spacecrafts are subject to solar and cosmic radiation, which includes high energy ions that promote the formation of defects in the different materials composing the solar cells, thus significantly affecting their performance. The formation of defects in such materials has been abundantly studied, but usually assuming that the system stays in its electronic ground state during the whole process. On the other hand, when the target is irradiated with high energy particles, its electronic subsystem is significantly excited as a consequence of the projectile' passing. These electronic excitations may significantly alter the defect formation in the material in comparison to the ground-state conditions. Here we present a study of the influence of the electronic excitations on the formation of defects on GaAs. We model the excitations by introducing a finite electronic temperature, and simulate the subsequent formation of different types of defects in the material for excitations of varying extent via first-principle Molecular Dynamics. We will show that the electronic excitations have a significant impact on the defect formation, changing the threshold displacement energy and causing different types of defects, even promoting local phase changes in the target material.

P97

Revisiting greenhouse gases adsorption in carbon nanotubes: advances by ab initio optimized potentials

Several carbon nanotubes (CNTs) applications such as filtering and storage rely on the adsorption properties of these nanostructures [1]. For this reason, many studies have employed classical force fields and molecular dynamics and/or Monte Carlo methods to investigate gases' adsorption properties inside the nanotubes [2]. However, even though many other studies [3] use ab initio methods to investigate the interaction of gases with CNTs and graphene, no studies have investigated the ability of the classical force fields in reproducing this data. In this work, we perform density functional theory (DFT) calculations with van der Waals functionals to investigate the interaction energies of CO2 with carbon nanotubes and graphene. We propose a new potential for the Lennard-Jones mixed parameters of the CO2-CNT interaction from the interaction energies. This potential is tested beyond the fitting data and compared with other DFT interaction curves. The final potential is used in Grand Canonical Monte Carlo simulations and compared with other classical force fields previously used in the literature. Our results show that, in general, the literature force fields, employed with the Lorentz-Berthelot rules, underestimate the amount of CO2 adsorbed in the CNTs.

P98

High throughput computational screening of perovskites for photovoltaics

Farha Naaz, M. S. Chauhan, and D. L. V. K. Prasad*

Department of Chemistry, Indian Institute of Technology, Kanpur 208016, India
Email: dprasad@iitk.ac.in

Perovskites are archetypal multifunctional materials—they could be inorganic, organic or their hybrid variants. Recently these classes of perovskites emerged as promising photovoltaic multi-junction solar cell materials, much needed for energy. But, that said, the structure stability and earth-friendly are some of the major concerns that may impede the development of an efficient photovoltaic cell. Perhaps, due to the inherent structural tolerance that there is no other crystal structure-type that could be a better sponge as perovskite for the elements in the periodic table, and therefore, one may predict appropriate compounds that tailored to have all the necessary distinctive attributes of a productive photovoltaic cell. To this end, in an effort to realize such a material from first principles, here we predict perovskites through combinatorial optimization and high throughput approaches. Various chemical filters have been applied to reduce the screening of the data-sizes and computer intensive calculations. The results are encouraging. The theoretical high throughput workflow developed and the results of the predicted perovskites will be presented. The forces and the phonons of the crystals are calculated within the density functional and density functional perturbation theoretical calculations. The band gaps are accurately estimated using range-separated and quasiparticle schemes.

P99

First-principles calculation of magnetism and magnetocrystalline anisotropy in antiferromagnetic semiconducting chalcopyrite

N. Tsogbadrakh[1*], N. Jargalan[2], B. Batgerel[3] and Kh.Tsookhuu[12]

[1] Department of Physics, National University of Mongolia, Ulaanbaatar-14201, Mongolia
[2] Institute of Physics and Technology, Mongolian Academy of Sciences, Ulaanbaatar-13330, Mongolia
[3] Institute of Mathematics and Digital Technology, Mongolian Academy of Sciences, Ulaanbaatar-13330, Mongolia

E-mail: Tsogbadrakh@num.edu.mn

Transition-metal sulfides are an important class of Earth materials with a fascinating diversity of structure types [1] that exhibit a host of technologically relevant electronic, magnetic, and catalytic properties. Because of the prominent role of sulfides as a source of nonferrous metals, the oxidation state of metals in these compounds has been extensively used in order to rationalize their fundamental crystal properties, the processes of mineral formation and breakdown, mineral processing, and their participation in environmental contamination associated with mining activities. However, it is surprising to find that, after numerous studies, there is still some debate on the assignation of oxidation states in a common mineral of prominent economic relevance such as chalcopyrite with the high Neel temperature (TN = 823 K), which represents the bulk of the world supplies of copper [2].

The most common naturally occurring ternary sulphide system is that containing copper, iron and sulphur. The ternary chalcogenide compounds have recently attracted great attention due to their important physical and chemical properties and promising potential applications in solar power engineering and spintronics [3, 4, 5].

We present the results of electronic structure, magnetism and magnetocrystalline anisotropy of antiferromagnetic (AFM) semiconducting chalcopyrite ($CuFeS_2$) by the first-principles method

within the framework of the spin- polarized density functional theory (DFT) using the Quantum Espresso packages. For the magnetocrystalline anisotropy energy, the calculation of noncollinear magnetism was performed using the Force Theorem. We predicted the lattice parameters, band-gap and atomic magnetic moment of the most stabilized ground state of AFM. We computed the magnetic anisotropy energy (MAE) of bulk and thin films, and our results agree with the results of neutron measurements.

References

1. Hulliger F (1968) Struct. Bonding (Berlin) p 83
2. Pearce C I, Pattrick R A D, Vaugham D J, Henderson C M B and van der Laan G (2006) Geochim. Cosmochim. Acta 70 4635
3. DiSalvo F J (1990) Science 247 649
4. Alivisatos A P (1996) Science 271 933
5. Heath J R, Kuekes P J, Snider G S and Williams R S (1998) Science 280 1716

P100

Ab-initio energetics of graphite and multilayer graphene: stability of Bernal versus rhombohedral stacking

Jean Paul Nery,[1,2] Matteo Calandra,[1,3,4] and Francesco Mauri[1,2]

[1] *Graphene Labs, Fondazione Istituto Italiano di Tecnologia, Via Morego, I-16163 Genova, Italy.*
[2] *Dipartimento di Fisica, Università di Roma La Sapienza, Piazzale Aldo Moro 5, I-00185 Roma, Italy.*
[3] *Sorbonne Université, CNRS, Institut des Nanosciences de Paris, UMR7588, F-75252, Paris, France.*
[4] *Department of Physics, University of Trento, Via Sommarive 14, 38123 Povo, Italy.*

There has been a lot of excitement around the observation of superconductivity in twisted bilayer graphene, associated to flat bands close to the Fermi level. Such correlated electronic states also occur in multilayer rhombohedral stacked graphene (RG) [1,2], which has been receiving increasing attention in the last years. However, multilayer stacked Bernal graphene (BG) occurs more frequently in both natural and artificial samples, making it desirable to determine under which conditions RG might be favored [3]. Here, we study the energetics of BG and RG in bulk and also multilayer stacked graphene using first-principles calculations [4]. It is shown that the electronic temperature, not accounted for in previous studies, plays a crucial role in determining which phase is preferred. We obtain that energy differences between BG and RG are of the order of 0.01 meV/atom, and justify why they are so small. We also show that the low energy states at room temperature consist of BG, RG and mixed BG-RG systems with a particular type of interface. Energies of all stacking sequences (SSs) are calculated for N = 12 layers, and are fit with an Ising model that uses only a few parameters and transfers to larger N. Our work clarifies inconsistent results in the literature, and sets the basis to studying the effect of external factors like curvature, doping or an electric field on the stability of multilayer graphene systems in first principles calculations.

[1] D. Pierucci, H. Sediri, M. Hajlaoui, J.-C. Girard, T. Brumme, M. Calandra, E. Velez-Fort,G. Patriarche, M. G. Silly, G. Ferro, V. Soulire, M. Marangolo, F. Sirotti, F. Mauri, and A. Ouerghi, Evidence for flat bands near the Fermi level in epitaxial rhombohedral multilayer graphene, ACS Nano **9**, 5432 (2015).
[2] H. Henck, J. Avila, Z. B. Aziza, D. Pierucci, J. Baima, B. Pamuk, J. Chaste, D. Utt, M. Bartos, K. Nogajewski, B. A. Piot, M. Orlita, M. Potemski, M. Calandra, M. C. Asensio, F. Mauri, C. Faugeras, and A. Ouerghi, Flat electronic bands in long sequences of rhombohedral-stacked graphene, Physical Review B **97** (2018), 10.1103/physrevb.97.245421.
[3] J. P. Nery, M. Calandra, and F. Mauri, Long-Range Rhombohedral-Stacked Graphene through Shear, Nano Lett. **20**, 50175023 (2020).
[4] J. P. Nery, M. Calandra, and F. Mauri, arXiv:2011.09614v1 (2020).

Acknowledgements: This project has received funding from the European Unions Horizon 2020 research and innovation programme Graphene Flagship under grant agreement No 881603.

P101

THEORETICAL INSIGHTS INTO MAGNETIZATION IN GRAPHENE CONTAINING SINGLE AND INTERACTING NANOPOROUS DEFECTS

F. B. S. NKOU[1], D. H. Douma[1], B. R. Malonda-Boungou[1,2], B. M'passi-Mabiala[1,2], A. T. Raji[3], and S. Kenmoe[4]

[1]Groupe de Simulations Numériques en Magnétisme et Catalyse, Faculté des Sciences et Techniques, Université Marien Ngouabi, B.P. 69, Brazzaville, Congo
[2]Unité de Recherche en Nanomatériaux et Nanotechnologies, Institut National de Recherche en Sciences Exactes et Naturelles (IRSEN), Brazzaville, Congo
[3]Department of Physics, College of Science, Engineering and Technology (CSET), University of South Africa (UNISA-Florida Campus), Corner of Christiaan de Wet Road & Pioneer Avenue, Florida, 1709, South Africa
[4]Department of Theoretical Chemistry, University of Duisburg-Essen, Universitätstr. 2, D-45141, Essen, Germany

Abstract

Density-functional theory (DFT) has been used to calculate the electronic structures and magnetization in nanoporous graphene. We consider single nanopore (consisting of up to ten vacancies) and interacting nanopores (consisting in vacancy pairs, divacancy pairs and vacancy-divacancy pairs) separated at varying distances. We have notice that the interactions between the nanopores weaken as their separation distance increase and the formation energy tends to the value of single nanopore whereas the magnetic moment tends to the sum of individual ones. We proposed an empirical model for predicting the total magnetic moment as a function of nanopore size. This model is able to predict the magnetic moment of small and large nanopore sizes.

Computational Model

- Quantum ESPRESSO first-principles simulation package [**1**, **2**] has been used for all the calculations.
- Interaction between the nuclei and the electrons is modeled by ultrasoft pseudopotentials [**4**], and the exchange-correlation functional is modeled GGA-PBE [**3**].
- A 10a $\times$ 10a (a = 2.46 Å) hexagonal graphene supercell of 200 carbon atoms to model our nanoporous defects.
- Two different nanoporous graphene structures containing single nanopores S_i i = 1, 2, 3, ...10 and those with double nanopores S_iS_j (i, j) = (1, 1), (1, 2), (2, 1), (2, 2) . The indices i and j stand for the number of carbon vacancy.

Result and discussion

We calculate the formation energy of all our structures and we obtain values in agreement with others DFT calculations. Throught the sum of local partial density of states (LPDOS) calculations and the electron spin density of all our structures we notice the extent of Carbon vacancies on the electronic and magnetic properties of graphene.

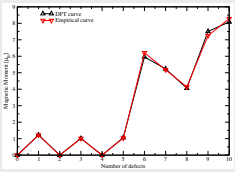

Fig. 1: Magnetic moments calculated from DFT (black curve) and obtained from the empirical equation (2) (red curve). [**5**]

We establish a relationship between the single nanoporous graphene ground-state magnetic moment and the number of dangling bonds presents in the nanopore by an empirical equation :

$$\mu_{V_n} = N_{DB}(1 + |\epsilon_{V_n}|)\mu_B \quad (1)$$

N_{DB} is the number of carbon atoms containing the dangling bonds, μ_B is the Bohr magneton and ϵ_{V_n} a dimensionless real number ($|\epsilon_{V_n}| < 1$), calculated as function of vacancy defects's number n :

$$\epsilon_{V_n} = exp(-n/a_0) - a_2 * sin(\pi\, n + a_1) + a_3 \quad (2)$$

$a_0 = 0.509306$, $a_1 = -0.123454$, $a_2 = 0.204424$ and $a_3 = 0.04$.
Moreover, our model is applies for large nanopore sizes and give good results, this has been tested for 22, 30 and 40 nanopores sizes and were in agreement with DFT results (see Table I).

Single nanoporous graphene structures

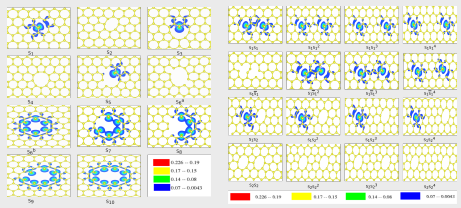

Fig.2 : Spin density distribution around single nanoporous graphene structures. The nanoporous structure S_i^j differts to S_i^k by the geometrical form. (Right) Spin density distribution around the double nanoporous structures. ([**5**].)

The calculated Local partial Density of states (LPDOS) of carbons atoms neighboring the nanopore, the 2p and 2s orbitals of S_1, S_3, S_5, S_5^0, S_7, S_8, S_9 and S_{10} nanostructures exhibit asymmetric DOS between spin-up and spin-down electrons. This can be explained by the fact that electron spins of carbon atoms neighboring each nanopore are aligned by exchange interactions which leads to a magnetic moments of 1.22, 1.01, 1.06, 5.96, 5.23, 4.06, 7.51 and 8.08 μ_B, respectively.
σ and π dangling bonds remains after the creation of the nanopores are responsible of the induced magnetism. The structures S_2, S_4 and S_6^a the 2p and 2s orbitals exhibit perfect symmetrical spin-up and spin-down DOS,

Table 1
The formation energy E_f and the total magnetic moment μ_{DFT} calculated from our DFT simulations, the estimated value μ_{V_n} calculated from equation (2) for the different nanostructures. These values are compared with previous DFT calculations E_f^* and μ^*. N_{DB} is the number of carbon atoms containing the dangling bonds while the dimensionless real numbers ϵ_{DFT} and ϵ_{V_n} are calculated from equation (2) for $\mu_{V_n} = \mu_{DFT}$ and the polynomial of equation (3) respectively. The notation for the defect systems has been described in the text.

System	n	E_f(eV)	E_f^*(eV)	N_{DB}	$\mu_{DB}(\mu_B)$	$\mu_{V_n}(\mu_B)$	$\mu^*(\mu_B)$	$\lvert\epsilon_{DFT}\rvert$	$\lvert\epsilon_{V_n}\rvert$
S_1	1	7.55	7.65 [18], 7.60 [19]	1	1.22	1.22	1.33 [18], 1.16 [19]	0.220	0.220
S_2	2	5.68	4.50 [18]	0	0.00	0.00	0.00 [18]	–	0.018
S_3	3	3.55	3.96 [18]	1	1.01	1.01	1.02 [18]	0.010	0.011
S_4	4	2.72	3.30 [18]	0	0.00	0.00	0.00 [18]	–	0.055
S_5	5	2.95	–	1	1.06	1.05	–	0.060	0.050
S_5^0	6	2.71	2.72 [18]	0	0.00	0.00	–	–	–
S_6^a	6	2.81	2.87 [18]	6	5.96	6.12	6.00 [18]	0.006	0.021
S_7	7	2.57	–	5	5.23	5.06	–	0.046	0.012
S_8	8	2.48	–	4	4.06	4.15	–	0.015	0.038
S_9	9	2.43	–	7	7.51	7.45	–	0.073	0.065
S_{10}	10	2.26	–	8	8.08	8.08	–	0.010	0.011
S_{22}	22	1.68	–	4	4.01	4.09	–	0.003	0.022
S_{30}	30	1.27	–	12	12.32	12.30	–	0.026	0.025
S_{44}	44	0.99	–	8	8.13	8.23	–	0.016	0.029
S_1S_1	2	7.27	–	2	2.55	–	–	–	–
$S_1S_1^1$	2	7.47	–	2	2.77	–	–	–	–
$S_1S_1^2$	2	7.49	–	2	2.58	–	–	–	–
$S_1S_1^3$	2	7.49	–	2	2.49	–	–	–	–
$S_1\bar{S}_1$	2	5.03	–	0	0.00	–	–	–	–
$S_1\bar{S}_1^1$	2	7.52	–	2	1.98	–	–	–	–
$S_1\bar{S}_1^2$	2	7.45	–	2	2.22	–	–	–	–
$S_1\bar{S}_1^3$	2	7.49	–	2	2.35	–	–	–	–
$S_1S_1/S_1\bar{S}_1$	3	3.45/7.09	–	1	1.16	–	–	–	–
$S_1S_1^1/S_1\bar{S}_1^1$	3	3.61/7.41	–	1	1.36	–	–	–	–
$S_1S_1^2/S_1\bar{S}_1^2$	3	3.62/7.42	–	1	1.21	–	–	–	–
$S_1S_1^3/S_1\bar{S}_1^3$	3	3.62/7.44	–	1	1.22	–	–	–	–
S_2S_2	4	2.91	–	0	0.00	–	–	–	–
$S_2S_2^1$	4	3.34	–	0	0.00	–	–	–	–
$S_2S_2^2$	4	3.50	–	0	0.00	–	–	–	–
$S_2S_2^3$	4	3.57	–	0	0.00	–	–	–	–

Electron spin densities presented above (Fig. 2), revealed that the magnetization is concentrated on C atoms around nanopores.

Double nanoporous graphene structures

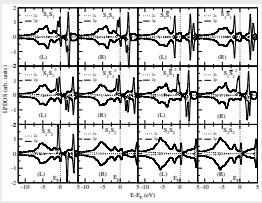

Fig. 4: Sum of local partial density of states (LPDOS) 2p and 2s for the carbon atoms surrounding each single nanopore belonging to S_iS_i. $S_iS_{\bar{i}}$, S_iS_2, S_iS_2, $S_iS_{\bar{i}}^1$ and $S_iS_i^1$. (L) and (R) stand for the left and right nanopores in these double structures

The formation energy is lesser than that of single nanopore.
However, as the separation between nanopore increases, the formation energy tends to that of isolated nanopore.
The structure $S_1\bar{S}_1$ is made of single magnetic nanopores S_1 but it's has zero magnetic moment (see Fig. 4).

Conclusion

- Induced magnetism by carbon vacancy defects in single and interacting nanopores is related to the presence of σ and π dangling bonds resulting from the creation of the vacancies making up the nanopores.
- Our empirical model predicts the total magnetic moment in single nanoporous graphene in good agreement with the DFT values.
- The interactions between nanopores in graphene play a fundamental role in its magnetic behavior.
- The magnetic properties of individual nanopores participating in the interactions appear to also have an impact on the magnetization.
- The nanopores may interact with each others resulting in an increase or total annihilation of the magnetic moment.

Acknowledgements

The computational resources are provided by the Center for High Performance Computing (CHPC) in South Africa through the MATS0988 project.

References

[1] Paolo Giannozzi, Stefano Baroni, et al., Quantum espresso: a modular and open-source software project for quantum simulations of materials, J. Phys. Condens. Matter 21 (39) (2009) 395502

[2] Paolo Giannozzi, Oliviero Andreussi, et al., Advanced capabilities for materials modelling with quantum espresso, J. Phys. Condens. Matter 29 (46) (2017) 465901.

[3] John P. Perdew, Kieron Burke, et al. Generalized gradientn approximation made simple, Phys. Rev. Lett. 77 (18) (1996) 3865.

[4] David Vanderbilt, Soft self-consistent pseudopotentials in a generalized eigenvalue formalism, Phys. Rev. B 41 (11) (1990) 7892.

[5] F. B. S. Nkou, D. H. Douma, et al., Theoretical insights into magnetization in graphene containing single and interacting nanoporous defects, Physica E: Low-dimensional Systems and Nanostructures 128 (2020) 114564

P102

Structural, Electronic, Magnetic and Thermodynamic Properties for XCrGe (X: Hf and Zr) Half-Heusler compounds: First Principle Calculations

The structural, electronic and magnetic properties of XCrGe (X = Hf and Cr) half-Heusler alloys have been studied using first principle DFT calculations by using the state of the art full-potential linearized augmented plane wave (FP- LAPW) method. Both compounds are observed to be ferromagnetic and half metallic in nature with a small band gap in their spin up (majority) channels. The magnetic moment are found to be 2 and 3μB for HfCrGe and ZrCrGe respectively and they obey the Slater-Pauling rule. Their mechanical properties show that they are mechanically stable and ductile in nature. The directional dependences of the Young's modulus, shear modulus, poisson ratio and linear compressibilty (in the xy, xz and yz planes) were presented. This theoretical investigation has clearly shown that the two materials have the potential of being used as spintronics devices.

P103

# of intermolecular interaction using Hirshfeld surface analysis and DFT calculations of chalcone derivatives

Chalcone and its derivatives are well known for their various biological activities such as anti-oxidant, anti-inflammatory, anti-bacterial, anti-fungal, anti-tumor etc. The compounds 1-(2-hydroxy-methylphenyl)-3-(2-methylphenyl)prop-2-en-1-one (I) and 1-(2-hydroxy-4-methoxy phenyl)-3-(4-ethyl- phenyl)prop-2-en-1-one (II) are chalcone derivatives. The molecule (I) crystallizes in the orthorhombic space group Pbca. The molecule (II) belongs to a primitive monoclinic system and the space group is P2 1 /c. Both the molecules exhibit intermolecular hydrogen bonds of the type O-H...O. Hirshfeld surface analysis was employed to analyze the intermolecular interactions. Hirshfeld surface is mapped over normalized contact distance d norm. The bright red and blue regions on the surface are from the contacts which are shorter and longer than the van der Waals' radii respectively. It helps in the study of the internuclear distances, angles, and crystal packing. Molecular geometry optimization and the analysis of frontier molecular orbitals HOMO and LUMO were done using density functional theoretical methods. The Hirshfeld surface analysis mapped over dnorm, and HOMO of the molecule (I) is shown in figure respectively.

P104

Title – Effect of electron-phonon interaction on Transport Properties of Lead Iodide(PbI_2) Monolayer

author- Vineet Kumar Pandey[a] Prasenjit Ghosh[ab]

[a] – Department of physics, Indian Institute of science education and research, Pune, India
[b] – Centre for energy sciences, Indian institute of science education and research, Pune, India

Abstract-

Electron-phonon interaction affects the dynamics of electrons in the crystal through renormalization of band structure and scattering of charge carriers. The real part of electron self-energy (Σ_{nk}) provides estimates of the band structure renormalization while the relaxation time (τ, measure of scattering of carriers by phonons) is obtained from the imaginary part of Σ_{nk}. These effects are known to be large for ionic materials. However, when computing transport properties of solids using Boltzmann transport equation, typically the effect of band structure renormalization is neglected. Moreover, τ is also estimated using deformation potential theory where the effect of carriers coupling with optical phonons are usually neglected.

In this work, in order to systematically understand the effect of these approximations on the transport properties of ionic solids, we have studied the effect of electron-phonon coupling (EPC) on transport properties of a monolayer of PbI_2. PbI_2 is chosen because it has very low thermal conductivity and a high density of states(DOS) at the valence band (VB) edge which might make it a plausible candidate for thermoelectric applications.

In this work, using Quantum ESPRESSO software, which is an implementation of density functional theory (DFT) and electron-phonon Wannier (EPW) code, we have studied the effect of electron-phonon interactions on electronic band structure and transport properties of PbI_2 monolayer. We notice that electron-phonon interactions significantly modifies the band structure and reduces the bandgap for PbI_2 monolayer owing to the strong coupling of the optical vibrational mode where motion corresponds to compression and expansion of the monolayer in the direction normal to its plane. These are further enhanced with the increase in temperature owing to the increase in phonon population. This leads to strong carrier scattering which results in reduced carrier relaxation time at high temperature. From the calculation of the transport properties with the renormalized band structure, we notice that a significant amount of electrical conductivity can be achieved even upon low doping. Further the electrical conductivity upon heavy doping owing to suitable modification in the band curvature. Unlike electrical conductivity, band gap renormalization reduces Seebeck coefficient significantly in the low doping region. Further decrease of Seebeck coefficient is obtained as we go for heavy doping due to strong electron-phonon interactions. The thermoelectric power factor of PbI_2 monolayer is significantly enhanced owing to the increase in electrical conductivity.

Thus our results reveal that it is crucial to include electron-phonon interaction in transport properties of PbI_2 monolayer.

P105

Cubic Phase Stability of Mixed-cation Perovskites: DFT calculations and machine-learning prediction

Heesoo Park[1], Adnan Ali[1], Raghvendra Mall[2], Halima Bensmail[2], Brahim Aïssa[1], Stefano Sanvito[3], Abdelhak Belaidi[1], and Fedwa El-Mellouhi[1*]

[1] *Qatar Environment and Energy Research Institute, Hamad Bin Khalifa University, P.O. BOX 34110, Doha, Qatar*
[2] *Qatar Computing Research Institute, P.O. BOX 34110, Hamad Bin Khalifa University, Doha, Qatar*
[3] *School of Physics, AMBER and CRANN Institute, Trinity College, Dublin 2, Ireland*

Mixing cations is a successful perovskite synthesis strategy to improve the perovskites' thermodynamic stability as well as their crystallographic phase and lattice parameter control [1,2]. Unfortunately, the relation between a given cation mixture and the associated structural deformation is not established linearly, hindering the identification of adequate chemical compositions from achieving optimal photovoltaic performance. Such challenges to control the synthesis of cubic-phase perovskites arise from the fact that local distortions and microscopic disorder influence the structural stability, besides, in some cases, phase segregation.

Material synthesis acceleration is nowadays surging due to exploring chemical composition spaces guided by machine-learning (ML) models. In this work, we have built an extensive database of mixed-cation perovskites based on planewave density functional theory calculations followed by an iterative training of ML models based on increasingly large and diverse chemical compositions aiming at perovskite synthesis acceleration. Halide perovskites ($A_xA_{(1-x)}MX_3$) consist of the monovalent cation (A and A' or their mixtures), divalent metal cation (M), and halide (X). Our supercells were built by varying the ratios of the A/A′-cations mixture by using $2 \times 2 \times 2$ supercells consisting of up to 104 atoms. Our database consists of 1864 unique compositions and accounts for all the relevant local distortions of the BX_6 octahedra induced by the cation mixture. We will discuss the performance of different models by applying linear regression, XGBoost as well as Neural network. Our optimal ML model allows us to determine the cubic phase stability at a given cation mixture regardless of the various cations' pair and concentration, even assessing very dilute concentrations [3]. We validated the optimal ML model by comparing the synthesized perovskite thin-films by analyzing them with XRD, SEM, absorption spectrum. Our work illustrates that an efficient ML modelling approach can significantly guide conventional or self-driving autonomous experimental laboratories that adopt this strategy for novel materials discovery.

Acknowledgements: This work is sponsored by the Qatar National Research Fund (QNRF) through the National Priorities Research Program (NPRP8-090-2-047 and NPRP12S-0209-190063) and by the Qatar Environment and Energy Research Institute (FE). Computational resources have been provided by the research computing group at Texas A&M University at Qatar. We are grateful to QEERI core labs for the XRD and SEM characterizations.

[1] Park et al. "Importance of Structural Deformation Features in the Prediction of Hybrid Perovskite Bandgaps" *Comput. Mater. Sci*., **2020**, *184*, 109858. https://doi.org/10.1016/j.commatsci.2020.109858
[2] Ali et al. "Machine Learning Accelerated Recovery of the Cubic Structure in Mixed-Cation Perovskite Thin Films" *Chem. Mater*., **2020**, *7*, 2998. https://dx.doi.org/10.1021/acs.chemmater.9b05342
[3] Park et al. "Data-driven Enhancement of Cubic PhaseStability in Mixed-cation Perovskites" *Machine Learning: Science and Technology*, **2021** https://doi.org/10.1088/2632-2153/abdaf9

P106

Ab-initio study of $CsPbCl_3$ and Mn-doped $CsPbCl_3$ monolayers as solar cell absorbers

Manushi J. Patel[a], Sanjeev K. Gupta[b], P. N. Gajjar[a,*]

[a]Department of Physics, University School of Sciences, Gujarat University, Ahmedabad,380 009, Gujarat, India

[b]Computational Materials and Nanoscience Group, Department of Physics and Electronics, St. Xavier's College, Ahmedabad,380 009, Gujarat, India

**Corresponding author: pngajjar@gujaratuniversity.ac.in*

Abstract

Inorganic perovskites are nowadays studied extensively because of their unique photovoltaic properties. Here study of band structures, total density of states (TDOS), partial density of states (PDOS) and vibrational properties of $CsPbCl_3$ and Mn-doped $CsPbCl_3$ monolayers have been done from density functional theory (DFT) point of view. The absence of imaginary frequencies in the phonon dispersion curve of unit cell of $CsPbCl_3$ monolayer shows its dynamical stability. The wide bandgap of $CsPbCl_3$ monolayer limits its application as absorber layer in solar cells. Therefore, in order to reduce the bandgap of this monolayer Mn has been doped at Pb-site, which not only reduces the concentration of toxic Pb but also decreases the band gap of the monolayer. Reason behind reduction of band gap in Mn-doped $CsPbCl_3$ monolayer is the creation of intermediate states due to Mn-3*d* state. Also the efficiencies of $CsPbCl_3$ and Mn-doped $CsPbCl_3$ monolayers have been obtained using Shockley-Queisser (SQ) limit and is seen that efficiency of Mn-doped $CsPbCl_3$ monolayer is quite enhanced compared to pristine $CsPbCl_3$ monolayer.

Computational Details

- **SIESTA code**
- **Calculations of exchange and correlation energies using GGA-PBE.**
- **Double zeta polarization.**
- **10x10x1 Monkhorst k-grid and energy cut-off 300 Ry.**
- **Optimization of monolayers until force on each atom was less than 10^{-2} eV/Å.**

Materials	Jsc (A/m²)	Voc (eV)	η (%)
$CsPbCl_3$ monolayer	9.94	2.84	2.48
Mn-doped $CsPbCl_3$ monolayer	526.10	0.62	25.99

Crystal structure

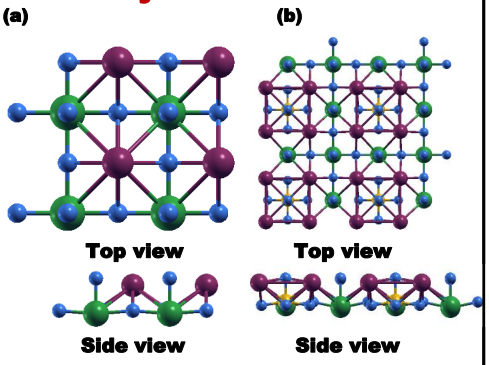

Fig 1: (a) Top and side view of $CsPbCl_3$ monolayer. (b) Top and side view of Mn-doped $CsPbCl_3$ monolayer. Here Mn is doped at Pb-site.

Vibrational property

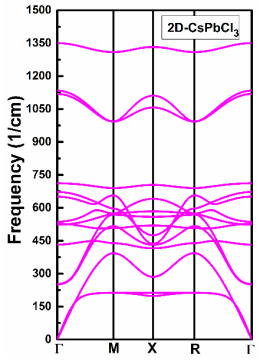

Fig 2: Phonon dispersion curve of 2D- $CsPbCl_3$.

J-V characteristics

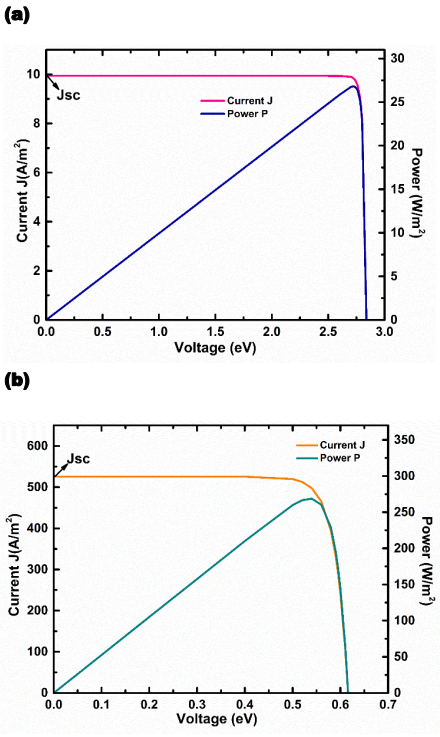

Fig 3: J-V characteristics and Power density of (a) $CsPbCl_3$ monolayer and (b) Mn-doped $CsPbCl_3$ monolayer.

Band structure, TDOS and PDOS

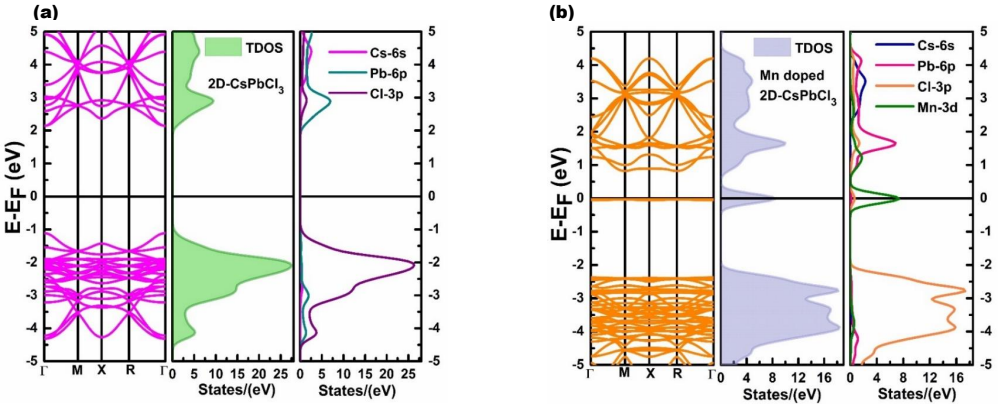

Fig 3: Band structure, TDOS and PDOS of (a) $CsPbCl_3$ monolayer and (b) Mn-doped $CsPbCl_3$ monolayer.

Conclusions

- **Thus it is seen that the doping of Mn at Pb-site in $CsPbCl_3$ monolayer not only decreases the concentration of toxic Pb but also increases the value of Jsc effectively which in turn increases efficiency of Mn-doped $CsPbCl_3$ monolayer.**
- **Therefore, it can be said that Mn-doped $CsPbCl_3$ monolayer is suitable candidate as absorber layer in solar cells.**

Acknowledgement

The computer facility and support under DST-FIST Level-I (No.SR/ FST/PSI-097/200 dated 20th December 2006 and No.SR/FST/PSI198/2014 dated 21 November 2014) programs of Department of Science and Technology, Government of India, New Delhi, India and DRS-SAP-I,II (No. F-530/10/DRS/2010 (SAP-I) dated November 2010 and No.F.530/17/DRS-II/2018 (SAP-I), dated 17th April 2018) of University Grants Commission, New Delhi, India are sincerely acknowledged. M.J.P would like to thank education department of Gujarat state for providing ScHeme of Developing High Quality Research (SHODH) fellowship.

References

1) **J.M. Soler, E. Artacho, J.D. Gale, A. Garcia, J. Junquera, P. Ordejon, D.S. Portal, J. Phys.: Condens. Matter 14 (2002) 2745-2779.**
2) **J.P. Perdew, A. Ruzsinszky, G.I. Csonka, O.A. Vydrov, G.E. Scuseria, L.A. Constantin, X. Zhou, K. Burke, Phys. Rev. Lett. 100 136406 (2008) 1-4.**
3) **N. Pandey, A. Kumar, S. Chakrabarti, RSC Adv., 9 (2019) 29556-29565.**
4) **N.N. Som, V. Sharma, V. Mankad, M.L.C. Attygalle, P.K. Jha, Sol Energy, 193 (2019) 799-805.**
5) **Bercx M., Saniz R., Partoens B., Lamoen D. (2018) Exceeding the Shockley–Queisser Limit Within the Detailed Balance Framework. In: Angilella G., Amovilli C. (eds) Many-body Approaches at Different Scales. Springer, Cham. https://doi.org/10.1007/978-3-319-72374-7_15**

P107

Electronic and magnetic properties of well defined Gr/Co/Ir(111) and Gr/Fe/Ir(111) heterostructures

Graphene’s coupling to ferromagnetic systems opens perspectives of efficient injection of spin-polarized electrons owing to graphene's long spin-diffusion lengths, gate-tunable carrier concentration, and high electronic mobility. Despite the large research effort dedicated t o Gr-metal heterostructures, only a few experimental results for graphene grown on Fe and Co surfaces are available, even Fe's cost is lower than other transition metal substrates and, most importantly, and it has a strong magnetic response. Here we report on the structural, electronic and magnetic properties of Fe and Co intercalation under graphene grown on Ir(111). We show that a ferromagnetic monolayer of Fe or Co can be successfully sandwiched between graphene and Ir, enhancing graphene’s corrugation while preserving the moiré structure. First principles electronic structure calculations and angular resolved photoelectron spectroscopy measurements show the redistribution of the electronic states due to the graphene/metal hybridization. X-Ray Magnetic Circular Dichroism the ferromagnetic response of the confined Fe and Co layers. In the case of Fe, there is an enhancement of the spin- and orbital-configurations with respect to the bcc-Fe bulk value, showing that graphene acts not only as a protective membrane, but also promotes a ferromagnetic order of the Fe layer.

P108

First-principles study of exchange-induced valley splitting in transition metal dichalcogenide monolayers

Monolayer transition metal dichalcogenides (TMDs) with spin-valley coupling are an emerging class of materials for valleytronics applications. Magnetic substrates have been shown to produce larger valley splitting than magnetic fields. In this work, we develop intuition for the physical mechanism driving valley splitting via magnetic substrates by performing first-principles density functional theory calculations for a series of Fe-decorated WSe2 and MoS2 monolayers. The valley splitting is computed as a function of different Fe heights above the TMD surface, different Fe alignment, and different Fe coverages. The non-Zeeman-like behavior of the valence band eigenvalues in the presence of variable magnetic atom position are rationalized using a magnetic impurity Hamiltonian, where the DFT trends in valley splitting can be recovered to second-order in the magnetic exchange coupling, a term that is strongly sensitive to TMD-4/5d-Fe 3d orbital overlap. These computed trends are used to rationalize prior experiments involving magnetic exchange coupling-induced valley splitting, and are used to suggest new substrates to achieve large valley splitting.

P109

Band-insulators with an odd numbers of electrons per unit cell and a restricted KS method for spin polarised systems

Conventional band theory suggests that the ground state of periodic systems with an odd number of electrons is metallic and that in order to open a band-gap in these systems it is necessary to double the unit cell, either by dimerisation of the chain (Peierls distortion) or by antiferromagnetism or both. Famously, band-theory fails to predict the insulating behaviour of Mott insulators, with the hydrogen chain as the archetype example. In fact, the well-known argument that a material with an odd number of electrons per unit cell has a metallic band structure strictly refers to a non-magnetic ground state and this poster shows how we can use spin-DFT methods to find insulating behaviour using only a primitive unit cell containing an odd number of electrons, by allowing for magnetic ground states. In our applications we use LSDA and spin PBE to study the metal-insulator transitions for a 3-dimensional lattice of hydrogen atoms under increasing atomic separation. Finally, a restricted Kohn-Sham (KS) method for performing spin-dependent calculations will be presented in which a common KS potential is used for both spin-up and spin-down electrons. This provides a simplified model with results similar to unrestricted spin-DFT for simple systems.

P110

Half-metallic ferromagnetism in XRuMnGa (X = Co & Ni) quaternary Heusler alloys -DFT study by using generalized gradient approximation (GGA) and modified Becke Johnson (mBJ) methods

Roshme P and * *G. Kalpana*

Department of Physics, Anna University, Chennai-25, India.

Abstract

The structural, electronic and magnetic properties of quaternary Heusler XRuMnGa (X = Co & Ni) alloys have been studied using FP–LAPW method within (GGA) and (mBJ) approximations. From the spin polarised total energy calculations, it is found that both the alloys XRuMnGa (X= Co & Ni) are stable in ferromagnetic (FM) phase. The spin-polarized energy bands of these alloys show that the majority spin channel has metallic nature and the minority spin channel has a semiconducting nature. Among the GGA and mBJ approximations used, mBJ approximation is found to enhances the band gap value. The obtained results show that CoRuMnGa and NiRuMnGa has a minority band gap of 0.063eV and 0.077eV with a half-metallic gap of 0.016eV and 0.014eV respectively. The total magnetic moment for CoRuMnGa and NiRuMnGa are 3.0 μB and 4.0 μB per formula unit respectively at their equilibrium volume. The integer magnetic moment confirms half-metallicity. Investigation of density of states of these compounds indicates that the magnetic moment mainly originates from the strong spin-polarization of 3*d* like states of Mn and partial contribution of 3*d* electrons of both Ru, Co and Ni atoms. From the calculated properties CoRuMnGa alloy shows promising feature for spintronics applications.

Keywords: spintronics, quaternary Heusler alloys, half metallic ferromagnetic.

*Corresponding- author
Email: g_kalpa@yahoo.com

P111

Tunable spin Hall and spin Nernst effects in Dirac nodal line semimetals XCuYAs (X=Zr, Hf; Y=Si, Ge)

Babu Baijnath Prasad [1,2] and Guang-Yu Guo [1,3,*]

[1]Department of Physics and Center for Theoretical Physics,
National Taiwan University, Taipei 10617, Taiwan

[2]Nano Science and Technology Program, Taiwan International
Graduate Program, Academia Sinica, Taipei 11529, Taiwan

[3]Physics Division, National Center for Theoretical Sciences,
Taipei 10617, Taiwan

XCuYAs (X=Zr, Hf; Y= Si, Ge) compounds have unique physical properties ranging from p-type transparent semiconductors to iron-based superconductors. So, we have studied the electronic structure, spin Hall and spin Nernst effects in these compounds based on DFT calculations. First, we have found the nonsymmorphic symmetry-protected Dirac line nodes along the Brillouin zone boundary A-M and X-R for the XCuYAs compounds having low density of states near the Fermi level. Second, the spin Hall and spin Nernst conductivities in some of these compounds are found to be large, e.g., the SHC and SNC (at room temperature) of HfCuGeAs are found to be as large as -514 (ħ/e)(S/cm) and -0.73 (ħ/e)(A/m-K), respectively. Also, the magnitude and sign of the SHC and SNC can be tuned via changing either applied electric field direction, spin current direction or by chemical doping or gating. A detailed analysis of the band-decomposed and k-resolved spin Berry curvatures reveals the origin of the such large values of SHC and SNC among these set of materials. Spin-orbit coupling gapped Dirac points near the Fermi level as well as gapless Dirac line nodes are the main source of origin for the XCuYAs compounds in exhibiting large spin Hall and spin Nernst conductivities. In conclusion, our findings thus not only provide a valuable platform for the interplay between band topology, SHE and SNE in the XCuYAs compounds, but they also have promising applications in spintronics and spin caloritronics.

Reference :-

1. Babu Baijnath Prasad and Guang-Yu Guo*, Tunable spin Hall and spin Nernst effects in Dirac line-node semimetals XCuYAs (X=Zr, Hf; Y=Si, Ge), Phys. Rev. Materials **4**, 124205 (2020).
[DOI: 10.1103/PhysRevMaterials.4.124205]

P112

In Silico prediction of antibacterial activity of sesquiterpene lactones using density-functional theory and quantitative structure-activity relationship methods

Fabián Puga*[1], Alicja Mikolajczyk[2], Paola E. Ordoñez[3] and Henry P. Pinto[3].
1 CompNano Group, School of Physical Sciences and Nanotechnology, Yachay Tech University, Ecuador
2 Laboratory of Environmental Chemometrics, University of Gdansk, Poland
3 School of Chemical Sciences and Engineering, Yachay Tech University, Ecuador

UNIVERSIDAD YACHAY TECH
ESCUELA DE CIENCIAS FÍSICAS Y NANOTECNOLOGÍA

Introduction

The growing resistance developed by bacteria to medicines is a problem that involves every social stratum; therefore, the development of new and effective anti-bacterial components is of vital importance for our society. *Sesquiterpene lactones* (STL) are a group of secondary metabolites isolated from plants that have shown a wide spectrum of biological activities including antimicrobial, antifungal, anti-inflammatory and anticancer. Unfortunately, the experimental methods to study the effectiveness of plant-based antibiotics are expensive and time consuming. An alternative to tackle these limitations is performing *in silico* studies of these molecules in order to predict their antibacterial activity. In this work computational studies combines quantum mechanical calculations at both levels semi-empirical tight binding and *ab~initio* density-functional theory (DFT) with appropriated hybrid functionals to predict the most energetically favorable conformers, their atomic and electronic structure, and physical chemical properties of the molecules. These computed values are processed on a quantitative structure-activity relationship (QSAR) models considering antibacterial activity. The obtained results on the training set of the *sesquiterpene lactones* molecules will allow us to propose and find more effective anti-bacterial *sesquiterpene lactones*-based compounds.

Methods

Twenty STL were selected based on the available documentation on the general structure of each molecule and its antibacterial activity. The first step is to computed the energetically favorable conformers and rotamers of each molecule using the Conformer – Rotamer Ensemble Sampling Tool (CREST) code that implements an efficient semi-empirical quantum mechanical method and xTB tight-binding method [1]. Since there can be several conformers for a molecule, those with more statistical weight and lower energy (most energetically favorable) were selected. Once the conformers have been identified, each selected structure is computed using *ab~initio* density-functional theory (DFT) as implemented in the ORCA [2]. The level calculation used hybrid functional B3LYP within the RIJCOSX approximation with def2-TZVPP basis set, def2/J auxiliary basis set and D3 for atom-pairwise dispersion correction. The obtained results were used to perform QSAR models which are a smart multidimensional fitting process capable to provide reliable predictions on the biological activity of these molecules on MRSA. In order to get the best fitting, different combinations of descriptors are performed giving different equations and correlation coefficient. Finally, the selected model will depend on the correlation coefficient and the relation between descriptors and toxicity.

Results

After full relaxation, the electronic structure was computed to obtain: the total energy, the electronic energy, the core–core repulsion energy, the energy of the highest occupied molecular orbital (HOMO), the energy of the lowest unoccupied molecular orbital (LUMO), the HOMO-LUMO energy gap (*Eg*), the dipole moment (*p*), the quadrupole moment (*Q*) and the polarizability α. All these values are tabulated in Table 1.

Mol	E_T	p	Q	α	E_e	E_{c-c}	HOMO	LUMO	E_g
1C1	-809,148	2,622	-84,427	176,831	-2228,420	1419,353	-0,249	-0,056	0,193
2C1	-807,952	1,887	-82,925	171,695	-2224,996	1417,122	-0,246	-0,058	0,187
3C1	-806,784	2,808	-80,323	175,883	-2180,431	1373,724	-0,238	-0,067	0,171
4C1	-808,014	1,472	-85,506	179,630	-2178,009	1370,071	-0,242	-0,066	0,176
5C1	-732,735	2,038	-78,493	173,552	-1976,871	1244,211	-0,250	-0,054	0,196
6C1	-769,855	2,405	-80,397	171,817	-2013,880	1244,099	-0,244	-0,055	0,189
7C1	-1115,691	1,717	-111,640	222,650	-3473,875	2358,299	-0,251	-0,060	0,190
8C1	-807,976	1,013	-88,877	194,548	-2088,269	1280,366	-0,248	-0,080	0,168
9C1	-804,3936	1,758	-82,465	216,219	-2039,560	1235,233	-0,224	-0,111	0,113
9C2	-804,3932	1,738	-82,522	216,272	-2038,595	1234,267	-0,225	-0,111	0,114
10C1	-883,210	1,517	-87,172	173,892	-2460,788	1577,663	-0,256	-0,066	0,189
11C1	-960,794	2,271	-91,429	181,086	-2820,069	1859,367	-0,264	-0,001	0,262
12C1	-883,202	1,208	-86,376	174,526	-2479,066	1595,950	-0,258	-0,069	0,189
13C1	-1187,2517	1,829	-111,392	230,787	-3582,943	2395,795	-0,255	-0,066	0,189
13C2	-1187,2519	1,682	-111,931	229,131	-3570,320	2383,172	-0,255	-0,065	0,189
14C1	-1456,847	2,444	-137,866	273,108	-4824,952	3368,243	-0,266	-0,088	0,178
14C2	-1456,846	2,496	-137,774	272,712	-4824,410	3367,701	-0,268	-0,088	0,179
15C1	-883,217	2,415	-88,628	182,558	-2413,820	1530,685	-0,253	-0,066	0,187
16C1	-883,219	2,432	-90,903	182,392	-2406,950	1523,813	-0,256	-0,068	0,187
16C2	-883,216	2,150	-90,647	183,797	-2395,546	1512,410	-0,256	-0,067	0,189
17C1	-1153,769	1,748	-112,731	234,708	-3634,849	2481,199	-0,255	-0,067	0,187
17C2	-1153,769	1,669	-112,572	233,191	-3631,054	2477,403	-0,254	-0,067	0,187
18C1	-1193,076	1,684	-116,937	249,757	-3823,539	2630,587	-0,253	-0,066	0,187
19C1	-1263,6289	1,825	-114,863	231,608	-3884,198	2620,684	-0,263	-0,058	0,204
19C2	-1263,6288	1,736	-114,951	230,541	-3881,459	2617,945	-0,263	-0,069	0,202
20C1	-1262,4611	2,474	-123,515	234,520	-3723,665	2461,311	-0,278	-0,076	0,201
20C2	-1262,4614	2,506	-122,789	234,104	-3732,371	2470,016	-0,278	-0,077	0,201

Table1. DFT-B3LYP computed properties for selected conformers of studied molecules: total energy *ET*, dipole moment *p*, quadrupole moment *Q*, polarizability α, electronic energy *Ee*, core–core repulsion energy *Ec–c*, HOMO, LUMO, HOMO-LUMO energy gap *Eg*. In this table, p, Q and α are in a.u. and the energies in Eh

Results

Different QSAR models were carried out using different combinations of 2 descriptors. Eq 1 is the equations of the most accurate QSAR model and is sketched in Fig 1. the equation was:

$$log(MRSA) = -6,6680 - (34,4472 * HOMO) + (5,3502e^{-06} * Eg)$$

Eq 1. Resulting equations of the best fitting process.

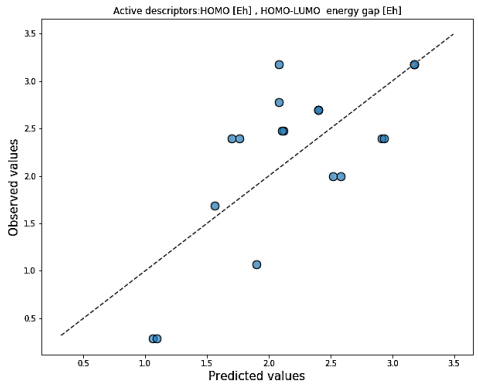

Fig 1. Graphic of the multilinear regression (Eq 1)

Conclusions and future work

- The calculations for the twenty molecules were carried out using xTB-CREST and the most energetically favorable conformers were selected and computed with ab initio DFT using ORCA at B3LYP level.
- The internal energy, dipole moment, quadrupole moment, polarization, electronic energy, nuclear repulsion, HOMO, LUMO and gap energy were calculated.
- The quantum mechanical computed properties are combined with experimental values of biological activity in a quantitative structure-activity relationship modeling (QSAR) [3].
- Preliminary QSAR results tested a variety of combinations which criteria used only two independent descriptors according to Table 1. Interestingly, among all the tested models, the best yields a $R^2 = 0,52$ that correlates HOMO energy and HOMO-LUMO energy as descriptors.
- These results suggest a relation between band gap energy and the mechanism of toxic actions: the smaller the band gap the easier is to detach one electron from the molecule that could migrate inside the bacteria producing free radicals that can damage and eventually contribute to kill the bacteria.
- Finally, the development of more affective descriptors to better describe the toxicity of Sesquiterpene lactones is needed; we are aware that more extensive exploration of parameters is needed to find the best correlation with the observed toxicity, this work is underway.

Acknowledgments

Fabian Puga and Henry Pinto thanks for the support of the School of Physical Sciences and Nanotechnology at YachayTech University.

References

1. S. Grimme, J. Chem. Theory Comput. 13, 1989–2009 (2017).
2. F. Neese, Rev.: Comput. Mol. Sci 2, 73–78 (2012).
3. T. Puzyn et al., Nature nanotechnology 6, 175 (2011).

P113

Ultrahigh carrier mobility and Strain Enhancement properties of 2D penta-PdX2 (X= As, P monolayer: A DFT study

Dhara Raval[1], Bindiya Babariya[2], Sanjeev K. Gupta[3] and P. N. Gajjar[4]

[1,2,4] Department of Physics, University School of Sciences, Gujarat University, Ahmedabad-380009, Gujarat, India

[3] Computational Materials and Nanoscience Group, Department of Physics, St. Xavier's College, Ahmedabad 380009, India

Abstract

In this study, we have investigated the geometrical and electronic properties of penta-PdX2 (X=As, P) using density functional calculation. The electronic structure calculations show that the penta-PdAs2 and PdP2 are semiconductors with direct band gaps of 0.34 eV and 0.30 eV, respectively. The dynamical stability of penta-PdX2 monolayer is proved by the absence of imaginary frequencies in the phonon dispersion curve. By applying a biaxial strain (for PdAs2 : - 6% to +6% and for PdP2 : -5.5% to +5.5%) on the monolayer, the effective mass and band edges are tuned effectively. Remarkably, the range of penta-PdX2 carrier mobility was obtained in an extremely high ~ 5,499,000 $cm^2 v^{-1} s^{-1}$ for holes and 43,120 $cm^2 v^{-1} s^{-1}$ for electrons. Our work would stimulate the fabrication of penta-PdX2 monolayer and it is envisioned that it is an appropriate future candidate for optoelectronic and ultra-fast electronic applications.

Results and Discussion

Stability of PdX2

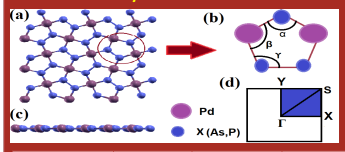

Phonon density of states

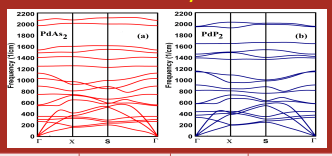

Penta-PdX_2	Angle of Pd-X-Pd α (deg)	Angle of X-Pd-X β (deg)	Angle of Pd-X-X γ (deg)	Lattice parameter (Å)	Bond length of X-X (Å)	Bond length of Pd-X (Å)	Cohesive Energy E_{coh} (eV/atom)
$PdAs_2$	128.657	90	115.677	6.295	2.31	2.46	-3.6364
PdP_2	126.042	90	116.98	6.032	2.09	2.39	-4.0979

Electronic properties

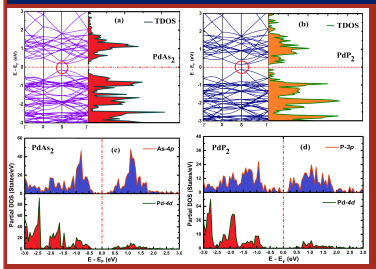

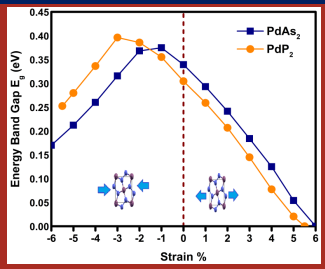

Figure 1. (Colour online) Electronic band structure and total density of states (TDOS). (a) For penta-$PdAs_2$ monolayer and (b) for penta-PdP_2 monolayer. The partial density of states (PDOS). (c) For penta-$PdAs_2$ monolayer and (d) for penta-PdP_2 monolayer. The Fermi level (E_F) is shifted at the zero energy as represented by the red dashed line. Figure 2. Energy band gap vs Strain %.

Acknowledgement

- ✓ I am thankful to my guide, Prof. P. N. Gajjar , for providing various facilities and Support during my research work.
- ✓ Research facility provided by the Department of Physics and computer facility developed under DST- FIST Level–I & DRS-SAP-I programme (New Delhi) is also acknowledged.
- ✓ I am also thankful for the project fellowship under DSR – II – SAP , dated 17/04/2018 of university Grants commission, New Delhi.

Introduction

- Research on 2D materials has grown exponentially, due to their unique physical, electronic, chemical and optical properties. From the last two decades, many of the 2D materials such as transition metal dichalcogenides (TMDCs), hexagonal boron nitride (h-BN), silicene, phosphorene and arsenene have been explored for nanodevices applications.
- Jing *et al.*[1] have reported the carrier mobility of GeP_3, 8.84 ×10^3 $cm^2 v^{-1} s^{-1}$ for holes and 8.48×10^3 $cm^2 v^{-1} s^{-1}$ for electrons. Yao *et al.*[2] have also predicted the carrier mobility of SbP_3 and GaP_3 monolayer, where SbP_3 monolayer has high electron mobility of 1600 $cm^2 v^{-1} s^{-1}$ and 2700 $cm^2 v^{-1} s^{-1}$ along the armchair and zigzag directions, respectively.
- Generally, these 2D materials exhibit the hexagonal phase. Nevertheless, 2D materials fully constructed have been reported in the pentagonal structure having unique electronic and optical properties such as high carrier mobility.
- Therefore, it is now the right time to investigate other novel two dimensional materials, which also have a moderate band gap, higher carrier mobility and other imperious properties.

Methodology

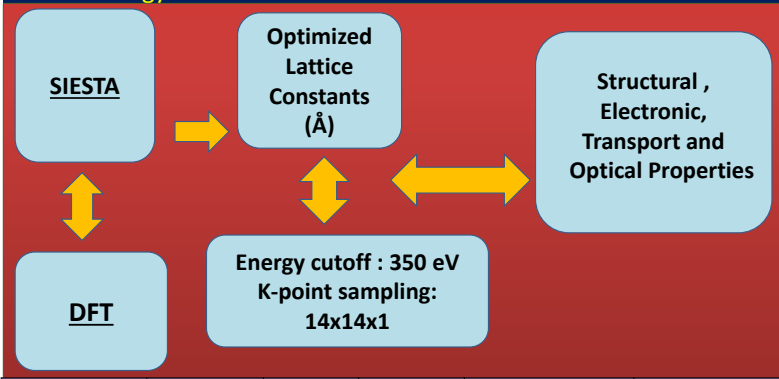

System	Carrier type	m*/me	C_{2D} (J/m^2)	E_1 (eV)	μ (x10^4 $cm^2 v^{-1} s^{-1}$)
$PdAs_2$	electron	0.30	263	-1.15	2.99
	hole	0.06	263	1.17	54.11
PdP_2	electron	0.13	277	-2.20	4.312
	hole	0.07	277	2.17	14.60

Conclusion

- ❖ In conclusion, we have explored the geometrical and electronic properties of penta-PdAs2 and penta-PdP2 monolayer with the first principles simulations. The positive phonon frequencies establish it's dynamically stability. The PdX2 (X= As, P) is a semiconductor with a direct narrow band gap of 0.30 and 0.34 eV, respectively.
- ❖ The density of states of the valence band is mainly formed by the 'd' orbital of the Pd metal atom and 'p' state of X-atom in the PdX2 monolayer. The electronic and optical properties could be affectively tuned by the applied biaxial strain.
- ❖ The hole mobility (~ 5.499 x105 $cm^2 v^{-1} s^{-1}$) of PdAs2 is much higher than the electron mobility of PdAs2 monolayer and difference between both carrier (electron or hole) mobilities is beneficial for separation of carriers in the photocatalytic applications.

References

[1] Y. Jing, Y. Ma, Y. Li and T. Heine, GeP_3: A small indirect band gap 2D crystal with high Carrier mobility and strong interlayer quantum confinement, Nano Lett., 2017, **17(3)**, 1833-1838.

[2] S. Yao, X. Zhang, Z. Zhang, A. Chen and Z. Zhou, 2D Triphosphides: SbP_3 and GaP_3 monolayer as promising photocatalysts for water splitting, Int. J. Hydrog. Energy, 2019, **44(12)**, 5948-5954.

P114

Pressure-induced Phase Transitions in Fe_4N

Sourabh Barua[1], Bohnni Shikha Biswas[2], Andrew C. Burgess[3], Jaime Dolado[4], Abdelali Elomrani[5], Wouter Heyvaert[6], Sri K[7], Victor Landgraf[8], Lórien MacEnulty[9], Stepan Marek[10], Adesh Rohan Mishra[11], Anoop A Nair[12], Riccardo Reho[13], Ahmed Subrati[14], Fatemeh Tabatabaei[15], Gulsum Efsun Tekneci[16], Seppe Van Dyck[17], Antonio Vázquez-López[18], Manoj Warrier[19] and Stefaan Cottenier[20]

[1]Department of Physics, Birla Institute of Technology Mesra, Ranchi, India, [2]Department of Physics, Jadavpur University, Kolkata, India, [3]School of Physics, Trinity College Dublin, The University of Dublin, Ireland, [4]Departamento de Física de Materiales, Universidad Complutense de Madrid, 28040, Spain, [5]Laboratoire de recherche en Science des Matériaux, des Mathématiques et de la Modélisation (LS3M), Université Sultan Moulay Slimane, Faculté Polydisciplinaire Béni Mellal, Morocco, [6]Department of Physics, University of Antwerp, Belgium, [7]Australia, [10]Department of Condensed Matter Physics, Charles University, Prague, Czech Republic, [8] Technical University Delft, the Netherlands ,[11]Department of Metallurgical and Materials Engineering, National Institute of Technology Roukerla,India, [12]Indian Institute of Science Education and Research - Thiruvananthapuram, [13]Debye Institute for Nanomaterials Science, Condensed Matter and Interfaces, University of Utrecht, Utrecht, Netherlands, [14]NanoBioMedical Centre, Adam Mickiewicz University, Wszechnicy Piastowskiej 3, 61614 , Poznan, Poland, [15]Université Claude Bernard Lyon 1, CNRS, Institut Lumière Matière, F-69622, Villeurbanne, France, [16]Izmir, Turkey, [17]Ghent University, Ghent, Belgium, [18]Departamento de Física de Materiales, Universidad Complutense de Madrid, 28040, Spain, [19]Bhabha Atomic Research Center, Visakhapatnam, India, [20]Center for Molecular Modeling & Department of Electromechanical, Systems and Metal Engineering, Ghent University, Ghent, Belgium,

γ'-Fe_4N is a magnetic alloy with a highly symmetric cubic structure that has been studied for decades and is applied, for instance, as a coating on steel and as a component in magnetic devices [1]. An analysis of the phonon band structure under applied pressure has recently pointed out a structural instability (soft mode), resulting in a phonon-induced phase transition at a few GPa [2]. The analysis in Ref. [2] is ambiguous in some respects, and therefore we performed an exhaustive analysis of all distortions that are consistent with the soft modes. Several of them were found to be stable and have energies that compete with the high-symmetry ground state structure at zero pressure. A scrutiny of these crystals shows that γ'-Fe_4N can lower its energy either by displacing some atoms or by modulating the magnetic moments, often opting for a combination of both. The total magnetization of these distorted cells is significantly smaller than that of the stable phase at 0 GPa γ'-Fe_4N. In addition, it is suspiciously close to the experimentally observed magnetization. Therefore, we speculate that these reduced-symmetry solutions may be relevant for the experimentally observed Fe_4N phase as well.

This work is being carried out by an *ad hoc* consortium of 20 former participants of an open online course on computational materials physics [3,4], as a spin-off of a course project that turned out to have particularly interesting results.

[1] E.L. Peltzer y Blancá et al., Phys. Status Solidi B 246 (2009) 909–928 (2009) (https://doi.org/10.1002/pssb.200844401)

[2] T. Cheng et al., Journal of Magnetism and Magnetic Materials 451 (2018) 87–95

[3] www.compmatphys.org

[4] https://youtu.be/LqoXYCDu-kw

P115

First principles calculation of the Hall coefficient in the high-temperature isotropic scattering-time limit

The Hall coefficient in the weak magnetic field semiclassical limit can be obtained using the geometrical construction of N. P. Ong (Phys. Rev. B 43, 193, 1991) in terms of the Stokes area swept out by the scattering path length vector on moving around the Fermi surface perimeter. We implement Ong's relationship within the Pyprocar software suite (Comput. Phys. Commun. 251, 107080, 2020) and use first-principles calculations to compute the Hall coefficient of copper and SrVO3, a prototypical strongly correlated system with a simple perovskite structure and isolated d-electron bands. For copper and SrVO3 we compute the Hall coefficient along specific crystallographic directions and find good agreement with transport measurements in the high-temperature isotropic scattering-time limit.

P116

RPA-OEP for solids

Stefan Riemelmoser[1], Merzuk Kaltak[2], Georg Kresse[1]
[1]University of Vienna, [2]VASP Software GmbH

Introduction

The optimized potential method (OEP) presents an unambiguous way to map an energy functional from many-body perturbation theory (MBPT) to a local exchange-correlation potential. The OEP framework combines in a sense the best of both DFT and MBPT worlds. It has all the formal and practical benefits of a local Kohn-Sham potential, whereas from MBPT it inherits the transparency of the Feynman diagrammatic representation and with it the possibility to obtain ever better approximations by taking higher order diagrams into account. Amongst other things, accurate KS potentials obtained in this way can serve as testing ground for lower-level approximations and starting points for various MBPT methods.

RPA-OEP method

- Unique mapping $\Sigma_{xc} \rightarrow v_{xc}$ (up to a constant) by the OEP equation [1]

$$\chi_0(1,2)v_{xc}(2) = G_0(1,2)\Sigma_{xc}(2,3)G_0(3,1)$$

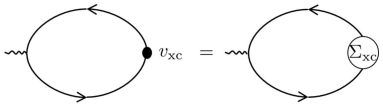

- Using the G_0W_0 self-energy corresponds to the random-phase approximation for the energy functional

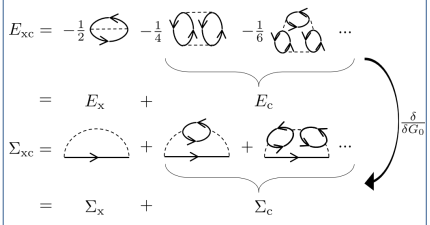

- Unlike semi-local functionals, the RPA-OEP exhibits the correct $1/r$ asymptotic behavior far away from an atom [2].
- Atomic shell oscillations are also described well by the RPA-OEP [3].

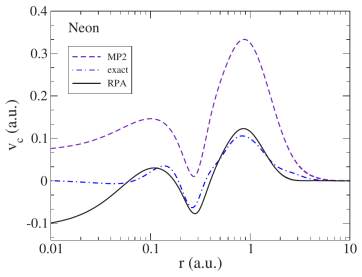

Figure 1. Self-consistent correlation potentials for the Ne atom [3].

Self-consistency

- Due to its high computational cost, RPA-OEP hasn't been broadly applied to solids
- One problem: like standard DFT methods, the OEP needs to be solved self-consistently
- The computational cost can be reduced by choosing a good starting point [4].
- Basis idea: pre-iterate the OEP on a sparse k-point mesh.

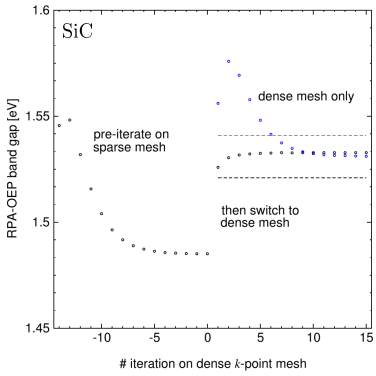

Figure 2. A single iteration on a $6x6x6$ k-point mesh is usually sufficient, if the OEP is pre-iterated on a $4x4x4$ mesh. Dashed lines indicate a tolerance-region of ± 10 meV [4].

Dynamical screening

- Quasiparticle approximation (QPA): Static approximation to the self-energy [5]

$$\Sigma^{QPA}_{mn} = \frac{1}{2}\left(\mathrm{Re}\Sigma_{xc,mn}(\varepsilon_m) + \mathrm{Re}\Sigma_{xc,mn}(\varepsilon_n)\right)$$

- Similar to Hedin's COHSEX approximation [6].
- This neglects certain dynamical screening effects, no spectral weight is given to satellites

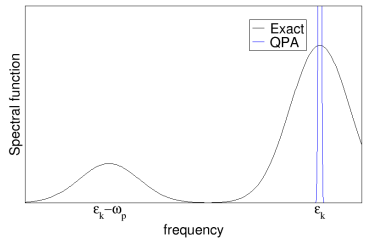

- in the QPA, the Z-factors are set to 1
  → QP lifetime is always infinite
  → some physical flaws [4].

- But: For the purpose of the OEP, the QPA becomes exact in metallic limit:
  → HEG is exactly described [2]!
  → The effect of the QPA on the band gap of a semiconductor can be approximated as [4]

$$\Delta E_g/E_g \approx \frac{(Z_c - Z_v)}{2Z_cZ_v}; \quad Z = \frac{1}{1 - \partial \mathrm{Re}\Sigma/\partial\omega}$$

Results

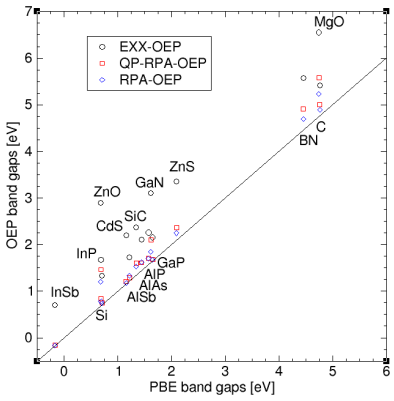

Figure 2. Minimal band gaps from EXX-OEP as well as RPA-OEP and RPA-OEP using the QPA, as compared to the PBE reference. Where the minimal gap is located along the Δ-axis, the Γ→X excitation energy is shown instead.

- Screening in the RPA reduces the EXX-OEP band gaps towards PBE
- The RPA-OEP band gaps are larger in the QPA
  → Same in COHSEX!
- Exact RPA-OEP is closer to PBE
  → Also true for the conduction band dispersion
- Largest effects of the QPA for ionic materials (ZnO, GaN, MgO) → Related to Z-factors!

Table 1. Macroscopic, ion-clamped dielectric constants in the RPA obtained from PBE and different RPA-OEP xc-potentials. Stars indicate, that experiments are performed at wurtzite rather than zinc-blende structure [4].

	PBE	RPA		expt.
		QPA	exact	
C	5.5	5.3	5.4	5.7
Si	12.1	11.6	11.7	11.9
SiC	6.6	6.2	6.3	6.5
BN	4.4	4.1	4.2	4.5
AlP	7.6	7.2	7.3	7.5
AlAs	8.6	8.1	8.1	8.2
AlSb	10.7	10.3	10.2	10.2
GaN	5.7	5.2	5.5	5.3*
GaP	9.7	9.2	9.4	9.1
InP	10.2	9.8	9.9	10.9
ZnO	5.1	3.9	4.2	3.7*
ZnS	5.6	5.3	5.4	5.1
CdS	5.8	5.7	5.7	5.3*
MgO	3.0	2.8	2.9	3.0
MRE	5%	0%	0%	
MARE	7%	5%	5%	

*wurtzite structure

- Effect of the QPA is reduced for dielectric constants, trends consistent with band gaps
- Both RPA-OEP methods are on average close to experiment

Conclusions

- Pre-converged OEP consistently speeds up self-consistency cycle
- QPA works well except for ionic materials
- In-itself closed RPA-OEP scheme yields dielectric constants in good agreement with experiment

Contact

Stefan Riemelmoser, MSc
University of Vienna
Email: stefan.riemelmoser@univie.ac.at
Website: cmp.univie.ac.at
Phone: +43-1-42777-5140

References

1. L. J. Sham and M. Schlüter, Phys. Rev. Lett. 51, 1888 (1983)
2. L. J. Sham, Phys. Rev. B 32, 3876 (1985)
3. M. Hellgren and U. von Barth, Phys. Rev. B 76, 075107 (2007)
4. S. Riemelmoser, M. Kaltak, G. Kresse (unpublished)
5. T. Kotani, M. van Schilfgaarde, and S. V. Faleev, Phys. Rev. B 76, 165106 (2007).
6. L. Hedin, Phys. Rev. 139, A796 (1965)

P117

Quantum HF/DFT-Embedding Algorithms for Electronic Structure Calculations

In the near future, material and drug design may be aided by quantum computer assisted simulations. These have the potential to target chemical systems intractable by the most powerful classical computers. However, the resources offered by contemporary quantum computers are still limited, restricting the chemical simulations to very simple molecules. In order to rapidly scale up to more interesting molecular systems, we propose the embedding of the quantum electronic structure calculation into a classically computed environment obtained at the HF or DFT level of theory. We achieve this by constructing an effective Hamiltonian that incorporates a mean field potential describing the action of the inactive electrons on a selected active space (AS). The ground state of the AS Hamiltonian is determined by means of the VQE algorithm. We show that with the proposed iterative DFT embedding scheme we can obtain significant energy corrections compared to the reference HF and DFT energies for systems of the size of the pyridine molecule.

P118

Constructing the energy landscape for Ti{x}Zr{1-x}O2 via a neural-network potential through charge equilibration technique

In simulating many different experimental phenomena like doped and mixed materials, coating on substrates, interfaces, surfaces, grain boundaries, many number of atoms in a complex landscape are involved which ab-initio calculation are very expensive and time consuming. So, to predict the properties of such systems a fast and accurate potential is demanded to enable us investigate large configurations in longer simulation times. In this work we generate a neural-network potential through charge equilibration technique(CENT) for Ti{x}Zr{1-x}O2 with 0 <=x<=1. Since the CENT potential was trained with vary diverse dataset in all boundary conditions with different cation ratio in the framework of density functional theory, we expect it to reproduce the energy landscape of all mentioned applications. the reliability and transferability of the potential are verified by calculations of crystal structures and energies, phonon spectra. Moreover, to investigate the performance of potential for different crystal phases and cluster configurations which are not included in our training dataset , we applied a structural search method called minima hopping to explore the local minimum of potential energy surfaces. The results show that our potential can reproduce the energy surfaces in good agreement with our DFT reference data and can predict very diverse new structures.

P119

Prediction of Structural, Electronic, Magnetic and Thermoelectric Properties for the InverseHeusler alloy Mn2NiSn: A first-principles study

In the framework of Density Functional Theory (DFT), we studied the inverse Heusler alloy Mn2NiSn using the Full Potential - Linearised Augmented Augmented Plane method as implemented in the WIEN2k code. Mn2NiSn inverse Heusler alloy structural stability, electronic structure, magnetic moment, Curie temperature, spin polarization and thermoelectric properties were determined. Generalised Gradient Approximation (GGA) and Local Spin Density Approximation (LSDA) schemes were implemented in the calculation. To get precise band gap effects, we used Tran Blaha-modified Beck-Johnson (TB-mBJ) correction. Mechanical stability was calculated by the measurement under ambient conditions of their elastic constants C11, C12, C44. In the ferromagnetic phase, the electronic structure of the Mn2NiSn inverse Heusler alloy shows half metallicity with a 100 percent spin polarization at Fermi level EF. The determined magnetic moment of total spin is 4μB, which is well in line with Mt=Slater-Pauling Zt-24's law. The measured temperature of Curie is higher than room temperature. We predicted the electronic transport properties such as thermal and electrical conductivity, the Seebeck coefficient and the figure of merit by using semi classical Boltzmann theory implied in the BoltzTrap code. In the framework of Density Functional Theory (DFT), we studied the inverse Heusler alloy Mn2NiSn using the Full Potential - Linearised Augmented Augmented Plane method as implemented in the WIEN2k code. Mn2NiSn inverse Heusler alloy structural stability, electronic structure, magnetic moment, Curie temperature, spin polarization and thermoelectric properties were determined. Generalised Gradient Approximation (GGA) and Local Spin Density Approximation (LSDA) schemes were implemented in the calculation.

SCHOOL OF PHYSICAL SCIENCES AND ENGINEERING

P120

YACHAY TECH

Ab initio studies of ultra-thin CaF_2 layer on the Si(100) surface

Joshua Salazar[1], Damien Riedel[2], Henry P. Pinto[1]

1: CompNano Group, School of Physical Sciences and Nanotechnology, Yachay Tech University, Urcuqui-Ecuador
Contact Information: joshua.salazar@yachaytech.edu.ec , hpinto@yachaytech.edu.ec
2: Institut des Sciences Moléculaires d'Orsay, ISMO, UMR 8214, CNRS, Université Paris Sud, 91405 Orsay Cedex, France

Abstract

An accurate atomic structure description for the stripe formation of CaF_2/Si(100) is unsolved yet [3]. The aim of this study is to provide a theoretical study of this interface using Density Functional Theory (DFT). To correctly simulate this multilayered system it is needed to take into account the weak van der Waals interactions arising between the CaF_2 and the Si(100) surface. In this work, we will use van der Waals density functional (vdW-DF) approach [4]. Employing this functional, we investigate the configuration and energetics of several interfaces, and the simulated scanning tunneling microscopy (STM) images of the most stable interfaces will be generated and compared directly with the experiment.

Methods

For the Density Functional Theory (DFT) simulation performed for this structure the plane wave code VASP v5.3 was employed. The bulk Si was simulated with a cutoff energy of 450 eV, and the k-point mesh chosen (9 x 9 x 9) and a grid spacing of 0.035 $Å^{-1}$. The parameters were converged over a range until the change in total energy was < 1 meV/atom in the cell. The Si(100) surface was constructed using the calculated cutoff energy and grid spacing parameters optimized from the bulk. The k-point mesh for the 1x1 surface used was (7 x 7 x 1) and for the 4x3 surface (2 x 2 x 1). The exchange-correlation functional used was optB86b-vdW. The (100) surface was constructed with 8 layers of silicon, freezing the last layer and passivizing it with Hydrogen. The wetting layer was constructed using the proposed etching process of the Si due to the CaF_2 exposure. Later, the cristalization of bulk CaF_2 in the [111] direction was considered to construct the stripes forming on top of the wetting layer. The STM images were calculated using the bSKAN program, which applies the Tersoff-Hamann approximation over the calculated and optimized structure.

Results

The calculated topographic states displaying the corrugation of the surface at -1 V (fig. 1) are qualitatively improved versus previous results of Chiaravalotti *et al.*. The computed STM images for -1 V correspond to the experimental measured ones at -1.5 V. The stripe configuration is shown (fig. 2) and compares the experimental STM image against the computed with the proposed atomic structure.

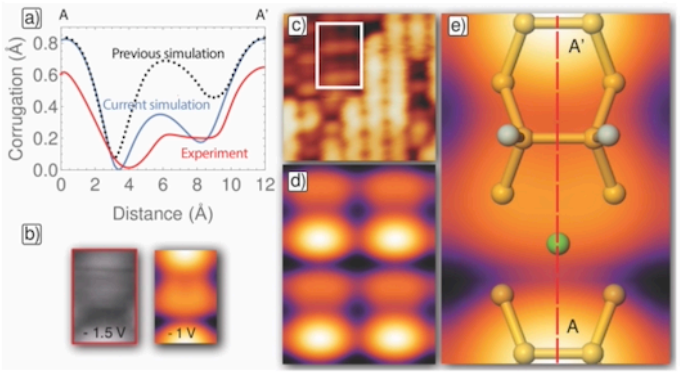

Figure 1: STM images computed for probing occupied levels at -1 V. (a) Comparisson between the computed and measured corrugation of the surface. (b) Experimental (@ -1.5 V) and calculated STM images for the 4x3 CaF_2/Si(100) supercell. (c) Experimental STM image of the CaF_2/Si(100) surface. (d,e) Computed STM images for the studied interface.

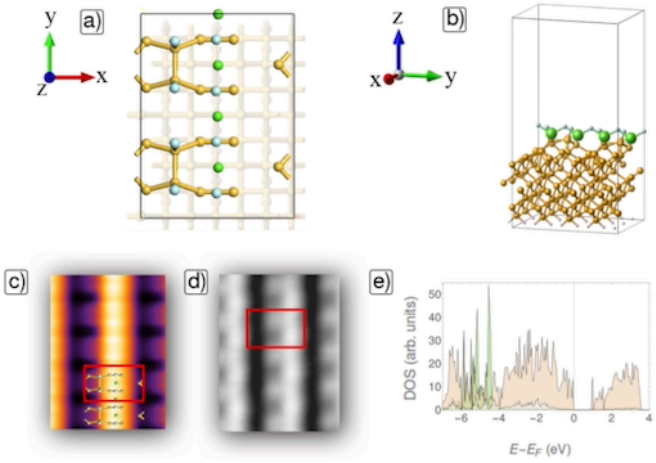

Figure 2: Proposed stripe structure that solves the experimentally observed stripe topography. (a) Top view of the atomic configuration of the stripe formation. (b) 3D view of the overall supercell used for the simulation. (c) simulated STM image

The proposed stripe configuration and their STM images are shown in fig. 2. The PDOS of the surface atoms (fig. 2e) displays a E_{gap} =0.878 eV, while the bare Si(100) has E_{gap} =0.206 eV, the experimental values are 1.3 eV and 3.8 eV respectively. The ratio $E_{gap,stripe}/E_{gap,bare}$ of our computed structures is found to be ∼3 and the experimental ones ∼4.

Conclusions

Molecular electronics development requires the effective electronic isolation of a given molecule with the substrate as well as a precise atomic manipulation [1]. In this work, we studied the CaF_2 / Si(100) interface that it is currently used for electronic manipulation of molecules at the nanoscale. This interface has been already grown experimentally for certain coverage regime [2,3]. After the DFT calculations, the computed STM images closely resemble the measured ones. Further research is needed in order to reproduce an accurate supercell configuration for the different patterns arising over the clustered islands of CaF_2 over the Si(100).

Acknowledgement

J. S. and H. P. acknowledge the support of the School of Physical Sciences and Nanotechnology at Yachay Tech University. The computation time was provided by the National Supercomputing Center in the QUINDE I supercomputer, grant: Computational Multiscale Modeling of Materials.

References

[1] Colton, R.J., Journal of Vacuum Science and Technology B: Microelectronics and Nanometer Structures 22 (2004) 1609.

[2] F. Chiaravalloti, G. Dujardin, H. Pinto, et al., Phys. Rev. B 84 (2011) 155433.

[3] F. Chiaravalloti, G. Dujardin, D. Riedel, J. Phys: Condens. Matter 17 (2015) 054006

[4] H. Rydberg, M. Dion, N. Jacobson, et. al., Phys. Rev. B 91 (2003) 12.

P121

A DFT Study on the Relationship Between Structure and Antioxidant Properties of Thymoquinone

Thymoquinone (TQ), an important naturally occurring phytochemical found in Nigella sativa seed. In present study, the structural properties of TQ is determined by using Density Functional Theory (B3LYP) method with 6-311G++(2d,2p) level of theory. Radical scavenging activity of TQ is elucidate by estimating C-H bond dissociation enthalpy (BDE) by means of hydrogen atom transfer (HAT) at different sites of H-abstraction, in gas, benzene, methanol and water solvent medium. It reveals that HAT mechanism is thermodynamically favoured in gas medium. 5-methyl site of TQ possess low BDE and this was confirmed by the interpretation of spin density distribution. The calculated values of global descriptors namely ionization potential, electron affinity, electronegativity softness, hardness and softness reveals that TQ have good antioxidant activity. Charge delocalization of TQ was investigated through frontier molecular orbital (FMO) distribution. The charge transfer mechanism is explored by natural bond orbital (NBO) analysis. The nucleophilic and electrophilic site of TQ were studied by Fukui function. The obtained properties confirm that TQ can act as radical scavenger against oxidative damage.

P122

Computational studies of the electronic structure and stability of TiO_2 nanoclusters.

Jennifer A. Sanchez*[1] and Henry P. Pinto[1]

[1]CompNano Group, School of Physical Sciences and Nanotechnology, Yachay Tech University, Urcuqui-Ecuador

jennifer.sanchez@yachaytech.edu.ec

UNIVERSIDAD YACHAY TECH

ESCUELA DE CIENCIAS FÍSICAS Y NANOTECNOLOGÍA

Introduction

Titanium oxide is an important transition metal oxide due to its photocatalytic properties; however, there are still problems in the use of TiO_2 as a photocatalyst due to its wide bandgap. Experimental and theoretical studies of nanoclusters can be very helpful in the understanding and prediction of catalytic properties of nanoparticles (*1*). Nanoclusters will be studied combining semi-empirical density-functional tight-binding (DFTB) with ab initio density-functional theory (DFT) methods to resolve the most stable nanocluster topology, related to the number of TiO_2 units contained. Molecular dynamics simulations are ap- plied to resolve the most likely atomic structure of (TiO_2)n (n = 4,6,7,8,10) nanoclusters. The electronic structure of the most likely candidates is computed using ab-initio DFT at the level of hybrid functional B3LYP. Physical-chemical properties like formation energies, dipole moment, quadrupole moment, polarizability, HOMO, LUMO and zero-point energy will be predicted.

Methods

Calculations were performed using Gaussian basis wave functions in XTB (*2*), a semi-empirical quantum mechanical program to obtain sets of stable structures for each cluster. Molecular dynamics (MD) at room temperature (T = 298.15 K) were implemented for 1 ns with time step 3 fs. The most energetically stable structures were selected for each phase of the MD, each of them was topologically different.

Afterward, relaxations were performed implementing ORCA, an ab initio molecular dynamics (AIMD) DFT and semiempirical SCF-MO package (*3*), along with the B3LYP hybrid functional which consist of Becke's three-parameter exchange functional and correlation functional of Lee–Yang–Parr (*4*). The calculations were performed at T = 0 K, relaxing different sets of stable structures per cluster of $(TiO_2)_n$ (n = 4, 6, 7, 8, 10) arranged in different configurations.

TiO_2 clusters structures

Titanium Oxide nanoparticles are able to arrange in different cluster configurations.

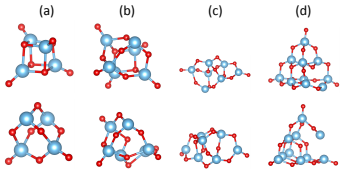

Figure 1. Before (***up***) and after (***down***) MD phase transition in xTB package. ***a*** : 4(2); ***b*** : 6(2); ***c*** : 7(3); ***d*** : 10(2) TiO_2 cluster structures.

The systems are named after the number of TiO_2 atoms present in the cluster, and a label next to it, to distinguish configurations with an equal number of atoms.

The original cluster structures (Fig. 1 (up)) were extracted from Arab. et al (*1*), and Fig. 1 (down) clusters are the result of the topological phase transition in MD at room temperature.

Molecular Dynamics

With the implementation of the molecular dynamics at room temperature (T = 298.15 K) we were able to obtain the most energetically stable structures in each of the phases per cluster.

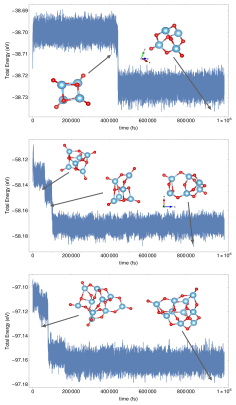

Figure 2. ***a*** : 4c2; ***b*** : 6f2; ***c*** : 10j3; TiO_2 cluster molecular dynamics.

As we see in Fig. 2, after the energy equilibrium the structure stabilizes to a range of energies for a period of time, in which the structure remains with a certain topologically. Then, occurs a phase transition, where we observe a lowering in the range of energies and a change in their topology.

Conclusions

With the implementation of Molecular dynamics at room temperature (T = 278.15 K) on TiO_2 clusters we were able to obtain different topological phases for each structure. After a relaxation (T = 0 K) of the phases, we could observe the role of the zero-point energy on the determination of the stability of the cluster in relation to their computation of the total energy. We observed that zero-point energy increases with the size of the clusters due to the modes of vibration.

Results

Though a relaxation at zero Kelvin (T= 0 K) we were able to compute the results displayed in Table 1. Different topological phases per cluster are labeled with a, b, c, d, depending on the order they appeared during the molecular dynamics time. The total energy displayed is the result of the combination of electronic, ionic, and zero-point energy.

Table 1. DFT B3LYP computed values of the Total Energy(E_{tot}) , Dipole moment(*D*), Quadrupole moment (*Q*), Isotropic polarizability (*P*), Electronic Energy (E_{elec}) , Nuclear repulsion (*NR*), HOMO, LUMO and Zero point energy (*ZPE*) , for TiO_2 clusters set up in different configurations.

System	E_{tot}(Eh)	D(a.u.)	Q(a.u.)	P (a.u.)	E_{elec}(Eh)	NR(Eh)	HOMO(Eh)	LUMO(Eh)	ZPE (Eh)
4c2a	-4000.048	0.245	-90.04	132.91	-5947.72	1947.64	-0.343	-0.18	0.0297
4c2b	-4000.078	4.84	-80.94	131.	-5901.01	1900.9	-0.266	-0.155	0.0305
6f1a	-6000.236	4.69	-125.5	196.58	-9944.51	3944.22	-0.274	-0.153	0.0474
6f1b	-6000.202	4.18	-127.7	198.68	-9885.53	3885.28	-0.286	-0.159	0.047
6f1d	-6000.221	2.26	-134.1	207.21	-9813.58	3813.31	-0.327	-0.161	0.047
6f2a	-6000.189	4.11	-132.	197.26	-9943.75	3943.51	-0.325	-0.192	0.0466
6f2b	-6000.187	3.1	-129.6	202.83	-9832.19	3831.96	-0.298	-0.168	0.0464
6f2c	-6000.236	4.38	-125.	204.27	-9813.97	3813.69	-0.302	-0.165	0.0473
7g1a	-7000.313	2.95	-150.7	239.19	-12152.9	5152.49	-0.311	-0.146	0.0551
7g2a	-7000.308	2.31	-147.4	241.87	-11909.	4908.67	-0.31	-0.163	0.0555
7g3a	-7000.339	0.944	-149.6	236.47	-12136.6	5136.23	-0.321	-0.14	0.0563
7g3b	-7000.31	0.494	-150.4	238.77	-12015.3	5014.93	-0.321	-0.157	0.0557
8h2a	-8000.347	1.92	-174.3	279.87	-14273.	6272.57	-0.326	-0.153	0.0625
8h3a	-8000.392	1.97	-174.1	283.12	-14261.9	6261.41	-0.315	-0.149	0.063
8h4a	-8000.345	2.72	-174.2	278.41	-14329.2	6328.84	-0.323	-0.153	0.0628

The most energetically stable topological phases with respect to their own cluster are 4c2b, 6f1a, 6f2c, and 7g3a, meanwhile, the most stable clusters with the same number of atoms are 4c2, 6f2, 7g3, and 8h3. Also, the difference in zero-point energy between phases is of the order of 0.01 eV and it reduces with the increase of the cluster size.

Acknowledgements

Special thanks to Alicja Mikołajczyk PhD. for her fruitful discussions and to the School of Physical Sciences and Nanotechnology for its support to this research.

References

1. A. Arab, F. Ziari, M. Fazli, *Computational Materials Science* **117**, 90–97, (https://doi.org/10.1016/j.commatsci.2016.01.031) (May 2016).
2. C. Bannwarth *et al.*, *WIREs Computational Molecular Science*, (https://doi.org/10.1002/wcms.1493) (Aug. 2020).
3. F. Neese, *WIREs Computational Molecular Science* **2**, 73–78, (https://doi.org/10.1002/wcms.81) (June 2011).
4. C. Legler *et al.*, *Spectrochimica Acta Part A: Molecular and Biomolecular Spectroscopy* **145**, 15–24, (https://doi.org/10.1016/j.saa.2015.02.103) (June 2015).

P123

Strong chemisorption of CO2 on B10–B13 planar-type clusters

An ab initio density functional study was performed investigating the adsorption of CO2 on neutral boron Bn (n = 10–13) clusters that are characterized by planar and quasiplanar groundstate atomic structures. For all four clusters, we found large chemisorption binding energies, reaching 1.6 eV between CO2 and B12, with the adsorbed molecule oriented in the plane of the cluster and adsorbed along the cluster edge. A configuration with chemisorbed dissociated CO2 molecule also exists for B11 and B13 clusters. The strong adsorption is due to the bending of the CO2 molecule, which provides energetically accessible fully in-plane frontier molecular orbitals matching the edge states of the clusters. At the same time, the intrinsic dipole moment of a bent CO2 molecule facilitates the transfer of excess electronic charge from the cluster edges to the molecule.

P124

Stability of variable protonation state of citrate on Fe3O4 nanoparticles

The structure of citrate layers on iron oxide nanoparticles (FeONPs) was investigated. A unique structure of adsorbed citrate is determined, and a pH-induced structural transition is presented. The stability analysis probes dangling dihydrogen anions (H2Citrate-) and hydrogen bonding of carboxylic acid groups between adsorbed and dangling citrate anions. A contribution of steric repulsion between citrate layers to particle stability is characterized.

P125

Rotopolar coupling driving the antiferroelectric phase transition in PbZrO3

Konstantin Shapovalov (1), Massimiliano Stengel (2,1). (1) Institut de Ciència de Materials de Barcelona, ICMAB-CSIC, Campus UAB, 08193 Bellaterra, Spain. (2) ICREA – Institució Catalana de Recerca i Estudis Avançats, 08010 Barcelona, Spain

PbZrO3 is, by far, the best known antiferroelectric material. During its antiferroelectric phase transition, Pb ions displace forming the characteristic ”up-up-down-down” pattern. This transition is accompanied by the condensation of a complex set of seemingly unrelated distortions, physical origin of which has been a subject of a considerable debate over the years. Here we combine ab-initio simulations with Landau theory modelling to study the physics behind the antiferroelectric phase transition. We show that > 99% of the distortions in the antiferroelectric phase of PbZrO3 can be equivalently described by polarization P, antiphase oxygen octahedra tilts ϕ and their modulations. We demonstrate that these modulations are stabilized by the trilinear rotopolar gradient coupling between P and ϕ, having form $W_{ijkl} P_i \phi_j ((\partial \phi_k)/(\partial x_l))$. Our theoretical framework has features of two main existing models that explain the antiferroelectric phase transition in PbZrO3: locked-in incommensurate modulations by Tagantsev et al. [1] and trilinear coupling between distortions by Íñiguez et al. [2]. We compare the new rotopolar mechanism with the flexoelectric one considered in model [1], discuss how the two mechanisms coexist in PbZrO3, and show how they can drive together the incommensurate/antiferroelectric phase transition in related perovskites. [1] A. K. Tagantsev et al., Nat. Commun. 4, 2229 (2013). [2] J. Íñiguez et al., Phys. Rev. B 90, 220103 (2014).

P126 **Title : Structural, electronic and and transport properties of BiI_3/ZrS_2 van der Waals heterostucutre : A first principle investigation**

Aurthor(s): Gautam Sharma[1], Shouvik Datta[1,2], Prasenjit Ghosh[1,2]*
Affiliations: (1) Department of Physics, Indian Institute of Science Education and Research, Pune, Maharashtra 411008, India (2)-Centre for Energy Sciences, Indian Institute of Science Education and Research, Pune, Maharashtra 411008
email:gautam480@gmail.com, gautam.sharma@students.iiserpune.ac.in

Using density functional theory combined with the semi-classical Boltzmann transport theory, we have investigated structural, electronic and transport properties of a van der Waals (vdW) vertical heterostructure (HS) of BiI_3 and ZrS_2. We find that the elastic constant of the heterostructure is larger than the individual monolayers. Electronic structure calculations reveal that HS has a direct band gap of 1.2 eV which is smaller than the monolayers. The interaction between the layers results in subtle changes in the electronic properties of the heterostructure such that its transport properties are also affected. We have used deformation potential theory together with the effective mass approximation to compute relaxation times (τ) of charge carriers in HS and monolayers. We find that τ of electrons is significantly increased in HS compared to monolayers. As a result, for electron in HS, the power factor is about two and hundred times larger than that of a monolayer of ZrS_2 and BiI_3, respectively. This indicates that the maximum power output from a thermoelectric device made of n-doped heterostructure is larger than that obtained from the individual components. This suggests that this novel heterostructure might be a plausible candidate for n-type thermoelectric.

P127

Abinitio Studies on Permeation and Solubility of Hydrogen Isotopes in Iron (Fe), Tungsten (W) and Chromium (Cr)

The knowledge about permeation and solubility of hydrogen isotopes in metal is of great technological significance as it helps in controlling the hydrogen induced embrittlement and also in the selection of structural materials for reactors with minimum permeability of these gases. Atomistic understanding of the behavior of D/T with metal is highly desirable to design an efficient better material. We have performed DFT calculations to investigate the interaction and dynamical behaviours of hydrogen isotopes in pure bcc Fe, Cr and W. The adsorption and dissociation pathways for hydrogen isotopes were predicted on Fe(100), Cr(100) and W(100) surfaces. The activation barrier energy for H atom to diffuse from one interstitial void to nearest interstitial void has been computed using nudge elastic band method. The most favourable diffusion path of H was observed from one tetrahedral site to the nearest tetrahedral site. The calculated activation barrier for Cr is found to be higher compared to Fe and thus demonstrates that addition of Cr in Fe-Cr alloy helps in reducing permeation. The present observation is in correspondence with the experimentally observed low diffusivity of hydrogen in Fe-Cr steels. The calculated diffusion coefficients, permeability constants and solubility are found to be higher for H compared to its heavier isotopes D and T. Further, the calculated diffusion coefficients are shown to be lowest for W and thus might be the basis for considering W as plasma facing materials. The present talk will discuss about the recently carried out abinitio calculations on hydrogen isotopes barrier materials.

P128

Strain tuning of the anisotropy in the optoelectronic properties of the two-dimensional transition metal trichalcogenide TiS_3

Jose Angel Silva Guillén[1], Enric Canadell[2], Pablo Ordejón[3], Francisco Guinea[4], Rafael Roldán[5]
[1] School of Physics and Technology, Wuhan University, Wuhan 430072, China
[2] Institut de Ciència de Materials de Barcelona (ICMAB-CSIC), Campus Bellaterra, 08193 Bellaterra, Barcelona, Spain
[3] Catalan Institute of Nanoscience and Nanotechnology (ICN2), CSIC and The Barcelona Institute of Science and Technology,Campus Bellaterra, 08193 Bellaterra, Barcelona, Spain
[4] Fundación IMDEA Nanociencia, C/Faraday 9, Campus Cantoblanco, 28049 Madrid, Spain
[5] Instituto de Ciencia de Materiales de Madrid, CSIC, Sor Juana Ines de la Cruz 3, 28049 Cantoblanco, Madrid, Spain
Josilgui@gmail.com

Since the discovery of graphene in 2004, there has been a huge improvement in the fabrication and manipulation of layered materials. Recently, the discovery that a monolayer of MoS_2 changes its electronic properties with respect to the bulk brought much expectation in the scientific community towards the transition metal chalcogenides (TMCs). The MX_2 transition metal dichalcogenides (TMDCs) have been thoroughly studied both experimentally and theoretically. Nowadays, TMCs with different chemical stoichiometries such as the transition metal trichalcogenides (TMTCs) MX_3 are also being intensely studied. Interestingly, TiS_3 has shown to have cleavage energies close to that of graphite, showing that similar methods can be used to fabricate TiS_3 monolayers.

In the present work we explore the optoelectronic properties of TiS_3. Analysis of the band structure of TiS_3 single-layers suggests the possibility of changing their physical behavior by injecting electron carriers. The anisotropy of the valence and conduction bands is explained in terms of their complex orbital composition. The nature of the Fermi surface and Lindhard response function for different doping concentrations is studied by means of first-principles DFT calculations. It is suggested that for electron doping levels x (number of electrons per unit cell) ~0.18-0.30e^- the system could exhibit incommensurate charge or spin modulations which, however, would keep the metallic state whereas systems doped with smaller x would be 2D metals without any electronic instability. The effect of spin-orbit coupling in the band dispersion is analyzed. The DFT effective masses are used to study the plasmon spectrum from an effective low energy model. We find that this material supports highly anisotropic plasmons, with opposite anisotropy for the electron and hole bands.

Finally, we study the effect of strain in these properties. We find that the ellipticity of the valence band can be inverted under moderate compressive strain, which is accompanied by an enhancement of the optical absorption. It is shown that the strain tuning of the band anisotropy can be exploited to focus plasmons in the desired direction, a feature that could be used to design TiS_3 nanostructures with switchable plasmon channeling.

References

[1] J. A. Silva-Guillén, E. Canadell, P. Ordejón, F. Guinea and R. Roldán. 2D Materials **4**, 02508 (2017).
[2] J. A. Silva-Guillén, E. Canadell, F. Guinea, and R. Roldán. ACS Photonics **5**, 3231-3237 (2018).

P129

Compositional dependence of structure and chemical short-range order in Zr-Cu-Al Glass-forming alloys

K. G. Soni and K. N. Lad

Department of Physics, Sardar Patel University, Vallabh Vidyanagar-388120, Gujarat, India.

ABSTRACT

The genesis of glass formation is one of the most intriguing problems of glass-forming liquids. In the last three decades bulk metallic glasses have emerged as an important class of materials due to its excellent physical properties compared to its crystalline counterparts. Understanding the role of different physical factors affecting the glass-forming ability (GFA) of multicomponent metallic glass-forming alloys has been a leading area of research in this field. The GFA of multicomponent metallic alloys has been reported to increase significantly by a small change in the concentration of the constituent elements[1]. As short- and medium-range topological order evolves remarkably during the glass-formation in metallic alloys, the chemical short-range order (CSRO) is expected to play an important role in stabilizing the liquid alloys against crystallization. [2-4] CSRO can be studied with the help of the partial pair distribution functions which can be obtained using the classical molecular dynamics (MD) simulations. In the present work, we have carried out classical MD study of $Zr_{50}Cu_{-x}Al_x$ (x = 5,10,15,20,25,30,40) liquid alloys to understand the effect of the change in composition on the structure and the CSRO in these alloys. We also attempt to investigate the role of CSRO in governing the GFA. CSRO has been characterized in terms the Warren-Cowley parameter [5].

References

[1] W. H. Wang, Prog. Mater. Sci. 52 (2007) 540.
[2] Y. Q. Cheng, E. Ma and H. W. Sheng, Appl. Phys. Lett. 93 (2008)111913.
[3] Y. Q. Cheng, E. Ma and H. W. Sheng, Phys. Rev. Lett. 102 (2009) 245501.
[4] K. N. Lad, N. Jakse and A. Pasturel, J. Chem. Phys. 136 (2012)104509.
[5] B. E. Warren, B. L. Averbach, B. W. Roberts, J. Appl. Phys. 22 (1951)1493.

P130

Flexoelectricity in two-dimensional materials

Among their many prospective applications, “two-dimensional” (2D) materials have received in last few years considerable attention as a basis for novel electromechanical device concepts. In particular flexoelectricity, the generation of macroscopic polarization or voltage due to a uniform strain-gradient, is expected to be remarkably large in two-dimensional crystals. Several attempts have been carried out to calculate the flexoelectric response of a monolayer (or few layers) due to a flexural deformation, but generally with remarkable disagreement in reported values, highlighting the necessity of a rigorous first-principle treatment. Very recently we overcame this problem, providing a powerful and general method to calculate the open-circuit voltage response to a flexural deformation of a 2D crystal, fully from first principles. [1] In this poster, I will introduce the theoretical tools to define and calculate flexoelectricity in 2D materials, building on recent developments in electronic-structure methods. In particular, I will show that the voltage response to a flexural deformation can be calculated within the linear-response regime, by using the surface unit cell of the flat configuration; this provides an optimally converged solution. By applying our methodology to graphene, silicene, phosphorene, BN, and transition-metal dichalcogenide monolayers we demonstrate that two contributions exist, respectively of purely electronic and lattice-mediated nature. Within the former we identify a previously overlooked key metric term, consisting in the quadrupolar moment of the unperturbed charge density. Such metric term largely cancels out with the dipolar moment of the first-order electronic density, leading to a much smaller electrical response than reported earlier. [1] https://arxiv.org/abs/2010.08470

P131

Double-Hybrid DFT Functionals for the Condensed Phase: Gaussian and Plane Waves Implementation and Evaluation

Intermolecular interactions play an important role for the understanding of catalysis, biochemistry and pharmacy. Double-hybrid density functionals (DHDFs) combine the proper treatment of short-range interactions of common density functionals with the correct description of long-range interactions of wave-function correlation methods. Up to now, there are only a few benchmark studies available examining the performance of DHDFs in condensed phase. We studied the performance of a small but diverse selection of DHDFs implemented within Gaussian and plane waves formalism on cohesive energies of four representative dispersion interaction dominated crystal structures. We found that the PWRB95 and ωB97X-2 functionals provide an excellent description of long-ranged interactions in solids. In addition, we identified numerical issues due to the extreme grid dependence of the underlying density functional for PWRB95. The basis set superposition error (BSSE) and convergence with respect to the super cell size are discussed for two different large basis sets.

P132

Towards a systematic multi-scale method for excitations in molecular materials in the BigDFT code

Understanding excited states plays a critical role in spectroscopy and in improving the performance of devices. From a technological perspective an interesting example is thermally activated delayed fluorescence (TADF). This is a mechanism for designing the next generation of OLED materials being fully organic and less environmental harmful than previous generation. TADF emission is based on inverse inter-system crossing from triplet to singlet states. These excitations exhibit an intricate mixture of charge-transfer and local nature. Modelling TADF (e.g to identify the best performing material) as well as locating excited states, thus, requires a methodology able to provide high accuracy while explicitly including environmental effects. However, developing a versatile theoretical approach for the characterisation of excitations can be challenging due to the complexity of the methods available and the variety of sources of error associated with them. We are developing a multi-scale approach within the BigDFT code where we combine the needed accuracy with the ability of treating big systems, which would allow one to go beyond implicit models. BigDFT is designed to run on parallel architectures and can treat large systems while ensuring high, controllable precision. First, we assess the performance of a new promising constrained-DFT approach developed in our group and compare the results with standard methods (e.g. TDDFT) and simulation conditions. Such investigation is conducted on a set of molecules (e.g. TADFs, acenes) in order to cover various classes of excitations. This phase is carried out by also developing a portable jupyter-notebook for the analysis of excitations.

P133

Effect of the cations distribution on the magnetic properties of SnFe2O4: First-principles study

In this work, a study of the electronic and magnetic properties of SnFe2O4 spinel ferrite for different case of octahedral and tetrahedral distribution was carried out by using the Full Potential Linearized Plane Wave (FP-LAPW) method in density functional theory (DFT) implemented in the WIEN2K package, with the generalized gradient (GGA) and Tran-Blaha modified Becke-Johnson approximations for the exchange and correlation functional. Our spin-polarized calculations based on mBJ correction show a half metallic behavior for SnFe2O4 which confirm the usefulness of SnFe2O4 in spintronic application. From the magnetic properties calculations, it is found that the magnetic moment per formula unit is 8.0327 μβ, 0.000015 μβ and 3.99μβ in SnFe2O4 100% normal, 100% inverse and 50% inverse, respectively.

P134

Termination dependent Rashba-Dresselhaus band splitting in CsPbI3 slabs

Herein employing ab-initio techniques, the role of surface termination and interfacial electric field on the band-splitting are investigated systematically. Our findings indicate a different pattern for band splitting of CsI-and PbI2-terminated slabs in the presence of the external electric field.

P135

Automated design of a structural descriptor for radiation resistant perovskites

We present the automated design of a topological descriptor to predict the irradiation resistance of hybrid perovkites. These materials are promising for solar cells that are highly resistant to radiation, especially suited to be used in space applications. However, one of the main drawbacks of perovskite materials is their structural instability, caused predominantly by the migration of halogen atoms. This migration can be remedied by having the halogens stronger bound to the organic cations. We performed a virtual screening on a large database of perovskite materials studying the total bond strengths of the organic cation with the halogens. By using a compressed sensing technique, called SISSO, we correlate the total bond strength with topological features, thus establishing a structural descriptor for structural stability. Finally, this descriptor can be used to improve the design of structurally stable perovkites.

P 36

First Principle Study on Magneto-electric Multiferroics

Reshmi.T[1], Dr.Kartick Tarafder[2**]
Department of Physics, National Institute of Technology Karnataka, Surathkal

INTRODUCTION

❑ Multiferroic materials are special class of solid state compounds which are simultaneously ferromagnetic, ferroelectric and often ferroelastic.

❑ The coexistence of several ferroic order parameters in such materials brings out novel physical phenomena and offers possibilities for new functional devices.

❑ Multiferroics promises their potential applications including sensors, data storage recording technologies, random access multi-state memories, energy harvesting and photo-voltaic technologies.

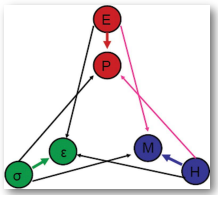

Figure showing possible coupling in multiferroics

OBJECTIVES

❑ Understanding the mechanism of coexistance of multiple ferroic orders in multiferroics.

❑ Investigate the multiferroic behaviour of Bismuth ferrite($BiFeO_3$) based on Density Functional Theory

❑ Implementation of Modern Theory of Polarization in the calculation of spontaneous polarization.

❑ Electronic structure and band structure studies on effect of doping at iron site by Cobalt (Co) in $BiFeO_3$ (BFO).

Density Functional Theory (DFT)

❑ DFT is a powerful tool in computational material science for the calculation of electronic, magnetic and structural properties of solids.

Many body Hamiltonian is given by

$$\hat{H} = -\sum_i \frac{\hbar^2}{2m_e}\nabla_{r_i}^2 - \sum_i \frac{\hbar^2}{2M_I}\nabla_{R_I}^2 + \frac{1}{2}\sum_{i\neq j}\frac{e^2}{|r_i - r_j|} - \sum_{i,I}\frac{Z_I e^2}{|r_i - R_I|} + \frac{1}{2}\sum_{I\neq J}\frac{Z_I Z_J e^2}{|R_I - R_J|}$$

Kohn-Sham scheme

Calculate $\rho(r)$ using trial basis $\{|\phi_i\rangle\}$

$$V_{eff}(r) = V_{ext}(r) + \int \frac{\rho(r')}{|r - r'|}dr' + \frac{\delta E_{xc}^{new}[\rho(r)]}{\delta\rho(r)}$$

$$\left[-\nabla_i^2 + V_{eff}[\rho(r)]\right]|\psi_i\rangle = \varepsilon_i|\psi_i\rangle$$

Calculate $\rho(r)$ using $\{|\psi_i\rangle\}$

$$E[\rho(r)] = T_{eff}[\rho(r)] + \int V_{ext}(r)\rho(r)dr + \iint \frac{\rho(r)\rho(r')}{|r - r'|}drdr' + E_{xc}^{new}[\rho(r)]$$

Compare Energy

Studies on Bismuth ferrite ($BiFeO_3$)

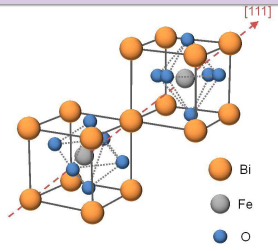

Electronic and Band structure calculation for pure and Co doped $BiFeO_3$

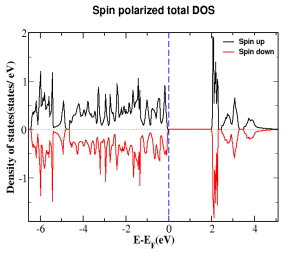

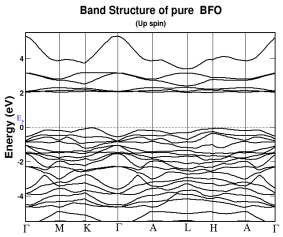

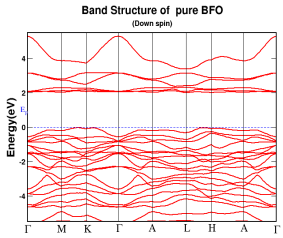

Polarization Calculations

- Pure BFO : 96 μC/cm²
- Co doped BFO : 99.75 μC/cm²

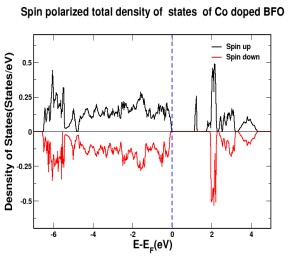

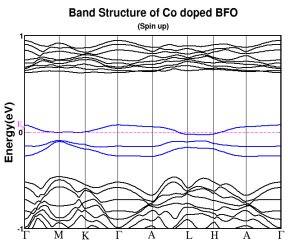

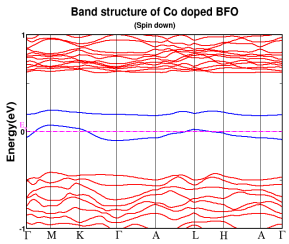

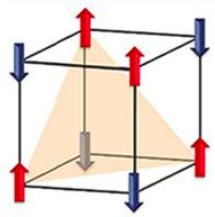

G – type Antiferromagnetic ordering is observed in pure Sample

CONCLUSIONS

❑ Our studies indicates a band gap of 2eV. This confirms the dielectric nature of the material.

❑ Even though pure BFO is antiferromagnetic , Cobalt doping enhanced its magnetic moment to 0.98 μB .

❑ Our calculations confirm the increased magnetic and ferroelectric properties in Bismuth Ferrite when Iron site doped with Cobalt. We can conclude that the magneto-electric coupling in BFO is enhanced by Co doping.

REFERENCES

1. C. Ederer, N.A. Spaldin, Phy. Rev. B – Condensed Matter and Materials Physics 71(6), 1-4 (2005).
2. N.A. Spaldin. A beginner's guide to modern theory of polarization J. Solid State Chem. 195, 2-10 (2012).
3. K.F. Wang, J.M. Liu, Z.F. Ren, Advances in Physics 58(4), 321-448 (2009).
4. N.A.Spaldin, S.W.Cheong, R.Ramesh, Multiferroics: Past, present, and future. Phy. Today, 63(10):38-43(2010).

P137

Pulay forces and stresses in density-functional theory with extended Hubbard functionals: From nonorthogonalized to orthogonalized manifolds

Density-functional theory with extended Hubbard functionals is a powerful method for studying complex materials containing transition-metal and rare-earth elements, owing to its accuracy in correcting self-interactions and its low computational costs. There are two key elements in these formulations which are closely interconnected: i) the choice of the on-site U and inter-site V Hubbard parameters, and ii) the choice of the Hubbard manifold. Recently, we developed an automated and reliable approach for the first-principles determination of U and V from density-functional perturbation theory [1], that can be used with nonorthogonalized and orthogonalized atomic orbitals as a Hubbard manifold. Achieving the self-consistency between the Hubbard parameters on the one hand and the crystal structure (lattice parameters and atomic positions) on the other hand requires computing Hubbard (Pulay) forces and stresses. While this calculation is straightforward for nonorthogonalized atomic orbitals, the use of an orthogonalized Hubbard basis set poses serious challenges. Here we present a derivation of the exact expression for Hubbard forces and stresses with orthogonalized atomic orbitals [2]. The key ingredient of this formulation - the derivative of the inverse square root of the orbital overlap matrix - is obtained as a closed-form solution of the associated Lyapunov (Sylvester) equation. We have implemented this method in Quantum ESPRESSO and benchmarked it with respect to finite differences of total energies for the case of NiO, finding excellent agreement. [1] I. Timrov et al., PRB 98, 085127 (2018), [2] I. Timrov et al., PRB 102, 235159 (2020).

P138

Heat transport in water from Deep Neural Network potentials

The computation of heat transport in general multi-component systems has been made feasible by recent theoretical advances [1], but is still extremely computationally expensive. However, the Deep Potential--Smooth Edition (DeepPot-SE) model [3], once properly trained, has proved to correctly predict liquid water properties, holding the promise to deliver the accuracy and transferability of ab initio methods at the cost of classical simulations. We discuss the crucial role of gauge [1] and convective [2] invariance principles. We present an explicit expression for the energy flux in DeepPot-SE, suitable for the computation of heat-transport coefficients in crystalline solids, glasses and liquids, using equilibrium MD. Our methodology is first validated against DFT-PBE ab initio results for liquid water [1]. It is then used to compute the thermal conductivity from a potential trained on accurate DFT data obtained from the SCAN functional. This work was partially funded by the EU through the MaX (Project No. 824143) and by the Italian Ministry of Research and education through the PRIN 2017 FERMAT grant. [1] A. Marcolongo, P. Umari, S. Baroni, Nat. Phys. , doi:10.1038/nphys3509. [2] R. Bertossa, F. Grasselli, L. Ercole and S. Baroni, Phys. Rev. Lett., 122, 255901 (2019). [3] L. Zhang, J. Han, H. Wang, W. A. Saidi, R. Car, Weinan E, Adv. Neural Inf. Process Syst. 31, 4436-4446 (2018)

P139

CO_2 capture, activation and dissociation on the Ti_2C surface and Ti_2C MXene: the role of surface structure

Aswathi Mohan T.[1], Nishamol Kuriakose[2], Krishnakanta Mondal[2] and Prasenjit Ghosh[2,3]

[1]Department of Chemistry, [2]Department of Physics, [3]Centre for Energy Science,
Indian Institute of Science Education and Research, Pune – 411008

ABSTRACT

Atmospheric CO_2 is one of the main components of the greenhouse effect. To overcome this problem there are ongoing efforts to convert CO_2 to some other useful and harmless products. The capture, activation and dissociation of CO_2 are the preliminary steps in this process. In an effort to understand the role of surface composition and structure in CO_2 adsorption and dissociation, in this work, with the help of first principles density functional theory based calculations, we have studied the same on the (100) surface of cubic Ti_2C and MXene (also the (0001) surface of trigonal Ti_2C). Our results show that CO_2 undergoes barrierless chemisorption on both of these surfaces with a preference towards (100) cubic Ti_2C. We attribute the reason for this to a lower value of the work function of the (100) surface. Furthermore, on MXene, the barrier for CO_2 dissociation is lower compared to that on the (100) surface. Coverage dependent CO_2 chemisorption studies on these two surfaces show that on the Ti_2C surface the CO_2 molecules form clusters around the C-vacancies while on MXene they are uniformly spread on the surface.

COMPUTATIONAL DETAILS

- DFT based Quantum ESPRESSO package
- Electron ion interactions described via ultrasoft pseudopotential
- PBE parameterisation of GGA exchange and correlation functional
- DFT-D2 used for dispersion corrections
- Energy cutoff of 55 Ry and 480 Ry used for wavefunction and charge density
- Marzari – Vanderbilt smearing of width 0.007 Ry used
- Spin polarised calculations for MXene. Vacuum separation of 15 Å and BZ sampled by 9*9*1 Monkhorst-Pack k-point mesh. Antiferromagnetic ground state having intralayer parallel and interlayer antiparallel spins.
- Non magnetic calculation for Ti_2C (100) surface. Vacuum separation of 16 Å and BZ sampled by 6*6*1 Monkhorst-Pack k-point mesh.
- CI-NEB used for finding minimum energy path. A minimum of 13 and 6 images used for CO_2 dissociation paths for MXene and (100) surface respectively.
- Adsorption energy of species X on surface is calculated as,

$E_{ads} = E_{tot}(X/surface) - E_{tot}(surface) - E_{tot}(X)$

Ti_2C SURFACES: STRUCTURE & STABILITY

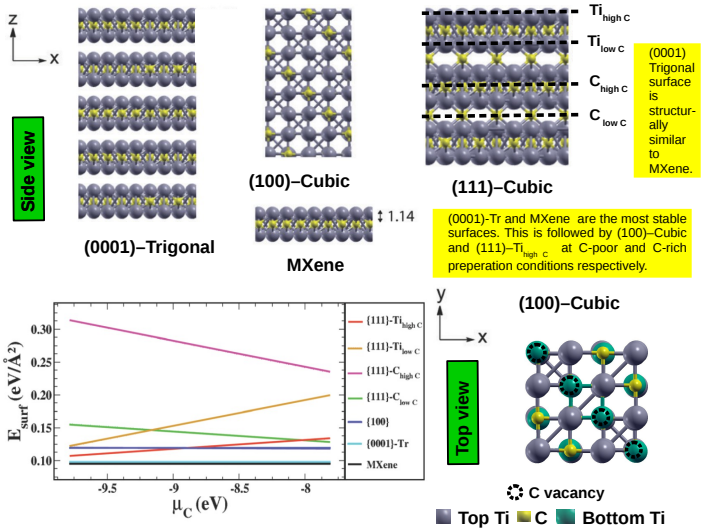

CO_2 ACTIVATION

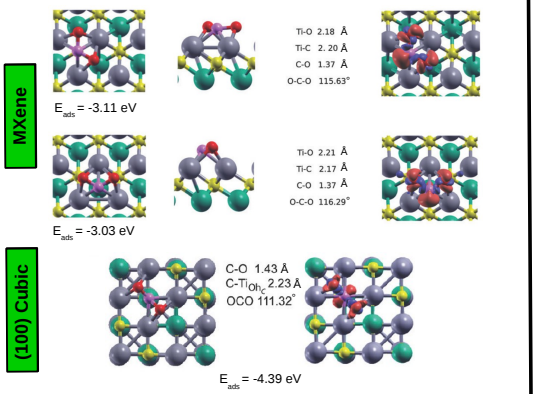

Charge transfer of 1.81 e and 2.25 e occur from MXene and (100) surface to CO_2 respectively. (100) surface has a lower work function hence has a higher reducing capacity.

CO_2 DISSOCIATION

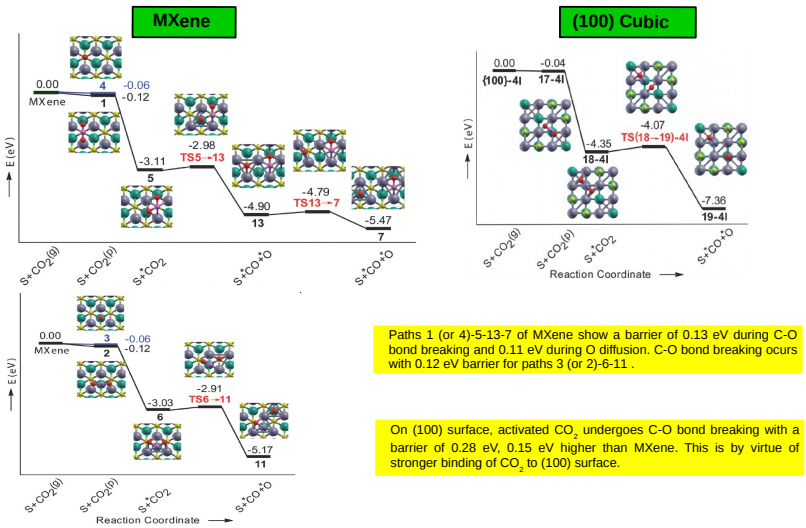

Paths 1 (or 4)-5-13-7 of MXene show a barrier of 0.13 eV during C-O bond breaking and 0.11 eV during O diffusion. C-O bond breaking ocurs with 0.12 eV barrier for paths 3 (or 2)-6-11 .

On (100) surface, activated CO_2 undergoes C-O bond breaking with a barrier of 0.28 eV, 0.15 eV higher than MXene. This is by virtue of stronger binding of CO_2 to (100) surface.

COVERAGE DEPENDENT ACTIVATION

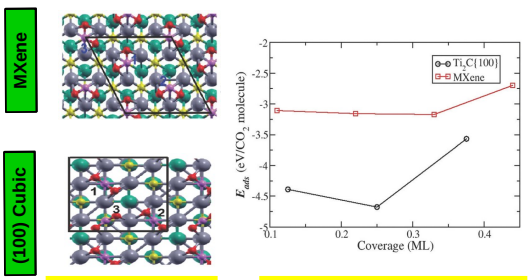

CO_2 molecules are more or less uniformly distributed on MXene while they cluster around C vacancy for (100) surface.

On MXene : Till coverage is 0.33 ML, CO_2 molecules do not interact. Above 0.33 ML, repulsive interaction is seen.
On TiC (100) : Attractive interaction till 0.25 ML and repulsive interaction thereafter.

CONCLUSIONS

- CO_2 activation and dissociation was studied on (100) cubic Ti_2C surface and MXene to understand the effect of surface structure.
- CO_2 activation requires no barrier on both substrates and has a stronger binding to (100) surface due to lower work function.
- CO_2 dissociation requires higher activation energy on (100) surface because of its stronger binding.
- As coverage increases CO_2 molecules are more or less uniformly distributed on MXene while they cluster around C vacancies on the (100) surface.

REFERENCES

This work is published as Phys. Chem. Chem. Phys., 2020, 22, 14599—14612.

ACKNOWLEDGEMENT

IISER Pune
DST-INSPIRE
DST-NANOMISSION
CDAC Pune
DST-SERB

P140

Two-dimensional ABO_3/Me oxide quasicrystal approximants : insights from Density Functional Theory

T. T. Dorini[1,3], F. Brix[1,3], C. Chatelier[1,3,4], M. Sicot[1,3], J. Ledieu[1,3], V. Fournée[1,3], A. Kokalj[2,3], É. Gaudry[1,3]

[1] *Univ. Lorraine, CNRS, IJL, 2 allée André Guinier, Nancy, France*

[2] *Jožef Stefan Institute (IJS), Jamova cesta 39, 1000 Ljubljana, Slovenia*

[3] *IRP PACS2 CNRS Universite de Lorraine, Nancy, France*

[4] *Synchrotron SOLEIL, Gif-sur Yvette, France*

Perovskite oxide present a wide range of composition and physical properties, that have been extensively studied. Recently, a conceptual breakthrough – the discovery of the quasiperiodic order in ultra-thin perovskite films [1] – reinvigorated the field, and raised the question of the reasons behind the emergence of the quasiperiodic order in these systems. In this work, starting from the structural model derived for the $BaTiO_3$/Pt(111) approximant [2], the structural, thermodynamic, electronic, and magnetic properties of freestanding two-dimensional oxide quasicrystalline approximants as well as their characteristics when deposited over metallic substrates, are systematically investigated to unveil the structure-properties relationships within the series. Our thermodynamic approach suggests that the formation of such aperiodic systems is likely for a large range of compositions. Electronic effects are identified as the main driving force for their formation, while the effect of size-mismatch appears to be weak. The control of the magnetic properties and the work functions of these metallic supported ultrathin oxide films is achievable by tuning their chemical composition. Our results provide well-founded general guidelines for the discovery of new oxide quasicrystalline ultra-thin films with interesting physical and chemical properties.

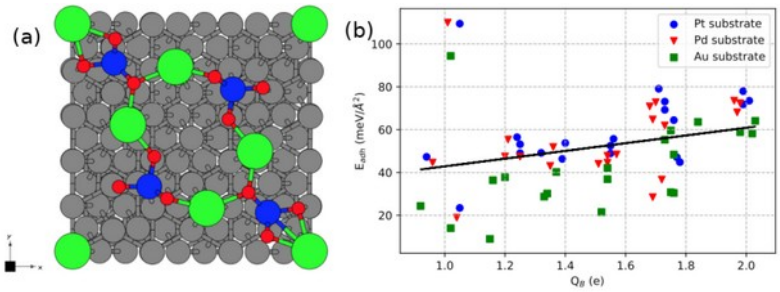

Figure : (a) Structure of the 2D oxide quasicristalline approximant $BaBO_3$/Pt(111) (top view); (b) Adhesion energy (E_{ads}) of the 2D oxide layer as a function of the Bader charge on the B-type atoms (Q_B).

[1] S. Förster et al. "Quasicrystalline structure formation in a classical crystalline thin-film system", Nature 2013, 502, 215;

[2] S. Förster et al. "Observation and structure determination of an oxide quasicrystal approximant", Physical Review Letters 2016, 117(9), 095501.

Additional information:
Type of contribution: oral
Presenting author: Thiago Trevizam Dorini
Status: PhD student
Phone: +33 07 66 71 08 22
e-mail: thiago.trevizam-dorini@univ-lorraine.fr

P141

Hydrogen Storage on TM metal doped Mgn and ZTC - A denstiy functional Investigation

n this work, we reported the interaction of hydrogen molecule with Mgn(Rh, Co) clusters using density functional formalism with an objective to study (a) the reactivity of small sized MgnRh and MgnCo clusters with H2 molecule and (b) the catalytic effect of Rh and Co on the Mgn cluster for adsorption and dissociation of hydrogen. From the variation of thermodynamic parameters, adsorption and chemisorption etc. with the size of the cluster, we found that the most stable lowest energy structure in the series is Mg6Rh, whereas, Mg9Rh is the most effective hydrogen storage cluster, while with Co doping, Mg5Co is most suitable for hydrogen storage. Interaction of H2 with MgnRh/MgnCo cluster shows a significant reduction in the activation barrier energy, which helps in the hydrogen dissociation. The chemisorptions energy reveals that Mg9Rh/Mg5Co cluster act as an effective catalytic agent for hydrogen adsorption and dissociation. On the other hand ZTC consists of microporous ordered nanostructures and synthesized in the confined space of nano channels in zeolite-Y. They are promising hydrogen storage materials because of their large surface area and uniform micro pores suitable for hydroge storage. Using the density functional theory we have studied hydrogen storage capability of Y doped ZTC. [On going work]

P142

Enhancing the speed and precision of Wannier interpolation with `WannierBerri` code.

Stepan S. Tsirkin*
Department of Physics, University of Zurich, Winterthurerstrasse 190, CH-8057 Zurich, Switzerland
(Dated: January 14, 2021)

`WannierBerri` [1,2] is a new Python code for Wannier interpolation, which is close in spirit to the post-processing module of the well-known Wannier90 code [3] (postw90.x), but improves over it by in a few directions.

- First, it is faster - sometimes by a factor of thousands, despite being a python "script" rather than an high-performance Fortran90 code. This is achieved by implementing a series of methods which include a combination of fast and slow Fourier transforms, explicit use of symmetries and other algorithms.

- Second, it allows to achieve convergence of Brillouin zone integration with less k-points. This is done by a special adaptive-refinement algorithm. Moreover, in some cases, e.g. in evaluation of Berry curvature dipole, use of Fermi-sea formulation with analytical Berry curvature derivatives also improves the k-grid convergence.

- Third, the pythonic structure of the code and its interface are aimed to be friendly to both users and developers.

A plethora of quantities are implemented, such as anomalous Hall conductivity, orbital magnetization, Berry curvature dipole, and spin Hall conductivity, among many others. More features, such as Wilson loops, magnetoresistance, and electrical magneto-chiral anisotropy, are under active development, and `WannierBerri` aims to serve as a platform for developing new Wannier interpolation functionalities.

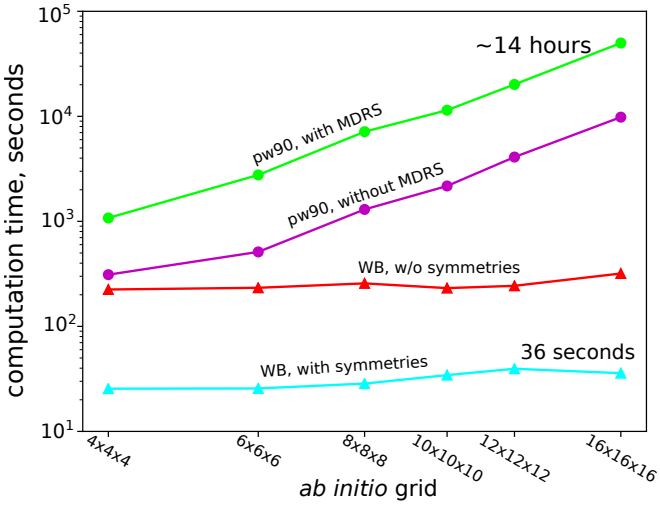

Computational time for AHC. Time for calculations with `WannierBerri` (`WB`, triangles) and `postw90.x` (`pw90`, circles) for different *ab initio* grids. For `WB` the calculations are done with (cyan) and without (red) use of symmetries. For `WB` the minimal-distance Replica method does not affect the computational time.

[1] http://wannier-berri.org
[2] https://arxiv.org/abs/2008.07992
[3] http://wannier.org

* *e-mail*: stepan.tsirkin@uzh.ch

P143

Higher order many-body perturbation theory applied to atomic systems

While the GW method has been the subject of an intense work of validation, higher-order many-body perturbation theory (MBPT) methods have received much less attention. Here we investigate the performance of beyond-GW MBPT approaches in atomic systems described within the spherical approximation. By using a dedicated numerical treatment based on a B-spline/spherical harmonics representation [1], we obtain benchmark results avoiding many commonly adopted approximate procedures (including complete basis set extrapolations and frequency descriptions). A number of MBPT schemes is explored, involving GW, 2nd Born, and SOSEX [2] self-energies. We present a variety of results obtained through their employment, including static polarizabilities, ionization potentials, and Kohn-Sham exchange and correlation potentials as obtained from the solution of the Sham-Schlüter equation (SSE). [1] M. Hellgren and U. von Barth, Phys. Rev. B 76, 075107 (2007). [2] X. Ren et al., Phys. Rev. B 92, 081104 (2015).

P144

Synthesis, Spectral, Hirshfeld surface analysis, DFT calculations and molecular docking studies on dioxol derivatives as potential antibacterial inhibitors

V.Vetri velan *

* Department of Physics, Thanthai Periyar Government Institute of Technology, Vellore-632 002. Tamilnadu, India.

Corresponding author. Tel.: +91 9486898120. Email address: vetri.tpgit@gmail.com (V. VETRI VELAN)

Abstract

The title compound (2Z)-3-(2H-1,3-benzodioxol-5-yl)-1-(6-chloropyridin-3-yl) prop-2-en-1-one has been synthesized and single crystals were grown by slow evaporation solution growth technique at room temperature. FT-IR, Raman, UV and NMR spectra of synthesized compound in the solid phase were recorded and analyzed. The minimum energy conformer has been found by PES (Potential Energy Surface) and then the structure is optimized. The optimized geometry and vibrational wave numbers were computed using DFT method. The NLO, Mulliken, MEP, HOMO-LUMO energy gap and thermodynamic properties were theoretically predicted. The hyperpolarizability calculation reveals the present material has a reasonably good propensity for nonlinear optical activity. The NBO analysis explained the intramolecular hydrogen bonding. The global chemical reactivity descriptors are calculated for compound and used to predict their relative stability and reactivity. Molecular Electrostatic Potential (MEP), Electron Localization Function (ELF) and Localized Orbital Locator (LOL) have been depicted to know the chemically active regions. Hirshfeld surface analysis and Fukui functions calculation were also performed. All the calculations were carried out by B3LYP/6-311++G (d,p) method using Gaussian 09. The antibacterial and antifungal activity of the compound was also tested against various pathogens. The molecular docking studies concede that title compound may exhibit antibacterial inhibitor activity.

Keywords: DFT, FT-IR, FT-Raman, Hirshfield surface analysis, DOS, Molecular docking

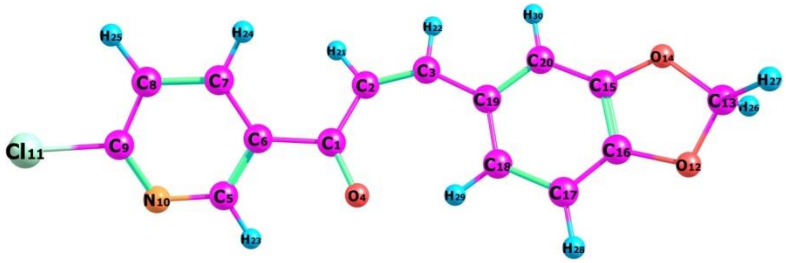

References:

1. Mehmood M.H, Gilani A.H, J. Med. Food 13 (2010) 1086.
2. Sudjarwo S.A, Folia Medica Indonesiana, 41 (2005) 190.

P145

Improving density functional calculations of molecular polarizabilities using locally scaled self-interaction corrections

We examine the effect of removing self-interaction error (SIE) on the calculation of molecular polarizabilities in the local spin density (LSDA) and generalized gradient approximations (GGA). To this end, we utilize a database of 132 molecules to assess the influence of SIE on polarizabilities by comparing results with accurate reference data. Our results confirm that the general overestimation of molecular polarizabilities by these density functional approximations can be attributed to SIE. However, removing SIE using the Perdew-Zunger self-interaction-correction (PZ-SIC) method, implemented using the Fermi-Löwdin Orbital SIC approach, leads to an underestimation of molecular polarizabilities, showing that PZ-SIC overcorrects when combined with LSDA or GGA. Application of a recently proposed locally scaled SIC is found to provide more accurate polarizabilities. We attribute this to the ability of the local scaling scheme to selectively correct for SIE in the regions of space where the correction is needed most.

P146

First-principles studies of the electronic and mechanical properties of α-Al/γ-Al2O3(111) multilayer composite

Edwin M. Vásconez* [1] [2], Jerzy Leszczynski[3], and Henry P. Pinto[1]

[1]Universidad San Francisco de Quito, Escuela de Ciencias e Ingenierías, Cumbayá-Ecuador

[2]CompNano Group, School of Physical Sciences and Nanotechnology, Yachay Tech University, Urcuqui-Ecuador.

[3]Interdisciplinary Center for Nanotoxicity, Department of Chemistry, Physics and Atmospheric Sciences, Jackson State University, Jackson, MS 39207, USA.

*edwin.vasconez@yachaytech.edu.ec

Introduction

The γ-Alumina (γ-Al2O3) phase is mainly used in the catalysis, electronics and automotive industries due to its interesting electronic and mechanical properties [1][2]. Recent experiments on multilayered α-Al/γ-Al2O3 are found to exhibit improvement of the mechanical properties in comparison with individual layers [2]. However, the actual atomic structure of γ-Al2O3 is slightly known and has motivated a large number of experimental and theoretical studies [3][4]. The proposed research will start considering the γ-Al2O3 bulk structure that was already predicted using density-functional theory (DFT). Interestingly, this theoretical model predicted the decomposition of the γ-Al2O3(110) surface to (111) nanofacets and has been already confirmed experimentally. The knowledge on these surfaces is applied in the construction of four atomic models for α-Al/γ-Al2O3(111) multilayer. The study will consider the atomic interface reconstruction of the metal/oxide interface, which structure will be resolved using simulated annealing. The electronic and mechanical properties of the most stable multilayered structures obtained will be computed and analyzed in the light of available experimental data. The electronic properties showed that the composite acquires a metal-like behavior. We found that there is an enhancement of the mechanical properties in the multilayered models, also founded in experimental results.

Methods

The plane wave Vienna *ab initio* simulation package (VASP) was used for the DFT calculations. This package uses plane-waves basis set ideal for crystalline systems. The necessary parameters for the simulations are: Functional GGA-PBE, core electrons described with PAW potential, an appropriate cutoff energy and k-points with an energy convergence < 1 meV/atom, and ionic relaxations < 0.01 eV Å^{-1}. Using those parameters, we computed the optimal structures for both, α-Al and γ-Al2O3 bulks. Four α-Al/γ-Al2O3 multilayered models were built using the slabs γ-Al2O3(111)a and γ-Al2O3(111)b. Simulated annealing was used to solve the metal/oxide multilayered models: equilibration was performed at 1000 K and then cooled down to 0 K, followed by full relaxation. In all cases, the equation of state was computed using the Birch-Murnagham of 3th order.

α-Al and γ-Al2O3 bulks

In this study we considered both, fcc α-Al and γ-Al2O3, Fig.1. Computed PBEsol mechanical properties are shown in Table 1, with their respective experimental values in this way we validate our theoretical approach of the multilayered models.

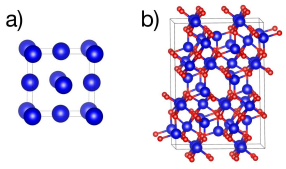

Figure 1. PBEsol computed structures of a) α-Al and b) γ-Al2O3; the blue and red spheres represent Al and O respectively.

Table 1. Mechanical properties for computed α-Al and γ-Al2O3.

System	V_o(Å^3)	B_o(GPa)	E_{coh}(eV/atom)	Hκ(GPa)
α-Al	16.198	81.59 (69±4)[5]	3.89 (3.39)[6]	1.03 (0.25-1.09)[7-8]
γ-Al2O3	371.191 (371.35)[9]	204.05 (250±9)[10]	5.642	22.26 (19-20.29*)[7-11]

* Data for corundum α-Al2O3.

According with the electronic properties we confirm the metallic behaviour of α-Al, while γ-Al2O3 is an insulator, see Fig.2.

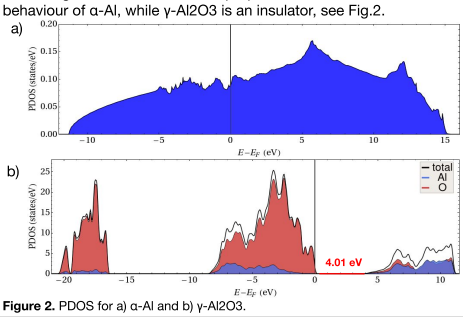

Figure 2. PDOS for a) α-Al and b) γ-Al2O3.

γ-Al2O3 surfaces

The multilayered models were done using the γ-Al2O3 surfaces: (111)a and (111)b. According to Pinto et al. [4], (111)a is the most likely surface reported and (111)b belongs to the same family, see Table 2 and Fig.3.

Table 2. Surface energies for γ-Al2O3 surfaces, after (σR) and before (σS) full relaxation.

Surface	σR (J/m^2)	σS (J/m^2)
γ-(111)a	0.95	1.62
γ-(111)b	1.85	3.57
γ-(001)	1.05	2.97
γ-(110)	1.53	3.43

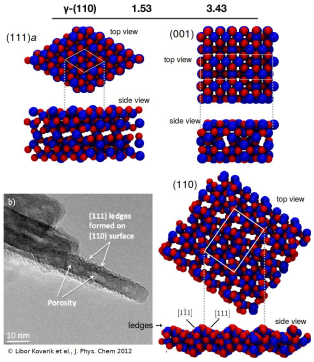

Figure 3. DFT computed structure of γ-Al2O3 (111)a, (001), and (110) surfaces. High-Resolution Electron Microscopy of γ-Al2O3 surface [1].

α-Al/γ-Al2O3 multilayered models

In this work we consider only the case of α-Al(111)/γ-Al2O3(111) multilayer where the α-Al and γ-Al2O3(111) have approximately the same thickness, 13.5 Å, along the crystallographic direction [111]. More specifically, the multilayer models were built using γ-Al2O3 slabs γ-Al2O3(111)a and γ-Al2O3(111)b shown in Fig.4 a) and b). The four multilayered models are shown in Fig.4 c).

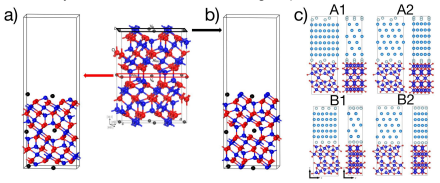

Figure 4. γ-Al2O3 a) (111)a, and b) (111)b slabs; the black spheres are the Al-vacancy sites. c) Multilayered models; the light blue spheres represent the Al of the α-Al, and the cyan spheres represent the Al atoms at the interface.

The mechanical and electronic properties of the multilayered models are shown in Table 3 and Fig.5 and 6.

Table 2. Mechanical properties for multilayered models.

Model	B_o(GPa)	Hκ(GPa)	E_{coh}(eV/atom)	δ(g/cm^3)	γ_{int}(eV/Å^2)
A1	108.47	6.672	3.95	3.13	0.653
A2	112.04	8.471	4.24	3.08	0.071
B1	113.07	8.505	4.49	3.21	0.083
B2	128.98	12.11	4.29	3.18	0.094
α-Al	81.59	1.03	3.89	2.77	-
γ-Al2O3	204.05	22.26	5.76	3.65	-

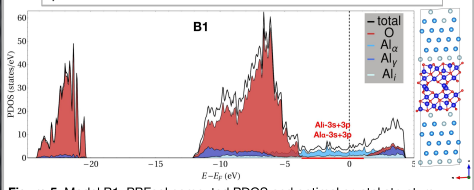

Figure 5. Model B1: PBEsol computed PDOS and optimal crystal structure.

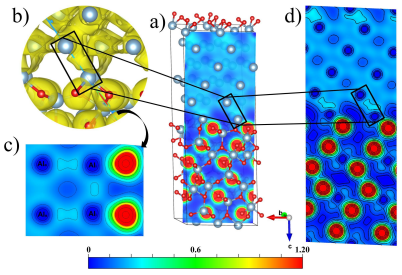

Figure 6. Model B1: Electron charge density. a) Electron charge density across (010) plane crossing certain. b) Close-up section showing a iso-charge density for the Aα and Ai bond. c) Contour plot of electron charge density of the bond. d) Contour plot of electron charge density across (010) plane (0 to 1.2 e/Å^3).

Conclusions and Outlook

A DFT study on α-Al and γ-Al2O3 was presented. Preliminary results of four multilayered models of α-Al/γ-Al2O3(111) were shown. According to the calculated data, the mechanical properties are predicted to be harder than α-Al and softer than γ-Al2O3. B2 model is the most resistant under compression and the hardest. The most stable structure is the B1. The composites acquire a metal-like behavior. Moreover, we are going to consider a multilayer system with different ratio thickness of the γ-Al2O3 and the α-Al regions.

Acknowledgement

The authors would like to thank the support of the School of Physical Sciences and Nanotechnology at Yachay Tech University. Edwin Vásconez and Henry Pinto want to acknowledge HPC-Europa3 (HPC17WE2EY) for providing state-of-the-art high-performance computing facilities for this research.

References

[1] Kovarik, L.; Bowden, M.; Genc, A.; Szanyi, J.; Peden, C. H.; Kwak, J. H. The Journal of Physical Chemistry C 2014, 118, 18051–18058.
[2] Goswami, R.; Pande, C.; Bernstein, N.; Johannes, M.; Baker, C.; Villalobos, G. Acta Materialia 2015, 95, 378–385.
[3] Ayoola, H. O.; House, S. D.; Bonifacio, C. S.; Kisslinger, K.; Saidi, W. A.; Yang, J. C. Acta Materialia 2020, 182, 257–266.
[4] Pinto, H. P.; Nieminen, R. M.; Elliott, S. D. Physical review b 2004, 70, 125402.
[5] Mearini, G.; Hoffman, R. Journal of electronic materials 1993.
[6] Kittel, C. Introduction to Solid State Physics, 8th ed.; Wiley, 2004.
[7]Sung, C.-M.; Sung, M. Materials Chemistry and Physics 1996.
[8] Holt, J.; Ho, C.; Mindlin, H. Structural Alloys Handbook; CINDAS/Purdue University, 1996.
[9] Ahuja, R.; Osorio-Guillén, J.; Almeida, J.; Holm, B.; Ching, W.-Y.; Johansson, B. Journal of Physics: Condensed Matter 2004.
[10] Dubrovinsky, L. S.; Saxena, S. K.; Lazor, P. Physics and Chemistry of Minerals 1998.
[11] Leger, J.; Haines, J.; Schmidt, M.; Petitet, J.; Pereira, A.; Da Jornada, J. Nature 1996.

P147

Polarons In Two-dimensional Pnictogens: DFT Study

Vasilchenko V.[1], Levchenko S.[1], Perebeinos V. [2] , Zhugayevych A. [1]

1 – Skolkovo Institute of Science and Technology, Moscow, Russia
2 – University at Buffalo, NY, United States
vasilii.vasilchenko@skoltech.ru

Present work is dedicated to the study of small polarons in emerging semiconductors: two-dimensional pnictogenes. They are great candidates for application in electronics and the work done will allow for better understanding of the nature of charge carriers in these materials. Up to this point, no information on their polaronic character has been provided and generally they were considered as free electrons and holes. First-principles cluster calculations and finite-size scaling show stability of a small hole polaron in blue phosphorene and arsenene. It is localized on a phosphorus atom, leading to the contraction of the bonds around it. Commonly used hybrids including PBE0, HSE06, B3LYP show consistent results with the adiabatic polaron relaxation energy slightly below 0.1 eV for phosphorene and 0.15 eV for arsenene. The adiabatic barriers for motion of the polaron are small compared to the frequency of strongly coupled phonons implying barrierless motion of the polaron.

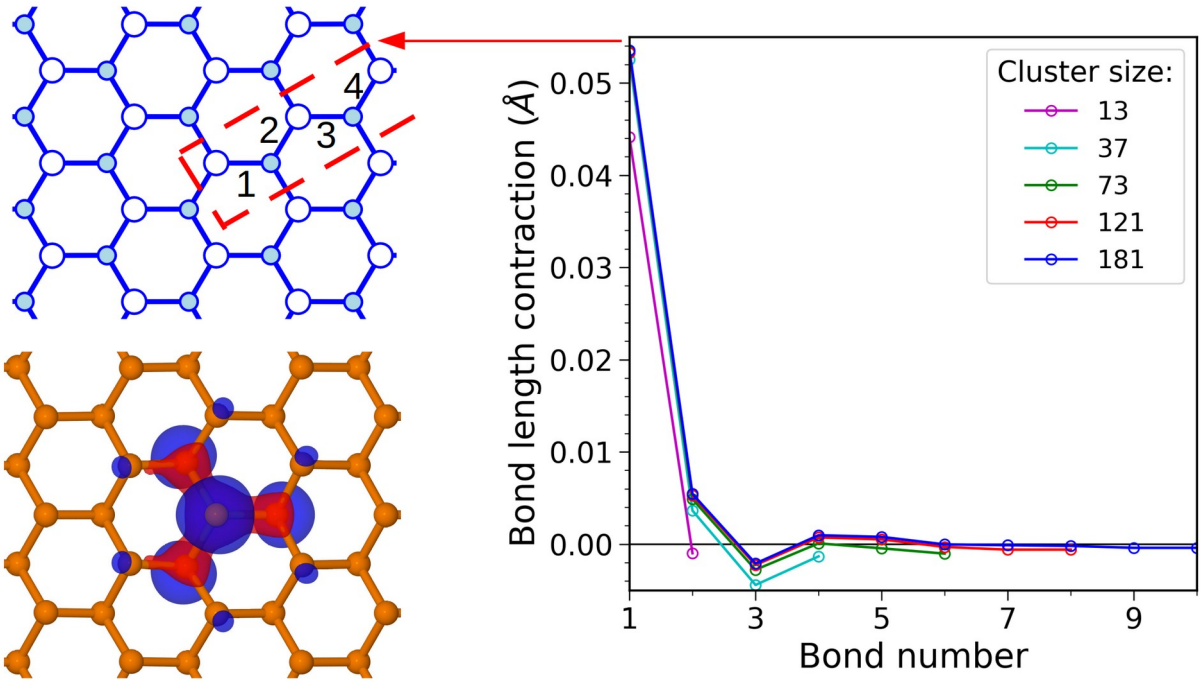

P148

Theoretical phase diagram of boron carbide from ambient to high pressure and high temperature

The phase diagram of boron carbide is calculated within DFT as a function of T and P up to 80 GPa, accounting for icosahedral, graphite- and diamond-like atomic structures [1]. Only some icosahedral phases turn out to be thermodynamically stable with atomic carbon concentrations (c) of resp. 8.7% (B10.5C), 13.0% (B6.7C), 20% (B4C) and 28.6% (B2.5C). Their respective ranges of stability under pressure and temperature are calculated, and the theoretical T-P-c phase diagram boundaries are discussed. At ambient conditions, the introduction in the phase diagram of the new phase B10.5C, with an ordered crystalline motif of 414 atoms, is shown to bring the theoretical solubility range of carbon in boron close to the experimental one. The effect of configurational entropy is studied at finite temperature, and the convex hull modified. We discuss the occurrence of the “single phase regime” in the light of these new results. [1] A. Jay, O. Hardouin Duparc, J. Sjakste and N. Vast, J. Appl. Phys. 125, 185902 (2019). https://doi.org/10.1063/1.5091000 *Results have been obtained with the Quantum ESPRESSO package, and computer time granted by PRACE (Project No. 2019204962) and by French GENCI-CINES and GENCI-TGCC (Project 2210). Supports from DGA and NEEDS-Matériaux are gratefully acknowledged.

P149

Effect of Adsorption of Co and Mn atoms on magnetic and transport properties of hydrogenated borophene nanoribbons

Effect of Adsorption of Co and Mn atoms on magnetic and transport properties of hydrogenated borophene nanoribbons In recent years, enormous research has focused on two-dimensional (2D) nanomaterials due to their attractive physical properties and various technological applications. Recently, two-dimensional (2D) boron sheets named as borophene have been synthesized on silver surfaces [1-2]. Borophene exhibits various structural polymorphs, all of them metallic and highly anisotropic. However, pristine borophene is inherently non-magnetic, which limits its use for spintronic applications. Several approaches can be used to induce magnetic properties in borophene. For example, the adsorption of 3d transition metals (TM) or the patterning of borophene into 1D strips, named as borophene nanoribbons (BNRs) [3-4]. In this work, by using density functional theory (DFT), the effect of adsorption of Mn and Co-transition atoms on the surface of hydrogenated zigzag borophene nanoribbons is investigated. The calculations are performed using density functional theory and non-equilibrium Green's function. The results indicate that the non-magnetic structure of hydrogenated zigzag borophene nanoribbons becomes magnetic by adsorbing Co and Mn atoms on its surface. Also, the direction of charge flow is from Co and Mn atoms to borophene nanoribbon, in other words, Co and Mn atoms are donors and B atoms are electron acceptors. References [1] Mannix, A. J. et al. Science 350, 1513 (2015). [2] Wang, H. F. et al. New J. Phys. 18, 073016 (2016). [3] Sevinçli, H. et al. Phys. Rev. B 77 195434 (2008). [4] Sahar Izadi .S. et al. Nanomicro Lett. 10 (2018).

P150

Ab Initio study of the structural and electronic properties of Niobium Sulfide (NbS2) and Lithium Niobium Sulfide (LiNbS2) bulk and (001) surfaces

In the context of the discovery of new materials, intercalation of Lithium (Li) atoms among layers of NbS2 can be performed. However, few experimental works deal with this material. Recently, Voiry et al. performed some experiments with LiNbS2 providing some insights about the properties of this system. Hence, we describe this material with state of the art non-empirical density functionals in the framework of density-functional theory (DFT). Specifically, we describe various insights regarding the electronic and atomic structure, lattice parameters, scanning tunnelling microscopy images and phonons of the bulk and surfaces of LiNbS2. We perform the computations with the meta-GGA SCAN functional and some variations of the hybrid HSE as implemented in VASP. We found out that SCAN+rVV10 performs very well in the description of certain properties of LiNbS2 and NbS2. Besides, we tested the hybrid HSE12 and HSE12s and compared with the customary HSE06. The performance of the hybrids is discussed too. Interestingly, we found that the intercalation of Li on NbS2 produces a considerable band-gap, making the material a semiconductor and providing promising technological applications.

P151

DFT insights into electrocatalytic reduction of CO2 reduction on PdCu(110) surface

Electrocatalytic reduction of CO2 is an important reaction considering the ever increasing CO2 levels in the atmosphere and their baneful effects such as global warming, ocean acidification, etc. There have been efforts in the last decade to find the stable, efficient and selective catalyst to carry out the electrocatalytic CO2 reduction towards desired products. Of which Cu based materials have shown some promising results, particularly PdCu alloy. Among different phases of PdCu alloy (ordered, disordered and phase separated alloy) the ordered alloy poses high C1 selectivity. In addition to that the formation of C2 products increases as the Cu fraction in the alloy increases. It is suspect that the Cu-Cu neighbors in the active site promotes the C-C coupling and hence the formation of C2 products. However, the mechanism for the C1 selectivity has not been understood thus far. In this work using the state-of-the-art DFT calculations and computational electrode model we studied the mechanism of electrocatalytic CO2 reduction towards C1 products.

P152

Electric field-induced band modulation of predicted ternary 2D MXC3 [M:X ¼ As:Ge, Sb:Sn and Bi:Pb] with strong stability and optical properties

The present work reports a new series of ternary two-dimensional MXC3 compounds whose stability and existence are confirmed through the phonon dispersion analysis, elastic properties, and ab initio molecular dynamics simulation. The developed compounds are further investigated with their electronic and optical properties using density functional theory. We have observed zero bandgap nature in MXC3 compounds, where AsGeC3 shows the graphene-like band structure with Dirac cone at K-point. We have systematically applied the external electric field to modulate the electronic and optical properties of these compounds. The increasing magnitude of the electric field has shown the increasing nature of bandgap in the AsGeC3 compound, while no effect was observed in the case of SbSnC3 and BiPbC3 compounds. Consequently, the bandgap of the AsGeC3 compoundis tuned up to 0.98 eV which is maximum at an optimum value of the applied electric field. All the three 2D MXC3 compounds have shown the broken symmetry of the structure after the optimum value of the electrical field that can be understood by the maximum tolerance limit of an applied electric field. Our results strongly suggest the excellent mechanical stability of the AsGeC3 compound under the applied electric field. We have also calculated the variation in the optical properties upon the external field for the AsGeC3 compound, which shows a good transparency nature and can be used in the regulation of the smart window applications. We sincerely believe that our outcomes reflect a significantachievementfor potential applications in future nanoelectronics.

P153

Chemical trends in the electronic structures of transition metal dichalcogenides

Small-angle twisted bilayer transition metal dichalcogenides (tBL-TMDs) exhibit rich phase diagrams as function of carrier density and temperature [1-5]. Similarly to twisted bilayer graphene, the competition of various electronic states, such as correlated insulating and superconducting phases, is attributed mainly to strong electron-electron interactions, due to the emergence of flat bands near the Fermi level [6]. At small twist angles (<5°), the large size of the moiré cells and the large chemical space associated with TMDs, makes first-principles calculations of the atomic and electronic structure challenging. To overcome this obstacle, we employ a multi-scale approach, in which classical force fields are used to find equilibrium atomic structures [8] and tight-binding calculations are carried out on the relaxed structures to determine electronic band structures [7]. We present results of single-particle quantities (band structures, wave function densities etc.) of different homo- and hetero-tBL-TMDs and discuss their dependence on twist angle as well as on chemical composition of the constituent monolayers. Refs. [1] Nat. Mat. 19, pages 861–866 (2020) [2] Nat. Mat. 19, pages 824–826 (2020) [3] arXiv.2006.05615 (2020) [4] Nat. Comm. 11, 2153 (2020) [5] arXiv:2007.12068 (2020) [6] Phys. Rev. Lett. 121, 266401 (2018) [7] Phys. Rev. B 92, 205108 (2015) [8] J. Phys. Chem. C, 123, 15, 9770–9778 (2019)

P154

Direct Comparison of Many-Body Methods for Realistic Electronic Hamiltonians

I will report on a large collaboration of more than 20 researchers, in which we carefully benchmark 20 first principles electronic structure methods on a test set of seven transition metal atoms, ions, and their monoxides. We were able to use a combination of 3 systematically improvable methods to establish total energy (not total energy) benchmarks with accuracy of approximately 1 mHa. These highly accurate total energy references allow us to examine how well different techniques solve the mathematical problem of the many-body Schroedinger equation, and make comments about cost/accuracy tradeoffs.

P155

The impact of chemical modification on charge injection at metal/polyolefin interfaces

The process of charge injection at metal/polymer interfaces is crucial to many areas of research and technology, such as organic light emitting and harvesting devices, high-voltage capacitors and cables. In this work, we study charge injection at metal/polymer interfaces for two polymers commonly used in high-voltage applications, namely polyethylene (PE) and polypropylene (PP). Using first-principles electronic structure methods, we compute charge injection barriers at model aluminium/PE and aluminium/PP interfaces. We show that the introduction of polar chemical groups (e.g., -COOH, -CH2Cl, and -CHO) in the polymer chains at the interface can tune the intrinsic charge injection barrier significantly. We take into account of thermal disorder by averaging over a large ensemble of interface structures obtained from first-principles molecular dynamics trajectories. Our results suggest the possibility of rational design of metal/polymer interfaces via localised chemical modification.

P156

PyQMC: an all-Python real-space quantum Monte Carlo code

PyQMC is a new, easy-to-use implementation of real-space quantum Monte Carlo (QMC) for highly-accurate simulations of correlated electron systems. The all-Python code enables rapid development of new techniques and flexible, complex workflows, such as the recent work from our group on QMC excited states [1]. Integration with the electronic structure package PySCF [2, 3] leverages available tools and facilitates direct comparison with many other ab initio methods. The wide availability of Python libraries offers additional flexibility. With PyQMC's parallelization implementation, cloud resources or HPC can be used with the same code. The vectorized architecture ensures good performance and will soon be GPU ready. PyQMC includes variational Monte Carlo, wave function optimization, and diffusion Monte Carlo on molecules and solids, as well as evaluation of one- and two-body density matrices. It also includes a method to find excited states by orthogonality-constrained VMC optimization. The code is freely available at https://github.com/WagnerGroup/pyqmc and is under active development. 1. S. Pathak, et. al. (2020). arXiv preprint arXiv:2009.13556. 2. Q. Sun, et.al. (2018). WIREs Comput. Mol. Sci., 8: e1340. doi:10.1002/wcms.1340 3. Q. Sun, et. al. (2020). J. Chem. Phys., 153, 024109 (2020). doi:10.1063/5.0006074. This work is funded by the U.S. National Science Foundation via Award No. 1931258.

P157

A first-principles Quantum Monte Carlo study of two-dimensional (2D) GaS/Se and Janus GaSSe

Two-dimensional (2D) post-transition metal chalcogenides (PTMCs) have attracted attention due to their suitable band gaps and lower exciton binding energies. Of the predicted 2D PTMCs, GaS/Se has been reliably synthesized and experimentally characterized. Despite this fact, results vary depending on which density functional theory (DFT) functional is used. In an attempt to correct these discrepancies, we employed Diffusion Monte Carlo (DMC) to calculate the ground and excited state properties of GaS/Se because the total energy calculated with DMC has a weaker dependence on the trial wavefunction. We benchmark these results with experimental data, DFT and many-body perturbation theory (GW-BSE). We confirm that monolayer GaSe and GaSe is an indirect gap semiconductor (Γ-M) with a quasiparticle gap in close agreement with experiment and low exciton binding energy. We also benchmark the optimal lattice parameter and cohesive energy with DMC and various DFT methods. In addition, we studied monolayer Janus GaSSe using QMC and compared with GaS and GaSe monolayers. We aim to present a terminal theoretical benchmark for pristine monolayer GaSe and alloys, which will aid in the further study of 2D PTMCs and alloys using DMC methods.

P158

Random structure searching with orbital-free density functional theory

Predicting the arrangements of atoms in materials from first principles is a longstanding challenge. Random structure searching, in which random configurations of atoms are relaxed to local minima in the energy landscape, is one fruitful strategy, but its computational expense can be high when driven by conventional density functional theory. Orbital-free density functional theory, while typically less accurate, is considerably cheaper as an engine for structure searching. Moreover, the results of an approximate search are easily refined with more accurate methods. We use this overall strategy to map the low-energy crystal structures of Li, Na, Mg, and Al at zero pressure. This new role for orbital-free density functional theory has the potential to expedite crystal structure prediction over wide ranges of compositions and pressures.

P159

Quantum transport with Spin Orbit Coupling

Authors: Nils Wittemeier, Nick Papior, Pablo Ordejon, Zeila Zanolli Spin polarized currents are instrumental in creating smaller, more efficient devices for memory storage and information processing, like magnetic random access memory or spin-polarized field effect transistors. Spin-orbit coupling (SOC) allows one to control spin polarization and gives rise to fundamental phenomena including the anomalous Hall effect and topological insulators. Existing (open source) codes implementing SOC can model equilibrium transport and cover the non-equilibrium/finite-bias cases in an approximate way. We present the implementation of SOC in the non-equilibrium Green's function (NEGF) code TranSIESTA [1,2]. TranSIESTA combines the NEGF formalism with DFT as implemented in SIESTA [3,4], including the solution of electrostatic equations, self-consistency of the NEGF density matrix and support for multiterminal devices. In the collinear spin approximation, the Hamiltonian splits into two independent spin-blocks and transport calculations are performed independently. In presence of SOC [5,6] off-diagonal terms coupling the two spin channels arise in the Hamiltonian and an independent treatment is no longer possible. We address this issue by extending the NEGF matrices into 2x2 blocks in spin-space. The new features of the code are tested for i) a monatomic iron chain with a spiral spin configuration, and ii) nanoribbons of topological bismuth. [1] M. Brandbyge et al., Phys. Rev.B 65, 165401 (2002). [2] N. Papior, et al., Comput.Phys.Commun. 212, 8 (2017). [3] J.M. Soler, et al., J.Phys.Condens.Matter 14, 2745 (2002). [4] A. Garcia et al., J.Chem.Phys. 152, 204108 (2020). [5] R. Cuadrado et al., J.Phys.:Condens.Matter 24, 086005 (2012).

P160

Exciton g-factors of van der Waals heterostructures from first-principles calculations

External fields are a powerful tool to probe optical excitations in a material. The linear energy shift of an excitation in a magnetic field is quantified by its effective g-factor. Here we show how exciton g-factors and their sign can be determined by converged first principles calculations. We apply the method to monolayer excitons in semiconducting transition metal dichalcogenides (TMDs) and to interlayer excitons in MoSe2/WSe2 heterobilayers and obtain good agreement with recent experimental data. The precision of our method allows to assign measured g-factors of optical peaks to specific transitions in the band structure and also to specific regions of the samples. This revealed the nature of various, previously measured interlayer exciton peaks. We further show that, due to specific optical selection rules, g-factors in van der Waals heterostructures are strongly spin and stacking-dependent. The presented approach can potentially be applied to a wide variety of semiconductors. [1] Recent measurements of electrons and holes g-factors in 1L TMDs additionally corroborate the validity and accuracy of our method. [2] [1] T. Woźniak, P. E. Faria Junior, G. Seifert, A. Chaves, J. Kunstmann, Exciton g factors of van der Waals heterostructures from first-principles calculations, PRB, 101, 235408 (2020). [2] M. Zinkiewicz, T. Woźniak, T. Kazimierczuk, M. Potemski, A. Babiński, M. Molas et al, Excitonic complexes in n-doped WS2 monolayer, arXiv:2012.11509 (2020).

P161

Novel low dense carbon allotropes from data mining approaches

Kedar Yadav, and D. L. V. K. Prasad*

Department of Chemistry, Indian Institute of Technology, Kanpur 208016, India
Email: dprasad@iitk.ac.in

Allotropes of carbon are very well known for their diverse structure and excellent properties. Diamond is the naturally occurring hardest elemental material known to the human kind. The graphite and its analogous structures, graphene and graphdiyne are omnipresent and they occupy a pivotal role in the chemistry and physics of contemporary materials. The nanoscience and engineering is spearheaded by fullerenes and nanotubes. In this multifarious carbon kinship, here, we propose different novel carbon networks built based on parental skeletons of carbon allotropes with molecular carbon spacers as linkers from data mining approaches. The model structures are calculated for their electronic structure and stability using density functional theory and density functional perturbation theoretical methods. The calculated structures are found to be remarkably stable; the phonon dispersions suggest that the structures are dynamically stable. All the carbon structures studied here with varied densities due spacers are found to be semiconductors with tunable band gaps. The predicted novel structures, structure-property correlations, and the results of the electronic structure calculations will be presented.

P162

Structural, elastic, electronic, and magnetic properties of MnNbZ (Z = As, Sb) and FeNbZ (Z = Sn, Pb) semi-Heusler alloys

The study of structural, electronic, magnetic, and elastic properties of a new series of semi-Heusler alloys MnNbZ (Z=As, Sb) and FeNbZ (Z=Sn, Pb) has been performed by density functional theory. The magnetic phase and hence the structural stability of the alloys were considered wherein the ferromagnetic state is found to be stable. The half-metallic states are observed from the density of states and band structure calculations. The total magnetic moments found for all studied compounds are 1 μ B /f.u., which obey the Slater-Pauling rule for semi-Heusler with ferromagnetic behavior. The calculated cohesive and formation energies confirmed the thermodynamical stability and elastic constant C ij confirmed the mechanical stability. Among the four systems, MnNbAs is found to have the highest ductility (i.e., non-directional metallic bonding) while the remaining systems are found to be brittle in nature (i.e., directional covalent bonding). These properties confirmed that among others, MnNbAs is one of the novel candidate for spintronic device applications.

P163

The study of Dirac cones in graphene flakes using band-unfolding method

Sefty Yunitasari[1], Fumiyuki Ishii[1], and Naoya Yamaguchi[1]

[1] Kanazawa University, Kakuma, Kanazawa 920-1192, Japan

The electronic band structure calculation is one of the essential tools to understand the electronic properties of the materials. The problem of band folding sets in when the supercell scheme is applied to study alloys or various perturbed systems with impurities and vacancies. The unfolding method is expected to get the meaningful energy-momentum relation by avoiding it. The unfolding method proposed by Chi-Cheng Lee et al. (2013) [1] was proven very useful for calculating the electronic structures of vacancy systems in the OpenMX code. By using it, we study the graphene flake size dependence of the electronic structure and observe the desirable Dirac cone features. The result could be a useful starting point to study twisted bilayer-graphene (tBLG). Moreover, tBLG is aperiodic the same as the flake system while the unfolding method strongly depends on the choice of the primitive cell.

Keywords: 2D material, graphene, band structures, unfolding method

[1] Chi-Cheng Lee *et al* 2013 *J. Phys.: Condens. Matter* **25** 345501.

P164

Defects in Transition Metal Dichalcogenides: towards quantum computing

Authors: Zeila Zanolli, Pedro M. M. C. de Melo, Matthieu J. Verstraete Even the best quality 2D materials have non-negligible concentrations of vacancies and impurities. It is critical to understand and quantify how defects change intrinsic properties, and use this knowledge to generate functionality. We address this challenge by employing many-body perturbation theory to obtain the optical absorption spectra of defected transition metal dichalcogenides [1]. Herein metal vacancies, which are largely unreported, show a larger set of polarized excitons than chalcogenide vacancies, introducing localized excitons in the sub-optical-gap region, whose wave functions and spectra make them good candidates as quantum emitters. Despite the strong interaction with substitutional defects, the spin texture and pristine exciton energies are preserved, enabling grafting and patterning in optical detectors, as the full optical-gap region remains available. A redistribution of excitonic weight between the A and B excitons is visible in both cases and may allow the quantification of the defect concentration. This work establishes excitonic signatures to characterize defects in 2D materials and highlights vacancies as qubit candidates for quantum computing. [1] P. M. M. C. de Melo, Z. Zanolli, M. J. Verstraete, Advanced Quantum Technology, accepted 2021, arXiv:2010.10222

P165

Enhanced optical adsorption at the surface of rutile TiO2 nanostructures by oxygen defects

Defective TiO2 nanoparticles (NPs) have been recently in particular interest because of wide applications in photocatalysis. To design a new metal-oxide based photocatalyst system with engineered defects and higher solar absorption, a precise description of the structural and electronic properties is necessary. Combining X-ray photoelectron spectroscopy (XPS) and density functional-tight binding (DFTB) calculations, we probed the effect of oxygen defects on the electronic structure of the rutile TiO2 NPs. We combined our experimental observations with electronic structure calculations to understand the origin of the enhanced photocatalytic performance of the defective rutile TiO2 NPs. According to the DFTB calculations, the fermi state shifted and touched the conduction band minimum with increasing the concentration of oxygen vacancies and adding OH groups on the (110) surface of the TiO2 slab. Furthermore, mid-gap states emerged below the Fermi level with increasing oxygen vacancies in the TiO2 slab. The DFTB calculations predict that TiO2 slab finds a metallic character with increasing the oxygen defects in the structure which is probably the origin of the visible light photocatalytic activity of the samples in our experiment. Time dependent (TD) DFTB calculations were also performed to investigate the optical properties of the TiO2 NPs and compared with the experimental results. The TD-DFTB results show enhancement in the visible light absorption with increasing the defect concentration which is in agreement with the experimental results.

P166

magneto electric response in rare earth orthoferrites

Rare earth orthoferrites have been studied for a long time due to their unique magnetic properties. Recently these materials have been shown to be multiferroic and magnetoelectric (ME). The ME responses measured in these material are shown to be among the strongest MEs. In this work we have studied the origin of this strong ME response using theoretical derivation which is supported by spin dynamics and DFT calculation. At first step we have made a Heisenberg model to describe the magnetic properties of these materials which is fitted with DFT calculations. Using these Hamiltonians, we then have expanded the ME response of these materials in odd orders of the magnetic field. We have shown that The response close to zero magnetic field is mainly governed by linear response of the material and going to higher magnetic field, the response becomes dominated by the higher order terms and the ME response shows a divergence close to magnetic phase transition point.

P167

Electrostriction by DFT: a methodological study

Recent discovery of materials exhibiting extremely large electrostrictive coefficients, a phenomenon known as "giant electrostriction" has opened a field with important applications for electromechanical devices. Giant electrostriction based systems offer advantages over current piezoelectricity based technology of increased temperature stability, low hysteresis, and lead-free materials. To date, few giant electrostrictors have been found, and the microscopic origins of this phenomenon remain unknown. This emerging field would thus benefit greatly from the application of ab. initio calculations to the high-throughput screening of materials for giant electrostriction, and also to the investigation of its origins. In this work we review the current finite field and energy difference methodologies by which electrostriction is calculated using DFT, and propose and validate a never before used method based on stress or strain derivatives of the permitivity. The efficiency, simplicity, and robustness of this method opens the door to high-throughput screening of the electrostriction in materials with large unitcells and possibly microscopic disorder necessitating a supercell approach, and offers a perspicuous approach by which the origins of electrostriction may be understood.